ELECTROSPUN PARTICLE/POLYMER FIBER MAT ELECTRODES FOR LI-ION BATTERIES

By

Ethan Craig Self

Dissertation
Submitted to the Faculty of the
Graduate School of Vanderbilt University
in partial fulfillment of the requirements
for the degree of

DOCTOR OF PHILOSOPHY
in

Chemical Engineering
May, 2017
Nashville, Tennessee

Approved:

Peter N. Pintauro, Ph.D., Chair
Paul E. Laibinis, Ph.D.
Cary L. Pint, Ph.D.
Bridget R. Rogers, Ph.D.

Dedicated to my lifelong childhood friend, Mitchell James Webb. May you rest in peace.

ACKNOWLEDGEMENTS

I thank everyone who made contributions which were essential to the completion of this dissertation. My most sincere gratitude goes to my thesis advisor, Professor Peter N. Pintauro, for accepting me into his research group and supporting my studies at Vanderbilt. Without his guidance, none of this work would have been possible. I thank Professors Paul E. Laibinis, Cary L. Pint, Bridget R. Rogers, and M. Douglas LeVan for providing valuable feedback on my research while serving on my thesis committee.

I also want to acknowledge all members of the Pintauro group for their support while I navigated my Ph.D. Professor Ryszard Wycisk and his expertise in polymer chemistry were vital resources in the laboratory, and his affable personality ensured the countless hours spent in Olin Hall were both productive and enjoyable. I also want to specially acknowledge Dr. Jason Ballengee for his mentorship during my early years at Vanderbilt and for being a model graduate student whom I strived to emulate throughout my studies. Daniel Anastos, Megan Burcham, and Emily McRen were undergraduate researchers who worked on various aspects of this project. Emily made substantial contributions to the studies on carbon anodes, Si anodes, and $LiCoO_2$ cathodes.

Several collaborators made significant contributions to this work. Professor Yang-Tse Cheng and his graduate student Jiagang Xu at the University of Kentucky taught me how to construct and characterize coin cells. Professor Rizia Bardhan and her graduate student William R. Erwin at Vanderbilt assisted with Raman analysis of $LiCoO_2$ nanoparticles. Drs. Jagjit Nanda, Michael Naguib, and Rose Ruther at Oak Ridge National Laboratory (ORNL) performed post-mortem analysis of electrospun Si-based anodes. Dr. Gao Liu at Lawrence Berkeley National Laboratory (LBNL) contributed to a

collaboration among Vanderbilt, ORNL, and LBNL by providing Si nanoparticles and electronically conductive polymer binder. Professor Sreeram Vaddiraju at Texas A&M University provided Si nanowires for anode fabrication.

I also want to thank several members of the Vanderbilt community for their diligent work which was vital for completion of my research. Mary Gilleran, Rae Uson, Julie James, Julie Canada, and Angie Pernell provided friendly administrative assistance and were always prompt in processing my purchase requests and travel forms. Mark Holmes helped install several pieces of laboratory equipment. Professors Anthony Hmelo and James McBride worked tirelessly to ensure laboratory facilities were available to the VINSE research community.

Fellow graduate students and members of the Nashville community made my time spent at Vanderbilt unforgettable. The past five years have been filled with some of the happiest moments of my life, and I am fortunate to have shared these experiences with so many compassionate individuals. Thanks to you all for your friendship and kindness.

Most importantly, I want to thank my family for their unwavering love and support. My parents and sister helped me put life in perspective throughout the highs and lows of graduate school. My nephews Kip and Ray Keyser constantly reminded me that there is beauty in life despite the myriad of problems that humanity faces.

This work was funded by the National Science Foundation (NSF EPS-1004083) through the TN-SCORE program under Thrust 2 and the United States Department of Energy (DE-EE0007215).

TABLE OF CONTENTS

Page

LIST OF TABLES

Table Page

LIST OF FIGURES

Figure Page

CHAPTER I

INTRODUCTION

Since the Industrial Revolution, human innovation has driven the development of new technologies that form the cornerstones of modern-day life. While this progress has vastly improved the average quality of life worldwide, humanity now faces an energy crisis caused by population growth and depletion of finite natural resources. The global energy demand is expected to double by 2050, so developing clean energy technologies is of utmost importance to ensure a sustainable future.[1-3] Many renewable energy resources—such as sunlight, wind, and tides—are intermittent by nature, and thus energy storage systems are required to store and release this energy as needed.

Secondary (i.e., rechargeable) batteries have several attractive features as energy storage devices including: (i) emissionless operation, (ii) high round-trip efficiency, (iii) low maintenance, and (iv) flexible energy and power characteristics.[1] The Ragone plot in Figure 1.1 shows that Li-ion batteries (LIBs) have the highest specific energy and power of any commercially available secondary battery technology. Furthermore, a low self-discharge rate and the lack of a memory effect make LIBs user-friendly for consumer devices.[4, 5] Since their commercial debut in 1991, LIBs have revolutionized the functionality of portable electronics, and the LIB industry continues to grow today due emerging applications such as electric vehicle propulsion. Despite the extraordinary commercial success of LIBs, many devices are still limited by battery performance, and

thus next-generation batteries must be developed to satisfy ever-increasing energy demands.[4-7]

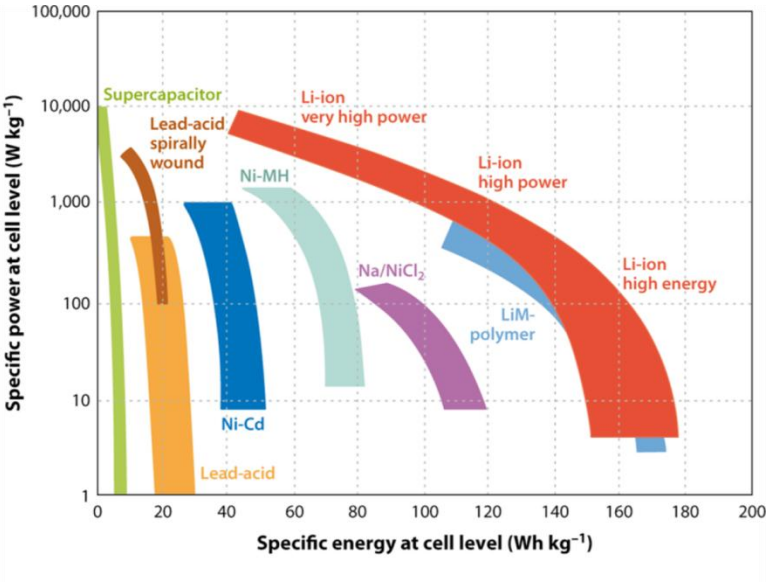

Figure 1.1. A Ragone plot showing the energy and power density of rechargeable batteries and supercapacitors. Image reproduced from Hayner et al.[8] with permission from Annual Reviews.

LIB performance is primarily limited by the lithium capacity, rate capabilities, and cycle life of conventional slurry cast electrodes. As described in Chapter II of this dissertation, the scientific community has dedicated considerable time and resources toward developing nanostructured battery materials (e.g., nanoparticles, nanowires, and nanofibers) to achieve higher capacities at faster charge/discharge rates.[9, 10] Moreover, for anodes such as Si which undergo large volumetric changes during charge/discharge processes, nanostructuring the active material prevents pulverization caused by lithiation-induced stresses, thus improving the cycling stability of these electrodes.[11, 12]

Despite their promising performance, such nanostructured electrodes remain distant from commercial applications due to their expensive fabrication methods and low areal and volumetric capacities.

To address the shortcomings of previously reported nanoscale battery electrodes, this dissertation details the fabrication and characterization of fiber mat LIB electrodes prepared using particle/polymer electrospinning, a technique originally developed by Pintauro and coworkers for fuel cell electrodes.[13-16] Electrospun fiber mat LIB electrodes typically contain three components—active material nanoparticles for Li storage, carbon powder for electrical conduction (only required when the other electrode components have low electronic conductivity), and a polymer binder. These particle/polymer fiber mats offer several advantages over conventional slurry cast electrodes, including: (i) a large electrode/electrolyte interfacial area, (ii) short Li^+ transport pathways between the electrolyte and active material in the radial fiber direction, and (iii) good electrolyte infiltration throughout the intra- and interfiber void space of the fiber mat. Furthermore, the presence of the polymer binder ensures the mats can be compacted under high pressure without fracturing, so thick, densely packed fiber mats can be used to achieve high gravimetric, areal, and volumetric capacities. For practical battery applications, high areal capacities are desired to reduce the amount of inactive cell components (e.g., current collectors, separators, etc.), and batteries with a high volumetric capacity allow more energy to be stored within a given space.[17]

Particle/polymer electrospinning is compatible with various active materials and binders, enabling the development of a wide range of fiber electrodes. Chapters III – VI of this dissertation detail the preparation and characterization of four types of

particle/polymer fiber mat LIB electrodes. Each chapter makes substantial contributions to the literature, and when considered as a whole, this dissertation demonstrates that particle/polymer electrospinning is an attractive technique for fabricating high performance electrodes for electrochemical energy storage devices.

Chapter III describes the first ever use of particle/polymer electrospinning for LIB applications. Fiber mat anodes containing titania nanoparticles and carbon powder distributed throughout a poly(acrylic acid) binder (TiO_2/C/PAA) were prepared and characterized. The electrochemical properties of electrospun and slurry cast TiO_2/C/PAA anodes were evaluated in half cells containing a Li metal counter/reference electrode. The performance of TiO_2/C/PAA fiber mats with thicknesses up to 1.4 mm was evaluated over a range of charge/discharge rates and compared to that of published data for anodes containing either titania, carbon, or silicon active materials.

Electrodes containing electronically conductive carbon active materials (active materials reversibly store Li during charge/discharge processes) do not require conductive additives and thus can be used to prepare electrospun mats with high active material loadings in the fiber. The use of carbon nanofiber anodes containing carbon powder and poly(vinylidene fluoride) (PVDF) binder is described in Chapter IV. The areal and volumetric capacities of electrospun C/PVDF mats with a range of thicknesses and fiber volume fractions were determined in half cells. The rate capabilities of C/PVDF nanofiber electrodes were compared to those of conventional slurry cast anodes.

Although most studies in the literature only discuss electrode performance in a half cell configuration, both anode and cathode materials are required for practical full cell devices. Chapter V details the preparation and characterization of electrospun LIB

cathodes containing $LiCoO_2$ nanoparticles, carbon powder, and PVDF ($LiCoO_2$/C/PVDF). The $LiCoO_2$/C/PVDF fiber mat cathodes were characterized in half cells and in full cells containing an electrospun C/PVDF anode (described in Chapter IV). The full cell results represent the first ever LIB prepared using a paired electrospun particle/polymer fiber mat cathode and anode. The performance of the electrospun electrodes was compared to that of conventional slurry cast electrodes of the same composition at slow and fast charge/discharge rates.

Si has been widely investigated as a replacement for graphite used in today's LIB anodes due to its high capacity and low operating potential, but Si-based anodes typically have poor cycling stability due to the large volumetric changes of Si during battery charge/discharge operation. Chapter VI describes electrospun Si-based anodes containing Si nanoparticles, carbon powder, and PAA (Si/C/PAA). Qualitative performance/composition/structure correlations were established by evaluating the performance of Si/C/PAA fiber mats with different compositions, fiber volume fractions, interfiber connectivities, thicknesses, and loadings in half cells. A full cell containing an electrospun Si/C/PAA anode and electrospun $LiCoO_2$/C/PVDF cathode (described in Chapter V) was also characterized. In addition to these studies on Si/C/PAA anodes, Chapter VI also describes electrospun and slurry cast anodes prepared with Si nanoparticles and one of two electronically conductive polymer binders (PFM and PEFM) where the electrodes contained 20 – 67 wt % Si.

References

[1] B. Dunn, H. Kamath, J.-M. Tarascon, *Science* **2011**, *334*, 928.
[2] A. Thatcher, P. H. Yeow, *Appl Ergon* **2016**, *57*, 1.
[3] N. S. Lewis, D. G. Nocera, *Proc. Natl. Acad. Sci. USA* **2006**, *103*, 15729.
[4] J.-M. Tarascon, M. Armand, *Nature* **2001**, *414*, 359.
[5] M. Armand, J.-M. Tarascon, *Nature* **2008**, *451*, 652.
[6] J. B. Goodenough, Y. Kim, *Chem. Mater.* **2010**, *22*, 587.
[7] J. B. Goodenough, *Acc. Chem. Res.* **2013**, *46*, 1053.
[8] C. M. Hayner, X. Zhao, H. H. Kung, *Annu. Rev. Chem. Biomol. Eng.* **2012**, *3*, 445.
[9] C. Liu, F. Li, L. P. Ma, H. M. Cheng, *Adv. Mater.* **2010**, *22*, E28.
[10] L. Ji, Z. Lin, M. Alcoutlabi, X. Zhang, *Energy Environ. Sci.* **2011**, *4*, 2682.
[11] H. Wu, Y. Cui, *Nano Today* **2012**, *7*, 414.
[12] U. Kasavajjula, C. Wang, A. J. Appleby, *J. Power Sources* **2007**, *163*, 1003.
[13] W. Zhang, P. N. Pintauro, *ChemSusChem* **2011**, *4*, 1753.
[14] M. Brodt, R. Wycisk, P. N. Pintauro, *J. Electrochem. Soc.* **2013**, *160*, F744.
[15] M. Brodt, T. Han, N. Dale, E. Niangar, R. Wycisk, P. Pintauro, *J. Electrochem. Soc.* **2014**, *162*, F84.
[16] M. Brodt, R. Wycisk, N. Dale, P. Pintauro, *J. Electrochem. Soc.* **2016**, *163*, F401.
[17] N. Nitta, G. Yushin, *Part. Part. Syst. Char.* **2014**, *31*, 317.

CHAPTER II

BACKGROUND

2.1 Principles of Li-ion Batteries

Li-ion batteries (LIBs) are electrochemical energy storage devices that convert chemical energy to electrical energy through redox reactions involving reversible Li storage in the electrodes. A LIB is constructed from two or more cells connected in series and/or parallel arrangements, and each cell is comprised of three components— a negative electrode, a positive electrode, and an ionically conductive electrolyte. The electrodes typically contain a mixture of active material that stores Li, electronically conductive carbon, and a polymer binder. Figure 2.1 shows a schematic of a LIB with graphite and $LiMO_2$ (where M = Co, Mn, or Ni) as the negative and positive electrodes, respectively. These electrode materials have a layered structure where the inter-plane spacing is sufficiently large to intercalate Li; similarly, other active materials (e.g., silicon and sulfur) store Li via conversion reactions which are accompanied by the formation and breakage of chemical bonds.[1] The electrolyte is ionically conductive to allow transport of Li^+ ions between the electrodes and electronically insulating to prevent short-circuiting of the cell. The electrolyte can either be a solid, liquid, or gel, but most commercial cells are prepared with a porous polyolefin separator soaked in a liquid electrolyte containing a Li-based salt (e.g., $LiPF_6$) dissolved in a mixture of organic carbonates (e.g., ethylene carbonate and diethyl carbonate).

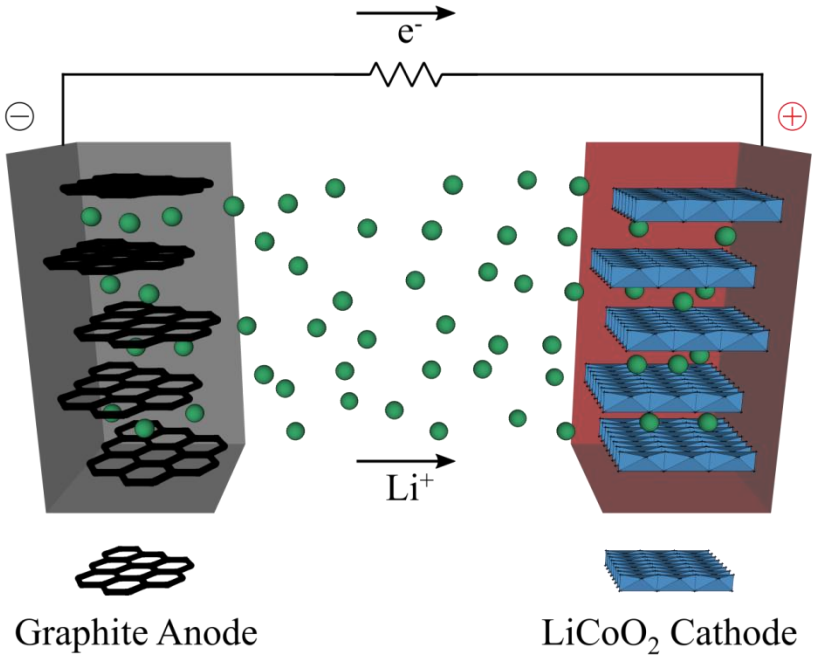

$$\text{Charge: } 2\,LiCoO_2 + 6\,C \longrightarrow 2\,Li_{0.5}CoO_2 + LiC_6$$
$$\text{Discharge: } 2\,Li_{0.5}CoO_2 + LiC_6 \longrightarrow 2\,LiCoO_2 + 6C$$
$$V_{cell} \sim 3.6\ V$$

Figure 2.1. Schematic of a Li-ion cell during discharge.

LIBs store and release energy by shuttling Li^+ ions between the two electrodes. During cell charging, oxidation at the positive electrode produces Li^+ ions and electrons. The electrons flow through an external circuit, and Li^+ ions diffuse/migrate across the electrolyte toward the negative electrode where they recombine with electrons and are stored in the active material. This process is reversed during cell discharging, and Li is spontaneously driven to positive electrode as shown in Figure 2.1. The battery community commonly refers to the positive and negative electrodes in full cells as the cathode and anode, respectively, but this nomenclature should be used with caution since the redox reactions switch directions during cell charging and discharging. By definition, reduction and oxidation occur at the cathode and anode, respectively.

2.2 Characterization of Li-ion Batteries

LIBs are characterized by the amount of energy stored/delivered during charge/discharge cycling. The specific energy of a cell E_{cell} (Wh kg^{-1}) is related to its lithium capacity Q (Ah) and operating potential V_{cell} (V) by equation 2.1,

$$E_{cell}(Q) = \frac{1}{m}\int_0^Q V_{cell}(Q')dQ' \quad (2.1)$$

where m is the mass of the cell. Similarly, the energy density of a cell (Wh L^{-1}) is normalized with respect to cell volume. Battery researchers typically characterize individual electrodes (either anodes or cathodes) in half cells where the working electrode is paired with a Li metal counter/reference electrode which contains a large excess of Li. This half cell configuration is a convenient and reliable setup which avoids constructing full cells where capacity matching of the anode and cathode can affect performance.[2] Half cells are characterized using charge/discharge experiments in which cells are cycled between upper and lower potential limits— which depend on the chemistry of the working electrode—by changing the direction of current flow between charging and discharging steps. These tests most commonly use galvanostatic (i.e., constant current) protocols.[3]

Charge/discharge curves which show cell potential as a function of lithium capacity give insight to the electrochemical processes occurring in a cell. Figure 2.2 shows charge/discharge collected over 3 cycles for a half cell containing a commercial graphite working electrode (from hereon referred to as the anode). The cell potential decreases/increases as graphite is lithiated/delithiated, respectively. The sloping profile at 0.25 – 1 V vs. Li/Li^+ during the first lithiation half cycle indicates formation of a solid electrolyte interphase (SEI) layer on the anode surface. The SEI layer, which is

comprised of various electrolyte decomposition products (e.g., lithium alkyl carbonates, Li_2CO_3, and LiF), forms when the working electrode's operating potential is outside the electrolyte's electrochemical stability window (approximately 1.3 – 4.5 V vs. Li/Li^+ for standard liquid electrolytes).[4] Desired SEI layer properties include: (i) good adhesion to the electrode surface, (ii) high Li^+ conductivity, (iii) low electronic conductivity, and (iv) low electrolyte permeability. During subsequent cycles, additional electrolyte decomposition is hindered by the SEI's low electronic conductivity and low electrolyte permeability. The voltage plateaus below 0.5 V vs. Li/Li^+ in Figure 2.2 correspond to lithiation/delithiation of graphite during half cell operation, and the end of the delithiation (charging) step indicates the graphite electrode has a reversible capacity of ~ 325 mAh g^{-1}. In general, charge/discharge experiments are used to characterize a wide range of LIB anodes and cathodes where the operating potential and lithium capacity depend on the chemistry of the active material, with several examples given in Figure 2.3.

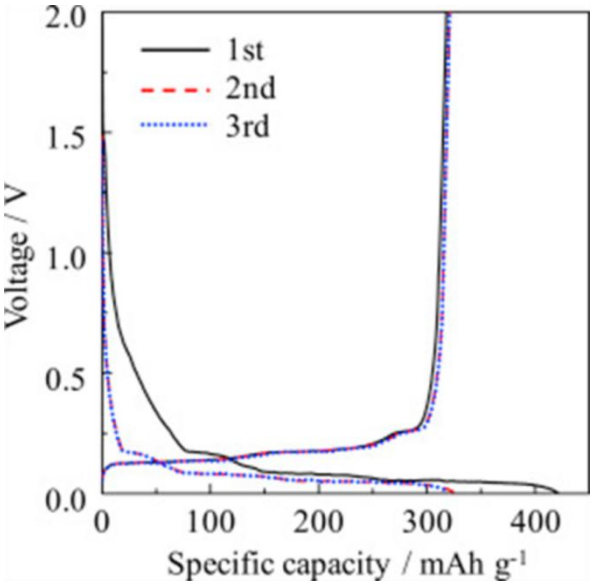

Figure 2.2. Charge/discharge curves for a commercial graphite anode collected over 3 cycles at 0.1 C. Image adapted from Towada et al.[5] with permission from Elsevier.

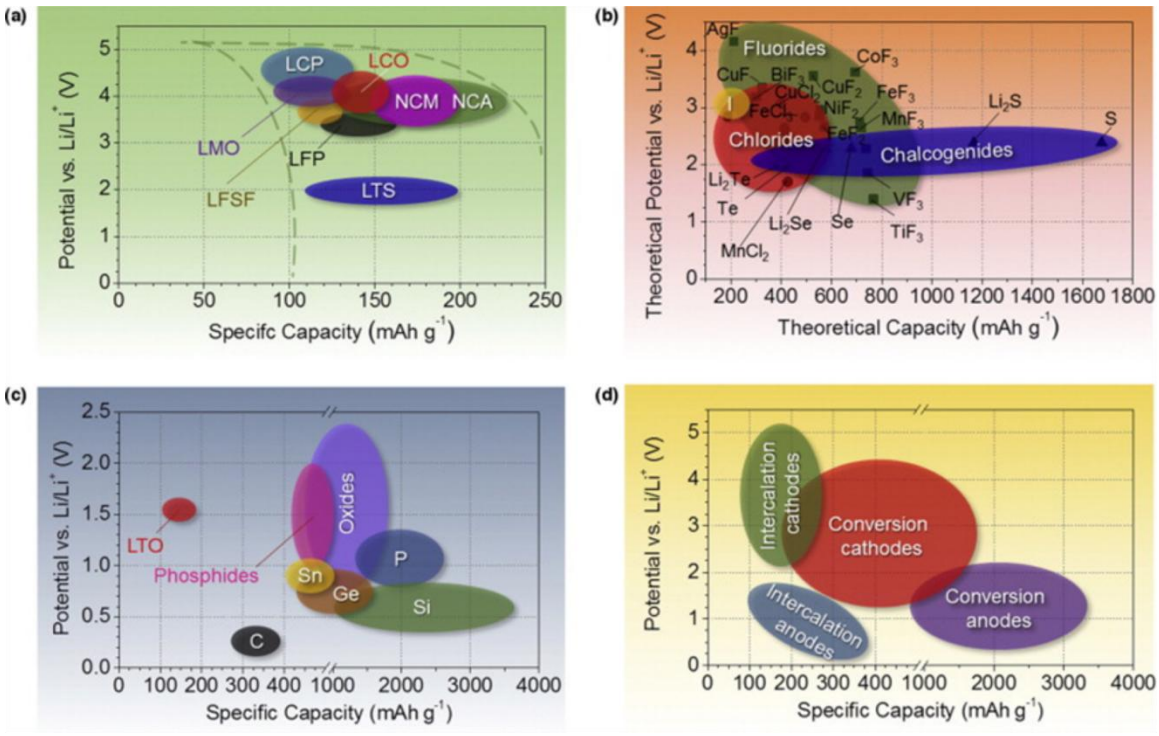

Figure 2.3. Specific capacity and operating potentials for (a) intercalation-type cathodes, (b) conversion-type cathodes, (c) conversion-type anodes, and (d) an overview of various anodes and cathodes. Image reproduced from Nitta et al.[1] with permission from Elsevier.

An active material's theoretical capacity is calculated based on the stoichiometry of the fully lithiated structure. For an active material AM that can be lithiated to form Li_xAM, the theoretical capacity $Q_{theoretical}$ (mAh g^{-1}) is given by equation 2.2,

$$Q_{theoretical} = \frac{xF}{M_w} \times \frac{mAh}{3.6\ C} \tag{2.2}$$

where F is Faraday's constant and M_w is the molecular weight of the active material. Battery electrodes typically contain multiple components including active material, conductive additive, and polymer binder, and the theoretical capacity $Q_{theoretical}$ (mAh g^{-1})

of these composite electrodes is calculated using the simple mixing rule shown in equation 2.3,

$$Q_{theoretical} = \sum_i x_i Q_i \tag{2.3}$$

where x_i and Q_i are the weight fraction and theoretical capacity of component i, respectively. The electrode's theoretical capacity is used to calculate the current used during galvanostatic charge/discharge experiments. This current is described using a charging rate (C-rate) notation where n^{-1} C is defined as the current needed to complete a half cycle (i.e., charge or discharge) in n hours. Charge/discharge experiments are often conducted over a wide range of currents (e.g., C-rates of 0.1 – 5 C) to evaluate an electrode's rate capabilities. In general, electrodes have lower reversible capacities at higher C-rates due to greater activation, ohmic, and Li^+ concentration overpotentials within the cell. Thus a primary goal of battery research is to minimize these overpotentials to achieve high reversible capacities at both slow and fast charge/discharge rates.

While an electrode's theoretical capacity is calculated using equations 2.2 and 2.3, experimentally measured capacities Q_{expt} (mAh g^{-1}) are determined by integrating the current I (mA) as a function of time t (s), as described by equation 2.4,

$$Q_{expt}(t) = \left(\frac{1}{m} \times \frac{mAh}{3{,}600\ mC}\right) \int_0^t I(t')dt' \tag{2.4}$$

where m is the overall electrode mass (g). During galvanostatic charge/discharge experiments in which constant current is used, equation 2.4 simplifies to equation 2.5:

$$Q_{expt}(t) = \frac{It}{m} \times \frac{mAh}{3{,}600\ mC} \tag{2.5}$$

The chemical reversibility of the Li storage reaction in an electrode is described by the coulombic efficiency (*CE*) calculated using equation 2.6,

$$CE = \frac{Q_{discharge}}{Q_{charge}} \times 100\ \% \tag{2.6}$$

where $Q_{discharge}$ and Q_{charge} are the corresponding half cycle capacities. In general, an electrode's discharge capacity is less than its charging capacity due to irreversible capacity losses caused by SEI layer formation, undesired side-reactions, electronic isolation of active material, etc.

Equations 2.4 and 2.5 describe gravimetric capacity which is normalized with respect to electrode mass. Although gravimetric capacity is the most common metric reported in the literature, an electrode's areal and volumetric capacities (normalized to electrode footprint and volume, respectively) should also be considered. Electrodes with high areal capacity reduce the number of inactive cell components (e.g., separators and current collectors) which contribute to a battery's overall size and weight. Similarly, batteries with high volumetric capacity store more energy in a given space.[3]

While individual electrodes are typically characterized in half cells, the Li metal anodes in these cells cannot be utilized in consumer devices due to safety issues associated with Li dendrite growth during charge/discharge cycling.[2, 6, 7] Thus, electrode performance in full cells containing a Li storage anode and cathode must be considered for practical battery applications. For full cell testing, the anode and cathode capacities should be well-matched to ensure good active material utilization in each electrode. In other words, the amount of Li available in the cathode should be similar to that which can be stored in the anode. The capacity matching of the negative and positive electrodes (i.e., anode and cathode, respectively) is described by the quantity *N/P* in equation 2.7,

$$\frac{N}{P} = \frac{Q_{anode}}{Q_{cathode}} \times 100\ \% \tag{2.7}$$

where Q_{anode} and $Q_{cathode}$ are the electrodes' reversible capacity. The N/P ratio in a full cell should be close to 1 to ensure good active material utilization in each electrode. Overall, full cell performance is evaluated using the same charge/discharge protocols previously described in this section.

2.3 Prior Research on Li-ion Battery Electrodes

Commercial LIB electrodes are prepared by slurry casting a solution containing active material, conductive carbon, and polymer binder onto an electronically conductive current collector (e.g., Cu foil for the anode and Al foil for the cathode).[8] While these slurry cast electrodes are used in all of today's commercial batteries, new electrode materials and designs must be developed to satisfy ever-increasing energy demands of consumers. Sections 2.3 and 2.4 summarize previous work on the fabrication and characterization of LIB electrodes.

2.3.1 Anode Materials and Designs

Carbon is one of the most versatile elements in the periodic table, and as such, many carbon allotropes have been investigated as active materials for LIB anodes. In general, carbon structures can be classified as either soft carbons, hard carbons, or nanostructured carbons, each of which has unique Li storage properties.[9, 10] Graphite is prepared from soft carbons by heating them at high temperature (> 1,000 °C) to align the graphene layers in a parallel arrangement. Despite their widespread use in commercial LIBs, slurry cast graphite anodes are limited by their theoretical capacity of 372 mAh g^{-1} (corresponding to LiC_6) and poor rate capabilities (e.g., 63 mAh g^{-1} at 2 C).[11] Hard

carbons have a disordered structure where the graphene layers are randomly oriented, and Li can be stored between these layers, at the edges of graphene planes, and on crystallite surfaces.[9] The reversible capacity of hard carbons typically ranges from 150 – 650 mAh g^{-1} depending on the exact structure of the material.[12-16] Yang et al.[13] characterized several hard carbon anodes with gravimetric capacities as high as 504 mAh g^{-1}, but these materials had low initial coulombic efficiencies of 28 – 47 % due to irreversible Li and electrolyte consumption in the cell. Nanostructured carbons such as carbon nanotubes and graphene flakes have attractive properties for use in LIB anodes due to their high surface area to volume ratio, high electronic conductivity, and good mechanical properties. Reversible capacities of 1,264 and 750 mAh g^{-1} have been reported for graphene[17] and carbon nanotubes[18], respectively. The high electronic conductivity of nanostructured carbons also make them useful as conductive additives in composite electrodes.[19, 20] Despite the attractive properties of these carbon nanomaterials, their high cost limits their use in commercial battery applications.

Ti-based anodes where the active material is either TiO_2 or $Li_4Ti_5O_{12}$ are attractive alternatives to carbon anodes due to their: (i) low volumetric strain during lithiation/delithiation (e.g., 0.2 % for $Li_4Ti_5O_{12}$ vs. ~ 8 % for graphite) which enables outstanding cycling stability and (ii) high operating potential (ca. 1.5 – 1.8 V vs. Li/Li^+) which lies within the electrochemical stability of common liquid electrolytes and thus avoids SEI layer formation.[21-26] These advantages are offset by the materials' low theoretical capacities (335 and 175 mAh g^{-1} for TiO_2 and $Li_4Ti_5O_{12}$, respectively) and low ionic and electronic conductivities which limits their rate capabilities. To improve the performance of Ti-based anodes at fast charge/discharge rates, several groups have

reported on the preparation and characterization of nanostructured TiO_2[27-32] and $Li_4Ti_5O_{12}$[33-35] anodes with large electrode/electrolyte interfacial areas and short Li^+ transport pathways. Liu et al.[34] described a carbon-coated $Li_4Ti_5O_{12}$ nanotube array grown directly on a stainless steel current collector with reversible capacities of 165 mAh g^{-1} at 1 C and 154 mAh g^{-1} at 10 C. In another study, Xiong et al.[32] showed that a TiO_2 nanowire anode consisting of mixed anatase and bronze phases had a gravimetric capacity of 166 mAh g^{-1} at 0.3 C and retained 46 % of this capacity at 4.8 C. Despite their moderate gravimetric capacities at high C-rates, these nanowire/nanotube arrays had very low electrode loadings which resulted in poor areal capacities (<< 1 mAh cm^{-2}). Thus, new nanoscale Ti-based anodes with areal capacities comparable to that of commercial electrodes (2.5 – 3.5 mAh cm^{-2}) at fast charge/discharge rates must be developed.

Active materials which electrochemically alloy with Li (e.g., Si, Ge, and Sn) have much higher capacities (theoretical values of 3,579, 1,600, and 994 mAh g^{-1}, respectively) compared to intercalation-based compounds.[1, 36] Si anodes will be the focus here since they have received the most attention in the literature. Lithiation of Si is accompanied by an active material volumetric expansion > 300 %. Repeated expansion and contraction of Si during battery cycling results in capacity fade due to: (i) Si pulverization, (ii) Si electronic isolation, and (iii) formation of an unstable SEI layer.[37, 38] A schematic of these phenomena is shown in Figure 2.4. Several groups have demonstrated that when Si materials are reduced to the nanoscale, the stresses required to induce crack formation and propagation are significantly increased.[39-42] Consequently, lithiation-induced

stresses are insufficient to drive Si fracture for Si nanomaterials with characteristic lengths below ~ 150 nm (e.g., Si nanowires, nanoparticles, etc.).

Although Si pulverization can be eliminated through the use of nanoscale active materials, effective electrode designs which prevent Si electronic isolation and unstable SEI layer formation are yet to be developed. Si volumetric changes disrupt the electrode's conductivity network, leading to electronic isolation of individual Si particles (see Figure 2.4b). Furthermore, the SEI layer can crack during cycling, which re-exposes the electrode surface and leads to more SEI formation during subsequent cycles (see Figure 2.4c). This unstable SEI growth results in irreversible Li and electrolyte consumption, Si electronic isolation, and increased Li^+ transport path lengths between the Si particles and electrolyte.[37, 43] To address these issues, researchers have investigated several nanoscale Si anode designs, including: (i) Si thin films, (ii) Si nanowires, (iii) Si nanoparticle/polymer composites, and (iv) core/shell structures. A summary of each of these approaches is given below.

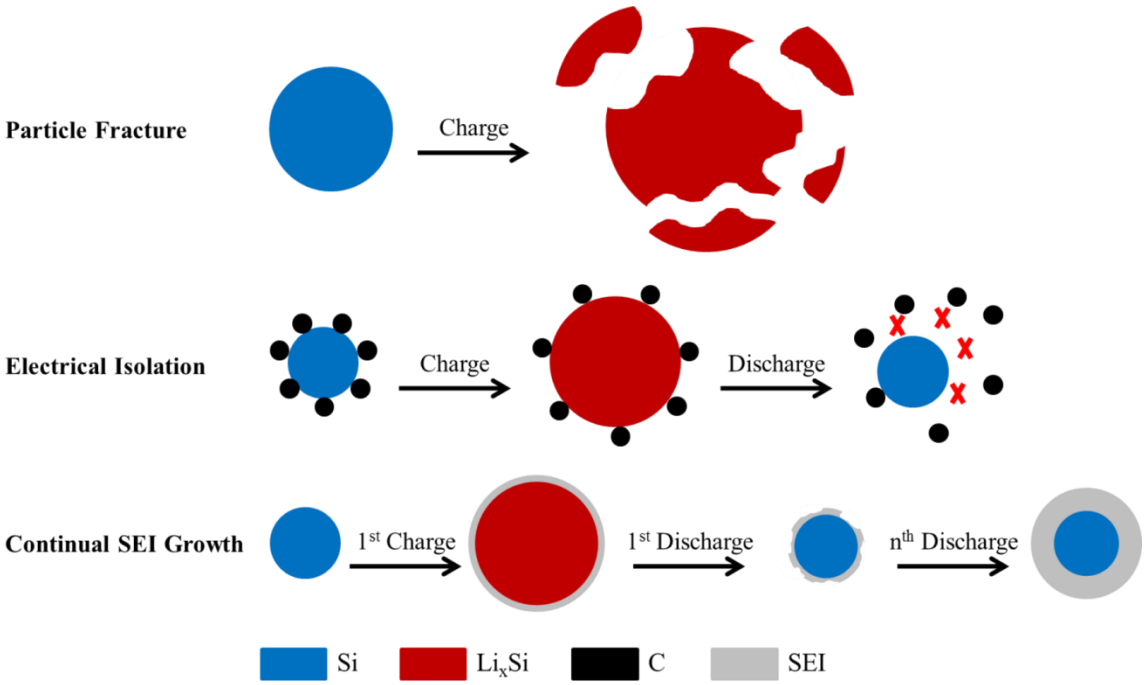

Figure 2.4. Si anode failure mechanisms: (a) material pulverization, (b) morphology and volume change of the entire Si electrode, and (c) continuous SEI growth. Image inspired by Wu and Cui.[37]

Si thin films are deposited onto a current collector using chemical or physical vapor deposition. High gravimetric capacities up to 3,500 mAh g^{-1} (equivalent to 3,500 mAh g_{Si}^{-1} since the anode is composed entirely of Si) have been demonstrated for Si thin film anodes, but these systems exhibit a tradeoff between electrode thickness and cycling stability. Films < 500 nm thick have been reported with stable capacities over several hundred cycles[44, 45], but Bourderau et al.[46] reported that a 1.2 µm thick film had poor performance (e.g., 80 % capacity loss after 20 cycles) due to pulverization of the electrode structure during cycling.

Similar to Si thin films, Si nanowire arrays can be grown using a vapor-liquid-solid method[47] or chemical vapor deposition.[48] Stable reversible capacities

up to 3,100 mAh g^{-1} (equivalent to 3,100 mAh g_{Si}^{-1}) have been reported for Si nanowires with diameters below 150 nm.[47] Furthermore, adequately spaced nanowires can expand and contract freely without inducing compressive stresses on one another.

Si-based slurry cast anodes containing Si nanoparticles, conductive carbon powder, and polymer binder have been widely investigated. Anodes prepared with binders which are electronically conductive[49-52] and/or contain functional groups that form hydrogen bonds with the SiO_x layer on the Si active material (e.g., poly(acrylic acid)[53], carboxymethyl cellulose[54], and alginate[55]) have been reported with gravimetric capacities exceeding 1,000 mAh g^{-1} (normalized to the overall electrode mass including conductive carbon and polymer binder) which are stable for several hundred cycles. In comparison, anodes prepared with a traditional PVDF binder exhibit severe capacity fade during cycling.[53, 56] Overall, these studies on slurry cast anodes demonstrate that strong interactions between the Si nanoparticles and binder are required to tolerate the volumetric changes of Si during battery operation.

Another Si anode design is the encapsulation of Si nanoparticles in a hollow shell that accommodates the volumetric changes of Si during cycling. A stable electrode microstructure can be obtained by appropriately sizing the void space to accommodate the swelling of Si without breaking the outer shell. Examples of these core-shell morphologies include yolk-shell particles[57, 58] and hollow nanofibers.[59-61] By eliminating direct contact between Si and the electrolyte, these structures allow a stable SEI layer to form. Furthermore, materials that utilize an electronically conductive shell ensure that Si remains electrochemically active during cycling. Core-shell anodes have

been reported with stable capacities exceeding 1,000 mAh g^{-1} (normalized with respect to the entire electrode's mass)

Despite the excellent performance of the various Si anode designs on a gravimetric basis, the electrodes often require expensive fabrication methods, and even more importantly, many studies on Si nanostructures utilized electrodes with low areal and/or volumetric capacities which limit their viability for practical battery applications. In general, nanostructured Si anodes with high areal capacities (> 1 mAh cm^{-2}) exhibit poor cycling stability due to the development of large lithiation-induced stresses throughout the electrodes.[62-65] Thus new anode designs which can tolerate Si volumetric changes while maintaining high gravimetric, areal, and volumetric capacities over many charge/discharge cycles must be developed.

2.3.2 Cathode Materials and Designs

$LiCoO_2$ is the most commonly used cathode in commercial LIBs, but development of cathodes with higher reversible capacities and/or operating potentials will ultimately lead to improvements in battery energy density.[66] A summary of previous work on LIB cathodes is provided in this section.

Cathode active materials that store Li through an intercalation reaction typically have a layered, spinel, or olivine crystal structure; the reversible capacity and operating potential of common intercalation compounds are listed in Table 2.1. Layered compounds have the general formula $LiMO_2$ where M is a transition metal, and Li is stored between parallel MO_2 layers. While $LiCoO_2$ is the most widely used commercial cathode, it is limited to a reversible capacity of 140 mAh $g_{LiCoO_2}^{-1}$ which is approximately

half its theoretical capacity (274 mAh $g_{LiCoO_2}^{-1}$) calculated based on complete utilization of Li in the structure. Extraction of more than half the Li from $LiCoO_2$ (i.e., $x > 0.50$ in $Li_{1-x}CoO_2$) results in poor cycling stability due to decomposition of the active material (e.g., oxygen evolution, cobalt dissolution in the electrolyte, and lattice shrinkage).[67] To address these issues, researchers have stabilized the $LiCoO_2$ structure by replacing some of the Co with other transition metals such as Ni and Mn.[68] Notably, $Li(Ni_{1/3}Mn_{1/3}Co_{1/3})O_2$ (NMC) containing a mixture of Co^{3+}, Ni^{2+}, and Mn^{4+} in the metal oxide layers has a high reversible capacity of 205 mAh g^{-1} at potentials ~ 3.9 V vs. Li/Li^+.[68, 69] Compared to layered compounds, Mn-based spinels (e.g., $LiMn_{3/2}Ni_{1/2}O_4$) have higher operating potentials up to 4.7 V vs. Li/Li^+, but these cathodes exhibit poor cycling stability due to oxygen loss from the active material and oxidation of the electrolyte which is electrochemically unstable at potentials > ~ 4.5 V vs. Li/Li^+.[1, 70] In contrast, olivine $LiFePO_4$ cathodes have excellent cycling stability and safety characteristics, although these advantageous are offset by a lower operating potential (3.4 V vs. Li/Li^+).

Table 2.1. Description of several active materials for cathodes which store Li through an intercalation reaction.[1, 70]

Active Material	Structure	Reversible Capacity (mAh g^{-1})*	Operating Potential (V vs. Li/Li^+)
$LiCoO_2$	Layered	140	3.9
$LiNi_{1/3}Mn_{1/3}Co_{1/3}O_2$	Layered	205	3.9
$LiNi_{0.8}Co_{0.15}Al_{0.05}O_2$	Layered	200	3.8
$LiMn_2O_4$	Spinel	125	4.0
$LiMn_{3/2}Ni_{1/2}O_4$	Spinel	130	4.7
$LiFePO_4$	Olivine	135	3.4

* Reversible capacity is normalized with respect to the active material mass.

The capacities listed in Table 2.1 are based on that of a conventional slurry cast cathode tested at a low C-rate (e.g., 0.1 C). To achieve high capacities at fast charge/discharge rates, many groups have developed nanostructured $LiCoO_2$, $LiMn_2O_4$, and $LiFePO_4$ cathodes where the active material is in the form of nanoparticles[71-73], nanowires[74, 75], nanorods[76], and thin films.[77-79] Xia et al.[74] reported on the fabrication of a $LiCoO_2$ nanowire array with excellent rate capabilities where the gravimetric capacity was 135 mAh g^{-1} at 0.1 C and 103 mAh g^{-1} at 10 C. In another study, Zhang et al.[72] prepared $LiMn_2O_4$ nanoparticles which had a high capacity of 124 mAh g^{-1} at 0.2 C and 84 % capacity retention at 10 C. Although these nanostructured cathodes exhibited good performance when normalized to the electrode mass, many studies used electrodes with low loadings and/or densities which limited their areal and volumetric capacities.

Compared to intercalation cathodes where reversible capacities range from 130 – 205 mAh g^{-1} (as listed in Table 2.1), sulfur cathodes have a much higher theoretical capacity of 1,672 mAh g^{-1} with an operating voltage of 2.2 V vs. Li/Li^+ (corresponding to an energy density of 3,678 Wh kg^{-1}).[1, 80-82] Sulfur stores Li through the multistep conversion process shown in equation 2.8.

$$S_8 \leftrightarrow Li_2S_8 \leftrightarrow Li_2S_6 \leftrightarrow Li_2S_4 \leftrightarrow Li_2S_2 \leftrightarrow Li_2S \quad (2.8)$$

Commercial adaptation of sulfur cathodes has been hindered by numerous drawbacks, including: (i) low electronic conductivity of elemental sulfur and its discharge products, (ii) large volumetric expansion/contraction of sulfur (~ 80 %) during battery operation, and (iii) dissolution of polysulfides in the electrolyte which causes loss of active material during cycling. To resolve these issues, researchers have developed various nanoscale

sulfur cathodes that accommodate the volumetric changes of sulfur while mitigating polysulfide dissolution during cycling. The most common methods to prepare sulfur cathodes include: (i) embedding sulfur in a porous carbon matrix and (ii) designing core-shell structures which prevent direct contact of sulfur with the liquid electrolyte. A summary of these approaches is given next.

Due to sulfur's low electronic conductivity, sulfur cathodes are often prepared by distributing sulfur throughout an electronically conductive carbon support, typically using sulfur melt, vapor, or solution infiltration techniques.[81] A number of different carbon substrates including carbon black, carbon nanotubes, and graphene have been investigated for sulfur cathodes. The pore size and surface functionality of these carbon supports are important factors that influence the sulfur loading and cathode cycling stability.[83-86] Ji et al.[83] showed that C-OH and C=O functional groups on graphene oxide immobilized polysulfides during cycling. They reported that sulfur/graphene oxide cathodes had high reversible capacities ranging from 950 – 1,400 mAh g_S^{-1} at 0.1 C with negligible capacity fade over 50 cycles. In another study, Qiu et al.[85] demonstrated that sulfur cathodes prepared with a nitrogen-doped graphene support had a high capacity of 1,167 mAh g_S^{-1} at 0.2 C and moderate stability with 44 % capacity retention after 2,000 cycles. Core-shell materials containing a sulfur core have also been shown to improve cathode cycling stability by preventing direct contact of sulfur with the electrolyte.[87-89] Wei Sei et al.[88] fabricated a yolk-shell structure in which sulfur was encapsulated by a hollow TiO_2 shell; this material had a high reversible capacity of 1,030 mAh g_S^{-1} at 0.5 C and stable performance over 1,000 cycles. Despite the recent advances on sulfur-based cathodes, these materials suffer from the same limitations as

many other nanoscale electrodes, namely expensive fabrication methods and poor areal and volumetric capacities.[90] Thus, future research should be directed towards the development of sulfur cathodes with high gravimetric, areal, and volumetric capacities using low-cost and scalable fabrication techniques.

2.4 Electrospinning Background

Electrospinning was first patented by John F. Cooley[91] in 1902, but the technique did not gain popularity for engineering applications until the pioneering work of Reneker and coworkers[92, 93] who electrospun more than 20 different polymers with fiber diameters ranging from 50 – 2,000 nm. Figure 2.5 shows a typical electrospinning setup consisting of a polymer solution or melt, syringe pump, single needle spinneret, high voltage power supply, and grounded collector. During electrospinning, surface charges are imparted on the solution as it exits the spinneret, and under the proper operating conditions, electrostatic repulsion forces exceed the solution's surface tension, resulting in formation of a Taylor cone. A charged polymer jet is emitted from this Taylor cone and accelerates toward the grounded collector. During this acceleration phase, solvent evaporates, and a whipping instability caused by charge repulsion elongates the fiber jet. Polymer chain entanglements prevent the jet from breaking into droplets during these steps, and a nonwoven fiber mat is collected on the grounded collector. Electrospinning conditions that influence the fiber mat properties include: (i) solution composition, (ii) solution flow rate, (iii) applied electric field strength, and (iv) atmospheric conditions (e.g., air temperature and relative humidity). In addition to neat polymer fibers, electrospinning can also be used to prepare composite nanofiber mats containing

functional nanoparticles (e.g., active material for LIB electrodes) distributed throughout a polymer binder.

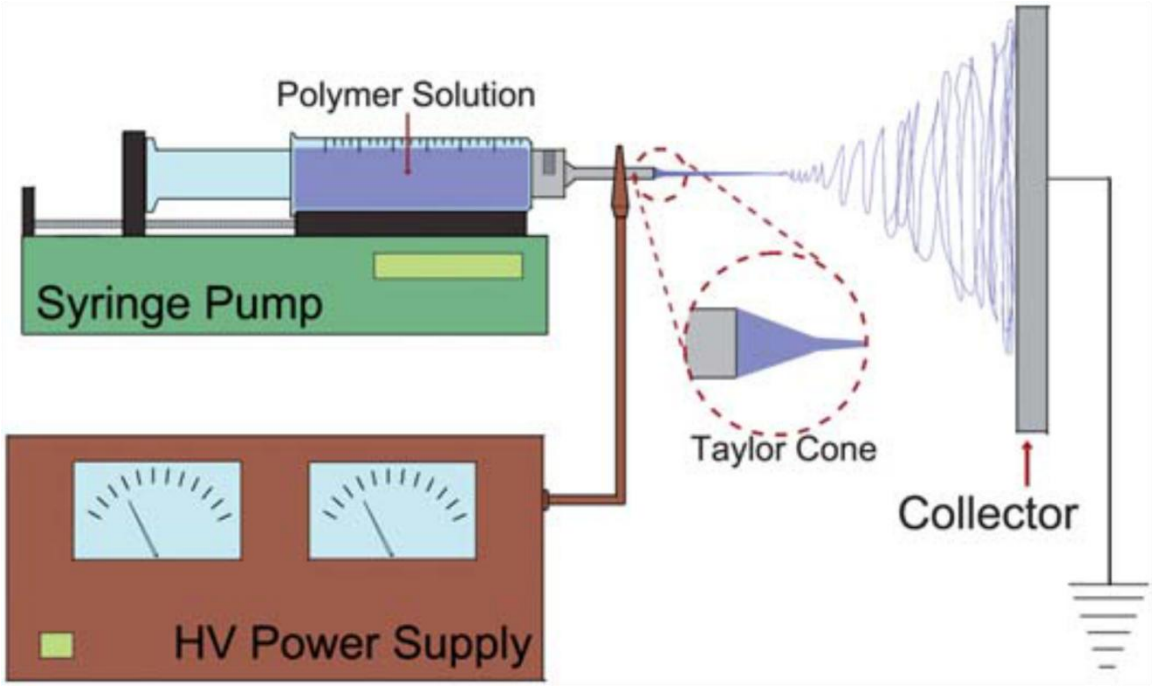

Figure 2.5. Schematic of a typical electrospinning setup. Image reproduced from Cavaliere et al.[94] with permission from The Royal Society of Chemistry.

2.5 Prior Research on Electrospun Fiber Mats as Li-ion Battery Electrodes

Previously reported electrospun LIB electrodes have been prepared by pyrolyzing polymeric fiber mats at high temperature to create a variety of electrodes including: (i) neat carbon nanofiber anodes and (ii) composite anodes and cathodes containing active material distributed throughout a carbon nanofiber mat. These electrospun nanofibers are typically evaluated as freestanding nanofiber mats or in slurry cast electrodes containing a mixture of crushed active material nanofibers, carbon powder, and polymer binder. The latter method is undesirable because the fiber structure is

destroyed during electrode processing. In comparison, freestanding fiber mat electrodes are attractive for LIB applications due to their interfiber void space and short Li^+ transport pathways. Previous work on electrospun LIB anodes and cathodes is summarized below.

Neat carbon nanofiber (CNF) anodes are prepared by pyrolyzing an electrospun polymer fiber mat at high temperature (typically 600 – 1,300 °C) in an inert atmosphere.[21] These CNF mats are often made from a poly(acrylonitrile) (PAN) precursor due to its high carbon yield (> 50 % after carbonization) and ease in electrospinning.[21] CNFs have been prepared from other polymer precursors, including poly(vinylpyrrolidone) (PVP)[95], poly(imide)[96], pitch[97], and lignin.[98] CNF mats with a high surface area (e.g., exceeding 1,000 $m^2 g^{-1}$) have been prepared by using additional chemical activation steps[99, 100] or by adding pore formers to the electrospun polymer fiber mat.[101-103] Ji et al.[104] reported on the preparation and characterization of the electrospun CNF mats shown in Figure 2.6. When used as a freestanding anode in a LIB, the CNFs had a high lithium capacity of 621 mAh g^{-1} at 0.13 C and good rate capabilities, with 345 mAh g^{-1} at 0.54 C. The CNF mat also exhibited good cycling stability with 73 % capacity retention after 50 cycles. Post-mortem analyses of these anodes showed the fiber structure and interfiber void space were preserved during cycling.

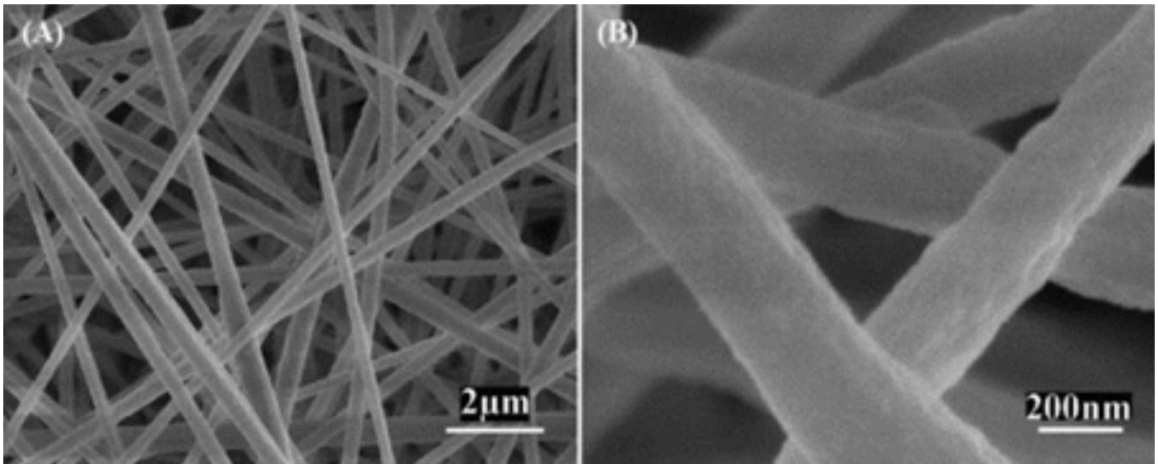

Figure 2.6. CNF mat prepared from a PAN/poly(pyrrole) (PPy) blend where the PAN/PPy weight ratio was 85/15. Image adapted from Ji et al.[104] with permission from Elsevier.

Electrospinning can also be used to prepare composite carbon nanofiber anodes and cathodes containing a Li storage active material. These electrodes are prepared by either: (i) electrospinning a solution containing Li storage nanoparticles and a polymeric carbon precursor or (ii) forming the active material *in-situ* after electrospinning via sol-gel or hydrothermal reactions. Table 2.2 summarizes the performance of such carbon nanofiber anodes and cathodes which store Li via intercalation. In general, the performance of these materials is very good and demonstrates that electrospinning can be used to prepare a wide range of nanofiber carbon composite electrodes for LIBs.

Table 2.2. Summary of previously reported electrospun carbon nanofiber mat anodes and cathodes for LIBs.

Active Material	Carbon Precursor	Electrochemical Performance	
		Capacity (mAh g^{-1})*	C-Rate
$Li_4Ti_5O_{12}$ Anode[105]	PVP	161	0.5
TiO_2 Anode[106]	PVP	86	0.1
$LiCoO_2$ Cathode[107]	PVP	85	1.5
Si Anode[108]	PAN	926	0.05
$LiFe_{0.5}Mn_{0.5}PO_4$ Cathode[109]	PVP	125	0.05
$LiFePO_4$ Cathode[110]	PAN	128	0.5
S Cathode[111]	PAN	354	0.03

* Capacity is normalized with respect to the total electrode mass

Electrospun CNF mats have also been used to prepare high capacity anodes (e.g., Si, Sn, and Ge) and cathodes (e.g., S) which experience large volumetric changes during battery operation (as discussed in Section 2.3). Compared to slurry cast electrodes where pore structure cannot be easily controlled, the interfiber voids of electrospun mats can accommodate the active material's volumetric changes to achieve good battery cycle life.[112, 113] Previous studies on high capacity electrospun anodes have been directed towards pyrolyzing polymer fibers containing active material nanoparticles such as Si[59, 108, 114-118], Sn[119-123], and Ge.[124-126] These nanofiber mats exhibited high gravimetric capacities (e.g., 800 – 1,600 mAh g^{-1}, normalized to the mass of the entire electrode) and stable performance over 30 – 100 cycles. Similarly, Zeng et al.[111] reported that a sulfur cathode prepared from an electrospun CNF mat had a stable capacity of 354 mAh g^{-1} (normalized to the overall electrode mass) over 100 cycles at 0.03 C and good rate capabilities with 216 mAh g^{-1} at 0.6 C.

While previously reported electrospun LIB electrodes have shown encouraging performance, these materials are limited in several ways. Low material loadings

corresponding to areal capacities < 1 mAh cm^{-2} were used in many reports on electrospun carbon nanofiber-based electrodes, and inspection of the SEM images in these reports indicates the fiber volume fraction of the nanofiber mats was < 0.25 which is far too low for practical battery applications. Furthermore, since the polymer binder is removed from the fibers during pyrolysis, these fiber mats cannot utilize high performance binders including electronically conductive polymers[49-52] and polymers such as poly(acrylic acid)[53], carboxymethyl cellulose[54], and alginate[55] which bind strongly to the active material. On the other hand, the creation of carbon fibers during pyrolysis means that electronically conductive carbon particles do not need to be added to the electrode.

2.6 Project Objectives

To improve upon the performance of previously reported LIB electrodes, this dissertation details the preparation and characterization of fiber mat LIB anodes and cathodes prepared using particle/polymer electrospinning, a technique originally developed by Pintauro and coworkers for fuel cell electrodes.[127-130] Compared to conventional slurry cast electrodes, particle/polymer nanofiber mats have a large electrode/electrolyte interfacial area, short Li^+ transport pathways, and intra and interfiber voids to ensure good electrolyte penetration throughout the electrode. These unique properties allow rapid Li transport between the electrolyte and active material nanoparticles, and thus electrospun mats should have high capacities at fast charge/discharge rates. Furthermore, unlike previously reported electrospun electrodes, particle/polymer fiber mats are fabricated at room temperature which preserves the

polymer binder, allowing the technique to incorporate new active materials and binders as they are developed. Electrospun particle/polymer fibers can also be made porous with a binder that absorbs electrolyte, ensuring that Li^+ ions have access to the active material nanoparticles throughout the electrode. Finally, the presence of the polymer binder allows the mats to be compacted under high pressure without fracturing, and thus thick, densely packed nanofiber mats can be prepared to achieve high gravimetric, areal, and volumetric capacities. When considered collectively, these advantages provide a compelling rationale for using particle/polymer electrospinning to prepare high performance LIB anodes and cathodes.

2.7 References

[1] N. Nitta, F. Wu, J. T. Lee, G. Yushin, *Mater. Today* **2015**, *18*, 252.
[2] D. I. Iermakova, R. Dugas, M. R. Palacín, A. Ponrouch, *J. Electrochem. Soc.* **2015**, *162*, A7060.
[3] N. Nitta, G. Yushin, *Part. Part. Syst. Char.* **2014**, *31*, 317.
[4] J. B. Goodenough, Y. Kim, *Chem. Mater.* **2010**, *22*, 587.
[5] J. Towada, T. Karouji, H. Sato, Y. Kadoma, K. Shimada, K. Ui, *J. Power Sources* **2015**, *275*, 50.
[6] V. Aravindan, Y.-S. Lee, S. Madhavi, *Adv. Energy Mater.* **2015**, *5*, 1402225.
[7] J. B. Goodenough, *Acc. Chem. Res.* **2013**, *46*, 1053.
[8] Y. Liu, Y. Yang, *J. Nanomater.* **2016**, *2016*, 1.
[9] A. R. Kamali, D. J. Fray, *J. New Mater. Electrochem. Syst.* **2010**, *13*, 147.
[10] S. Goriparti, E. Miele, F. De Angelis, E. Di Fabrizio, R. Proietti Zaccaria, C. Capiglia, *J. Power Sources* **2014**, *257*, 421.
[11] S. R. Sivakkumar, J. Y. Nerkar, A. G. Pandolfo, *Electrochim. Acta* **2010**, *55*, 3330.
[12] H. Fujimoto, K. Tokumitsu, A. Mabuchi, N. Chinnasamy, T. Kasuh, *J. Power Sources* **2010**, *195*, 7452.
[13] J. Yang, X.-y. Zhou, J. Li, Y.-l. Zou, J.-j. Tang, *Mater. Chem. Phys.* **2012**, *135*, 445.
[14] J. R. Dahn, T. Zheng, Y. Liu, J. S. Xue, *Science* **1995**, *270*, 590.
[15] E. Buiel, J. R. Dahn, *Electrochim. Acta* **1999**, *45*, 121.
[16] J.-H. Kim, J.-S. Kim, Y.-G. Lim, J.-G. Lee, Y.-J. Kim, *J. Power Sources* **2011**, *196*, 10490.
[17] J. Zhu, D. Yang, Z. Yin, Q. Yan, H. Zhang, *Small* **2014**, *10*, 3480.
[18] D. T. Welna, L. Qu, B. E. Taylor, L. Dai, M. F. Durstock, *J. Power Sources* **2011**, *196*, 1455.
[19] M. J. Ganter, R. A. DiLeo, C. M. Schauerman, R. E. Rogers, R. P. Raffaelle, B. J. Landi, *Electrochim. Acta* **2011**, *56*, 7272.
[20] J. E. Trevey, K. W. Rason, C. R. Stoldt, S.-H. Lee, *Electrochem. Solid-State Lett.* **2010**, *13*, A154.
[21] B. Zhang, F. Kang, J.-M. Tarascon, J.-K. Kim, *Prog. Mater Sci.* **2016**, *76*, 319.
[22] X. Su, Q. Wu, X. Zhan, J. Wu, S. Wei, Z. Guo, *J. Mater. Sci.* **2011**, *47*, 2519.
[23] C. Jiang, J. Zhang, *J. Mater. Sci. Technol.* **2013**, *29*, 97.
[24] T.-F. Yi, L.-J. Jiang, J. Shu, C.-B. Yue, R.-S. Zhu, H.-B. Qiao, *J. Phys. Chem. Solids* **2010**, *71*, 1236.
[25] G.-N. Zhu, Y.-G. Wang, Y.-Y. Xia, *Energy Environ. Sci.* **2012**, *5*, 6652.
[26] T. Ohzuku, A. Ueda, N. Yamamoto, *J. Electrochem. Soc.* **1995**, *142*, 1431.
[27] W. Wang, M. Tian, A. Abdulagatov, S. M. George, Y. C. Lee, R. Yang, *Nano Lett.* **2012**, *12*, 655.
[28] D. Guan, J. Li, X. Gao, C. Yuan, *J. Power Sources* **2014**, *246*, 305.
[29] G. F. Ortiz, I. Hanzu, P. Lavela, J. L. Tirado, P. Knauth, T. Djenizian, *J. Mater. Chem.* **2010**, *20*, 4041.
[30] T. Yiping, T. Xiaoxu, H. Guangya, Z. Guoqu, *Electrochim. Acta* **2014**, *117*, 172.

[31] W. Wei, G. Oltean, C.-W. Tai, K. Edström, F. Björefors, L. Nyholm, *J. Mater. Chem. A* **2013**, *1*, 8160.
[32] W. Xiong, Y. D. Wang, H. Xia, *Materials Technology* **2013**, *28*, 260.
[33] J. Kim, J. Cho, *Electrochem. Solid-State Lett.* **2007**, *10*, A81.
[34] J. Liu, K. Song, P. A. van Aken, J. Maier, Y. Yu, *Nano Lett.* **2014**, *14*, 2597.
[35] L. Shen, E. Uchaker, X. Zhang, G. Cao, *Adv. Mater.* **2012**, *24*, 6502.
[36] H. Tian, F. Xin, X. Wang, W. He, W. Han, *J. Materiomics* **2015**, *1*, 153.
[37] H. Wu, Y. Cui, *Nano Today* **2012**, *7*, 414.
[38] J. Li, N. J. Dudney, J. Nanda, C. Liang, *ACS Appl. Mater. Interfaces* **2014**, *6*, 10083.
[39] I. Ryu, J. W. Choi, Y. Cui, W. D. Nix, *J. Mech. Phys. Solids* **2011**, *59*, 1717.
[40] X. H. Liu, L. Zhong, S. Huang, S. X. Mao, T. Zhu, J. Y. Huang, *ACS Nano* **2012**, *6*, 1522.
[41] U. Kasavajjula, C. Wang, A. J. Appleby, *J. Power Sources* **2007**, *163*, 1003.
[42] M. W. Verbrugge, Y.-T. Cheng, *ECS Transactions* **2008**, *16*, 127.
[43] H. Wu, G. Chan, J. W. Choi, I. Ryu, Y. Yao, M. T. McDowell, S. W. Lee, A. Jackson, Y. Yang, L. Hu, Y. Cui, *Nat. Nanotechnol.* **2012**, *7*.
[44] S. R. Gowda, V. Pushparaj, S. Herle, G. Girishkumar, J. G. Gordon, H. Gullapalli, X. Zhan, P. M. Ajayan, A. L. Reddy, *Nano Lett* **2012**, *12*, 6060.
[45] S. Ohara, J. Suzuki, K. Sekine, T. Takamura, *J. Power Sources* **2004**, *136*, 303.
[46] S. Bourderau, T. Brousse, D. M. Schleich, *J. Power Sources* **1999**, *81-82*, 233.
[47] C. K. Chan, H. Peng, G. Liu, K. McIlwrath, X. F. Zhang, R. A. Huggins, Y. Cui, *Nat. Nanotechnol.* **2008**, *3*, 31.
[48] L. Hu, H. Wu, S. S. Hong, L. Cui, J. R. McDonough, S. Bohy, Y. Cui, *Chem. Commun.* **2011**, *47*, 367.
[49] G. Liu, S. Xun, N. Vukmirovic, X. Song, P. Olalde-Velasco, H. Zheng, V. S. Battaglia, L. Wang, W. Yang, *Adv. Mater.* **2011**, *23*, 4679.
[50] S. J. Park, H. Zhao, G. Ai, C. Wang, X. Song, N. Yuca, V. S. Battaglia, W. Yang, G. Liu, *J. Am. Chem. Soc.* **2015**, *137*, 2565.
[51] H. Zhao, Z. Wang, P. Lu, M. Jiang, F. Shi, X. Song, Z. Zheng, X. Zhou, Y. Fu, G. Abdelbast, X. Xiao, Z. Liu, V. S. Battaglia, K. Zaghib, G. Liu, *Nano Lett.* **2014**, *14*, 6704.
[52] M. Wu, X. Song, X. Liu, V. Battaglia, W. Yang, G. Liu, *J. Mater. Chem. A* **2015**, *3*, 3651.
[53] A. Magasinski, B. Zdyrko, I. Kovalenko, B. Hertzberg, R. Burtovyy, C. F. Huebner, T. F. Fuller, I. Luzinov, G. Yushin, *ACS Appl. Mater. Interfaces* **2010**, *2*, 3004.
[54] J. S. Bridel, T. Azais, M. Morcrette, J. M. Tarascon, D. Larcher, *Chem. Mater.* **2010**, *22*, 1229.
[55] I. Kovalenko, B. Zdyrko, A. Magasinski, B. Hertzberg, Z. Milicev, R. Burtovyy, I. Luzinov, G. Yushin, *Science* **2011**, *334*, 75.
[56] D. M. Piper, J. J. Travis, M. Young, S. B. Son, S. C. Kim, K. H. Oh, S. M. George, C. Ban, S. H. Lee, *Adv. Mater.* **2014**, *26*, 1596.
[57] N. Liu, H. Wu, M. T. McDowell, Y. Yao, C. Wang, Y. Cui, *Nano Lett.* **2012**, *12*, 3315.

[58] N. Liu, Z. Lu, J. Zhao, M. T. McDowell, H. W. Lee, W. Zhao, Y. Cui, *Nat. Nanotechnol.* **2014**, *9*, 187.
[59] H. Wu, G. Zheng, N. Liu, T. J. Carney, Y. Yang, Y. Cui, *Nano Lett.* **2012**, *12*, 904.
[60] B. Hertzberg, A. Alexeev, G. Yushin, *J. Am. Chem. Soc.* **2010**, *132*, 8548.
[61] J. Wang, Y. Yu, L. Gu, C. Wang, K. Tang, J. Maier, *Nanoscale* **2013**, *5*, 2647.
[62] L.-F. Cui, L. Hu, J. W. Choi, Y. Cui, *ACS Nano* **2010**, *4*, 3671.
[63] J. Ji, H. Ji, L. L. Zhang, X. Zhao, X. Bai, X. Fan, F. Zhang, R. S. Ruoff, *Adv. Mater.* **2013**, *25*, 4673.
[64] G.-H. Lee, S. Lee, C. W. Lee, C. Choi, D.-W. Kim, *J. Mater. Chem. A* **2016**, *4*, 1060.
[65] J. P. Maranchi, A. F. Hepp, P. N. Kumta, *Electrochem. Solid-State Lett.* **2003**, *6*, A198.
[66] K. Zaghib, A. Guerfi, P. Hovington, A. Vijh, M. Trudeau, A. Mauger, J. B. Goodenough, C. M. Julien, *J. Power Sources* **2013**, *232*, 357.
[67] A. Kraytsberg, Y. Ein-Eli, *Adv. Energy Mater.* **2012**, *2*, 922.
[68] P. Rozier, J. M. Tarascon, *J. Electrochem. Soc.* **2015**, *162*, A2490.
[69] C. M. Julien, A. Mauger, K. Zaghib, H. Groult, *Inorganics* **2014**, *2*, 132.
[70] D. Liu, W. Zhu, J. Trottier, C. Gagnon, F. Barray, A. Guerfi, A. Mauger, H. Groult, C. M. Julien, J. B. Goodenough, K. Zaghib, *RSC Adv.* **2014**, *4*, 154.
[71] C.-H. Lu, H.-H. Chang, Y.-K. Lin, *Ceram. Int.* **2004**, *30*, 1641.
[72] Q. Zhang, J. Mei, X. Wang, J. Guo, F. Tang, W. Lu, *J. Alloys Compd.* **2014**, *617*, 326.
[73] Y. Zhang, H. Zhang, X. Li, H. Xu, Y. Wang, *Nanotechnology* **2016**, *27*, 155401.
[74] H. Xia, Y. Wan, W. Assenmacher, W. Mader, G. Yuan, L. Lu, *NPG Asia Materials* **2014**, *6*, e126.
[75] W. Sun, H. Liu, Y. Liu, G. Bai, W. Liu, S. Guo, X. Z. Zhao, *Nanoscale* **2015**, *7*, 13173.
[76] F. Teng, S. Santhanagopalan, R. Lemmens, X. Geng, P. Patel, D. D. Meng, *Solid State Sciences* **2010**, *12*, 952.
[77] S. Tintignac, R. Baddour-Hadjean, J. P. Pereira-Ramos, R. Salot, *Electrochim. Acta* **2014**, *146*, 472.
[78] R. A. Davoglio, K. Irikura, S. R. Biaggio, N. Bocchi, R. C. Rocha-Filho, *J. Solid State Electrochem.* **2016**, *20*, 2019.
[79] A. Bünting, S. Uhlenbruck, D. Sebold, H. P. Buchkremer, R. Vaßen, *ACS Appl. Mater. Interfaces* **2015**, *7*, 22594.
[80] L. Chen, L. L. Shaw, *J. Power Sources* **2014**, *267*, 770.
[81] L. Borchardt, M. Oschatz, S. Kaskel, *Chemistry* **2016**, *22*, 7324.
[82] S.-K. Lee, Y. J. Lee, Y.-K. Sun, *J. Power Sources* **2016**, *323*, 174.
[83] L. Ji, M. Rao, H. Zheng, L. Zhang, Y. Li, W. Duan, J. Guo, E. J. Cairns, Y. Zhang, *J. Am. Chem. Soc.* **2011**, *133*, 18522.
[84] G. Zhou, L.-C. Yin, D.-W. Wang, L. Li, S. Pei, I. R. Gentle, F. Li, H.-M. Cheng, *ACS Nano* **2013**, *7*, 5367.
[85] Y. Qiu, W. Li, W. Zhao, G. Li, Y. Hou, M. Liu, L. Zhou, F. Ye, H. Li, Z. Wei, S. Yang, W. Duan, Y. Ye, J. Guo, Y. Zhang, *Nano Lett.* **2014**, *14*, 4821.

[86] Z. Wang, Y. Dong, H. Li, Z. Zhao, H. B. Wu, C. Hao, S. Liu, J. Qiu, X. W. Lou, *Nat. Commun.* **2014**, *5*, 5002.
[87] F. Wu, J. Chen, R. Chen, S. Wu, L. Li, S. Chen, T. Zhao, *J. Phys. Chem. C* **2011**, *115*, 6057.
[88] Z. Wei Seh, W. Li, J. J. Cha, G. Zheng, Y. Yang, M. T. McDowell, P. C. Hsu, Y. Cui, *Nat. Commun.* **2013**, *4*, 1331.
[89] X. Liang, L. F. Nazar, *ACS Nano* **2016**, *10*, 4192.
[90] N. Ding, S. W. Chien, T. S. A. Hor, Z. Liu, Y. Zong, *J. Power Sources* **2014**, *269*, 111.
[91] J. F. Cooley, *United States of America Patent 692,631*, 1902.
[92] J. Doshi, D. H. Reneker, *J. Electrostat.* **1995**, *35*, 151.
[93] D. H. Reneker, I. Chun, *Nanotechnology* **1996**, *7*, 216.
[94] S. Cavaliere, S. Subianto, I. Savych, D. J. Jones, J. Rozière, *Energy Environ. Sci.* **2011**, *4*, 4761.
[95] P. Wang, D. Zhang, F. Ma, Y. Ou, Q. N. Chen, S. Xie, J. Li, *Nanoscale* **2012**, *4*, 7199.
[96] N. T. Xuyen, E. J. Ra, H.-Z. Geng, K. K. Kim, K. H. An, Y. H. Lee, *J. Phys. Chem. B* **2007**, *111*, 11350.
[97] S. H. Park, C. Kim, Y. O. Choi, K. S. Yang, *Carbon* **2003**, *41*, 2655.
[98] S. X. Wang, L. Yang, L. P. Stubbs, X. Li, C. He, *ACS Appl. Mater. Interfaces* **2013**, *5*, 12275.
[99] Y. Chen, X. Li, K. Park, J. Song, J. Hong, L. Zhou, Y. W. Mai, H. Huang, J. B. Goodenough, *J. Am. Chem. Soc.* **2013**, *135*, 16280.
[100] L. Ji, X. Zhang, *Electrochem. Commun.* **2009**, *11*, 684.
[101] D. Nan, J.-G. Wang, Z.-H. Huang, L. Wang, W. Shen, F. Kang, *Electrochem. Commun.* **2013**, *34*, 52.
[102] L. Ji, X. Zhang, *Nanotechnology* **2009**, *20*, 155705.
[103] S.-H. Park, B.-K. Kim, W.-J. Lee, *J. Power Sources* **2013**, *239*, 122.
[104] L. Ji, Y. Yao, O. Toprakci, Z. Lin, Y. Liang, Q. Shi, A. J. Medford, C. R. Millns, X. Zhang, *J. Power Sources* **2010**, *195*, 2050.
[105] H. Xu, X. Hu, Y. Sun, W. Luo, C. Chen, Y. Liu, Y. Huang, *Nano Energy* **2014**, *10*, 163.
[106] R. Qing, W. Sigmund, *Ceram. Int.* **2014**, *40*, 5665.
[107] H.-W. Lu, L. Yu, W. Zeng, Y.-S. Li, Z.-W. Fu, *Electrochem. Solid-State Lett.* **2008**, *11*, A140.
[108] K. Fu, L. Xue, O. Yildiz, S. Li, H. Lee, Y. Li, G. Xu, L. Zhou, P. D. Bradford, X. Zhang, *Nano Energy* **2013**, *2*, 976.
[109] R. von Hagen, H. Lorrmann, K.-C. Möller, S. Mathur, *Adv. Energy Mater.* **2012**, *2*, 553.
[110] C. Zhang, L. Yao, Y. Qiu, *J. Appl. Polym. Sci.* **2016**, *133*, 43001.
[111] L. Zeng, Y. Jiang, J. Xu, M. Wang, W. Li, Y. Yu, *Nanoscale* **2015**, *7*, 10940.
[112] L. Liu, J. Lyu, T. Li, T. Zhao, *Nanoscale* **2016**, *8*, 701.
[113] H.-G. Wang, S. Yuan, D.-L. Ma, X.-B. Zhang, J.-M. Yan, *Energy Environ. Sci.* **2015**, *8*, 1660.
[114] Y. Liu, K. Huang, Y. Fan, Q. Zhang, F. Sun, T. Gao, Z. Wang, J. Zhong, *Electrochim. Acta* **2013**, *102*, 246.

[115] L. Ji, X. Zhang, *Energy Environ. Sci.* **2010**, *3*, 124.
[116] L. Xue, K. Fu, Y. Li, G. Xu, Y. Lu, S. Zhang, O. Toprakci, X. Zhang, *Nano Energy* **2013**, *2*, 361.
[117] Y. Xu, Y. Zhu, F. Han, C. Luo, C. Wang, *Adv. Energy Mater.* **2015**, *5*, 1400753.
[118] Z. Favors, H. H. Bay, Z. Mutlu, K. Ahmed, R. Ionescu, R. Ye, M. Ozkan, C. S. Ozkan, *Sci. Rep.* **2015**, *5*, 8246.
[119] Y. Yu, Q. Yang, D. Teng, X. Yang, S. Ryu, *Electrochem. Commun.* **2010**, *12*, 1187.
[120] I. Meschini, F. Nobili, M. Mancini, R. Marassi, R. Tossici, A. Savoini, M. L. Focarete, F. Croce, *J. Power Sources* **2013**, *226*, 241.
[121] F. Nobili, I. Meschini, M. Mancini, R. Tossici, R. Marassi, F. Croce, *Electrochim. Acta* **2013**, *107*, 85.
[122] X. Xia, X. Wang, H. Zhou, X. Niu, L. Xue, X. Zhang, Q. Wei, *Electrochim. Acta* **2014**, *121*, 345.
[123] S. Kim, J.-H. Choi, D.-S. Lim, J.-H. Lee, I.-D. Kim, *J. Electroceram.* **2014**, *32*, 261.
[124] W. Wang, Y. Xiao, X. Wang, B. Liu, M. Cao, *ChemSusChem* **2014**, *7*, 2914.
[125] W. Li, Z. Yang, J. Cheng, X. Zhong, L. Gu, Y. Yu, *Nanoscale* **2014**, *6*, 4532.
[126] Y. W. Lee, D. M. Kim, S. J. Kim, M. C. Kim, H. S. Choe, K. H. Lee, J. I. Sohn, S. N. Cha, J. M. Kim, K. W. Park, *ACS Appl. Mater. Interfaces* **2016**, *8*, 7022.
[127] W. Zhang, P. N. Pintauro, *ChemSusChem* **2011**, *4*, 1753.
[128] M. Brodt, R. Wycisk, P. N. Pintauro, *J. Electrochem. Soc.* **2013**, *160*, F744.
[129] M. Brodt, T. Han, N. Dale, E. Niangar, R. Wycisk, P. Pintauro, *J. Electrochem. Soc.* **2014**, *162*, F84.
[130] M. Brodt, R. Wycisk, N. Dale, P. Pintauro, *J. Electrochem. Soc.* **2016**, *163*, F401.

CHAPTER III

ELECTROSPUN TITANIA-BASED FIBERS FOR HIGH AREAL CAPACITY LI-ION BATTERY ANODES

Adapted from E. C. Self, R. Wycisk, P. N. Pintauro, *J. Power Sources* **2015**, *282*, 187 with permission from Elsevier.

3.1 Introduction

Despite widespread commercial success, Li-ion battery (LIB) technologies require significant improvements to keep pace with increasing energy demands.[1] The scientific community has dedicated considerable time and resources to develop superior LIB materials, most notably replacements for the graphite anode. Currently, LIB anode performance is limited in three primary ways: (i) lithium capacity, (ii) cycle life, and (iii) rate capabilities. To address the Li capacity problem, Li-alloying materials such as silicon have been examined with some success. In these studies, high capacities (near the theoretical limit of 3,579 mAh g_{Si}^{-1}) were obtained but at the expense of reduced lifetimes due to Si volume changes during charge/discharge cycling.[2] The use of nanostructured Si anodes in the form of nanowires, nanotubes, nanofibers, and nanoparticles improved cycle life and rate capabilities, but these nanomaterials often have low tap densities, resulting in poor volumetric and areal capacities.[3-17]

Titania has gained attention as a potential LIB anode material for two primary reasons: (i) TiO_2 anodes exhibit outstanding lifetimes due to limited volume changes

during battery cycling (< 4 % for anatase TiO_2 vs. ~ 8 % for graphite) and (ii) the high operating potential of a TiO_2 anode (1.5 – 1.8 V vs. Li/Li^+) minimizes safety issues associated with Li dendrite formation and solid-electrolyte interface (SEI) formation encountered with graphite materials.[18-20] These advantages are counterbalanced by the low lithium capacity of titania. The lithiation/delithiation reaction with TiO_2 is shown in equation 3.1.

$$TiO_2 + xLi^+ + xe^- \leftrightarrow Li_xTiO_2 \quad (3.1)$$

Assuming complete lithiation (x = 1), titania's theoretical capacity is 335 mAh g^{-1}, but attainable capacities are generally only ~ 168 mAh g^{-1} (x = 0.50) due to strong repulsive forces among Li^+ ions.[18] In comparison, the operational capacity of graphite is ~ 340 mAh g^{-1}. Another drawback of TiO_2 anodes is their poor rate capabilities arising from poor electronic conductivity (~ $1x10^{-12}$ S m^{-1}) and a low lithium diffusion coefficient (~ $1x10^{-15}$ cm^2 s^{-1}).[18, 21] Some improvements in rate capabilities have been attained when TiO_2 is fabricated into nanowires and nanotubes, but these approaches are limited to low areal capacities (< 1 mAh cm^{-2}).[22-26] For example, Wei et al.[26] tested a TiO_2 nanotube anode and reported excellent rate capabilities with ~ 45 % capacity retention at 5 C, but the areal capacity (0.6 mAh cm^{-2}) was about 5-times lower than that of graphite anodes (2.5 – 3.5 mAh cm^{-2}). To effectively compete with commercial graphite materials, titania anodes with areal capacities ≥ 3 mAh cm^{-2} at fast charge/discharge rates (≥ 2 C) must be developed.[27]

Battery researchers often focus on an electrode's gravimetric and volumetric capacities. While these properties are important for weight- and volume-sensitive applications, they do not always provide an indication of an electrode's usefulness for

practical batteries. For example, Wu et al.[6] prepared double-walled Si nanotube anodes that exhibited outstanding gravimetric and volumetric capacities of 1,780 mAh g^{-1} and 2,000 mAh cm^{-3}, respectively. Despite these impressive material-normalized metrics, the anode was limited to loadings < 0.1 mg cm^{-2}, corresponding to an areal capacity of only 0.178 mAh cm^{-2} (approximately 17 times lower than commercial graphite anodes). Unless material loading is reported separately, a mass- or volume-normalized capacity conceals the electrode's areal loading (i.e., mg cm^{-2}), an important parameter which directly impacts performance. Especially for anodes containing large-volume changing hosts (e.g., Si), simply increasing the material loading does not always provide good performance and a practical areal capacity. An electrode may perform well at a low areal loading but becomes less useful at higher loadings due to large internal stresses and/or transport resistances (i.e., low Li^+ and/or electronic conductivity).[27] Furthermore, a low areal loading increases the amount of inactive components (i.e., current collectors, separators, cell packaging, etc.) for full cell construction. Nitta and Yushin recently addressed these concerns and emphasized that areal capacity is an important metric for practical battery electrodes.[27] New electrode architectures should be prepared with areal capacities comparable to commercial graphite anodes (2.5 – 3.5 mAh cm^{-2}) to assess their practicality for consumer devices.

3D porous anodes show promise for achieving both high areal capacities and short recharge times. Complete electrolyte penetration throughout a porous anode results in good active material utilization even at high loadings. For example, Hu et al.[28] prepared 600 μm thick $Li_5Ti_4O_{12}$ anodes using a porous textile substrate. They reported high areal capacities but only at slow discharge rates (e.g., ~ 27 mAh cm^{-2} at ~ 0.06 C). In addition

to high areal capacity, Vu et al.[29] propose that a 3D porous network can enhance electrode rate capabilities. Previous studies suggest that conventional electrodes are limited by Li^+ concentration polarization under fast charging currents.[30, 31] A 3D porous structure addresses this limitation by utilizing a large electrode/electrolyte interfacial area to limit Li^+ depletion near the electrode during charging. This 3D structure enhances Li^+ transport within the pores and thus improves the electrode's rate capabilities.

Despite the promising performance of 3D porous LIB anodes, no reports to date have achieved high areal capacities ($\geq$ 3 mAh cm^{-2}) at fast charge/discharge rates ($\geq$ 2 C). To address these issues, the present study investigates the fabrication and use of electrospun fibrous anodes containing TiO_2 and carbon nanoparticles with a poly(acrylic acid) binder. Electrolyte penetration throughout the porous mat and short Li^+ transport pathways between the electrolyte and TiO_2 nanoparticles in the radial fiber direction allow for production of thick electrodes with a high areal capacity and excellent rate capabilities.

A key innovative aspect of the present study is the use of electrospun particle/polymer fiber mat anodes in a LIB. Electrospinning has been shown to be an inexpensive and scalable technique for fabricating high performance nanofibrous energy storage and conversion electrodes. For LIB applications, all prior electrospinning studies have been directed towards the pyrolysis of polymer fibers to create an electronically conductive carbon-based nanofiber network containing a Li host.[9, 11, 32-35] Zhang and coworkers,[9, 11] for example, prepared and characterized anodes containing silicon nanoparticles in carbon nanofibers. These materials achieved capacities up to 850 mAh g^{-1}, but neither areal capacity nor rate capabilities were investigated. Similarly,

Zhao et al.[36] electrospun a TiO_2 nanoparticle/carbon nanofiber anode which exhibited stable capacities at charge/discharge rates up to 30 C, but the authors did not discuss areal capacity or material loading effects.

The approach taken in the present study builds upon the work of Pintauro and coworkers who used particle/polymer electrospinning to fabricate high performance oxygen reduction Pt/C nanofiber cathodes for hydrogen/air fuel cells.[37, 38] In a manner similar to the fuel cell electrode work, composite fiber anodes for LIBs were prepared using particle/polymer electrospinning. Potential advantages of electrospun anodes over conventional slurry cast electrodes include: (i) a large electrode/electrolyte interfacial area for enhanced electrochemical oxidation/reduction kinetics, (ii) a controllable interfiber void volume to ensure good electrolyte infiltration into the electrode, and (iii) micron/sub-micron fibers with high nanoparticle content and short Li^+ transport pathways.[32, 39] Furthermore, the method can be adapted to a wide selection of particle/polymer combinations, making this a robust technology that is capable of incorporating new materials as they are developed.

Herein we present LIB performance data for an electrospun fiber anode containing TiO_2 nanoparticles, carbon powder, and a poly(acrylic acid) binder (from hereon referred to as TiO_2/C/PAA). TiO_2 was chosen as an active material due to its excellent cyclability, its minimal volume changes upon cycling, and its avoidance of SEI layer formation. Thin and thick anodes were characterized in terms of stability and rate capabilities; thin electrodes had an areal capacity of 0.099 mAh cm^{-2} and a thickness of 50 μm whereas thick electrodes had an areal capacity of 1.5 – 3.9 mAh cm^{-2} and a thickness of 600 – 1,400 μm. The performance of the electrospun material is compared

with that of conventional slurry cast electrodes of the same composition. These results are also contrasted with TiO_2, graphite, and Si anodes reported in the literature.

3.2 Experimental

Anode slurries were prepared by mixing titania nanoparticles (anatase, 15 nm, US Research Nanomaterials, Inc), conductive carbon black (Vulcan XC72R, Fuel Cell Store, Inc.), and poly(acrylic acid) (PAA, M_v = 450,000 g mol^{-1}, Sigma-Aldrich) in 1-propanol with a fixed composition of 19 wt % solids where the TiO_2/C/PAA weight ratio was 40/25/35. Electrodes were prepared from this mixture by either: (i) conventional slurry casting or (ii) electrospinning a nonwoven fiber mat. Slurry cast anodes were prepared by painting the electrode mixture onto Cu foil (9 μm, MTI Corp). The liquid slurries were stabilized at ambient conditions for at least 2 h to allow for partial solvent evaporation and subsequently dried overnight at 60 °C under vacuum. Electrospinning was conducted at room temperature on a custom-built rotating and oscillating drum collection apparatus as described elsewhere.[37] Well-formed fibers were deposited on an aluminum foil sheet at the following conditions: (i) 1.00 mL h^{-1} solution flow rate, (ii) 8 – 9 kV bias voltage, (iii) 8.0 cm spinneret-to-collector distance, and (iv) a relative humidity between 10 – 20 %. Small adjustments in bias voltage and relative humidity were needed to maintain batch-to-batch reproducibility of the fiber structure. Top-down surface images of mats were collected and analyzed by scanning electron microscopy (Hitachi S4200 SEM) after gold sputtering for 90 s.

The fiber volume fraction in an electrospun mat was determined from the ratio of the fiber mat density and the density of a slurry cast electrode. The as-spun mats typically

had a fiber volume fraction < 0.30, which was increased by mechanical compaction on a hydraulic press (typical compaction conditions were ~ 5 MPa for ~ 10 s). Unless otherwise stated, the fiber volume fraction of electrospun anodes was in the range of 0.40 – 0.60. The compacted electrospun mats were sufficiently robust such that they could be tested in a coin cell without the need for a Cu foil current collector.

CR2032 half cells were assembled in an argon-filled glovebox using a titania-based slurry cast or electrospun working electrode (dried overnight at 60 °C under vacuum) and a Li metal counter/reference electrode. The electrolyte was 1.0 M $LiPF_6$ in a mixture of ethylene carbonate, dimethyl carbonate, and diethyl carbonate (1/1/1 by volume, MTI Corp.). Two sheets of Celgard 2500 soaked in the electrolyte were used as a membrane separator. For electrospun fiber anodes, the desired loading was achieved by stacking several layers of uncompacted electrospun mats followed by mechanical compression as described above. For slurry cast electrodes, the amount of material painted onto the Cu foil was varied to control loading, which was determined by subtracting the Cu substrate mass from the total electrode mass. In the present study, electrodes were prepared with material loadings ranging from to 1.4 to 54.1 mg cm^{-2} (which includes the mass of TiO_2, carbon and PAA). Several drops of electrolyte were added to electrodes with high mass loadings (> 20 mg cm^{-2}) to ensure complete electrolyte infiltration throughout the electrode. Cells were crimped at 1,000 psi and evaluated electrochemically at room temperature after a 24 h resting period.

Cells were analyzed by cyclic voltammetry, where the anode was polarized between 1.0 and 2.6 V at a scan rate of 0.5 mV s^{-1} using a Gamry Reference 3000 potentiostat. During galvanostatic charge/discharge experiments, cells were cycled

between 1.0 – 2.6 V. To investigate anode rate capabilities, cells were cycled 5 times at current densities corresponding to 0.1 – 5 C, and the capacity during the 5^{th} cycle was recorded. Battery cycling experiments were performed on an 8-channel battery tester (5V/1mA, MTI Corp.) and a Gamry potentiostat (for high C-rate testing). At least two coin cells were tested for each sample to assess the reproducibility of these experiments. The electrochemical performance of each sample was reproducible within approximately 15 – 20 % among independent coin cell tests. Selected cells were disassembled after cycling, and the anodes were washed thoroughly with diethyl carbonate for post-mortem SEM imaging.

C-rates are based on a theoretical capacity of 335 mAh g^{-1} TiO_2 (i.e., 335 mA $g_{TiO_2}^{-1}$ corresponds to 1 C). Unless otherwise indicated, electrochemical capacities refer to TiO_2 delithiation. Areal capacities are based on the electrode's geometric footprint, and all potentials are referenced vs. Li/Li^+.

3.3 Results and Discussion

A scanning electron microscopy (SEM) image of an as-spun electrospun mat containing titania nanoparticles and carbon black with a poly(acrylic acid) (PAA) binder (average fiber diameter = 1.4 μm) is shown in Figure 3.1a. The fiber volume fraction of the as-spun mat was very low (< 0.30), so a compaction step on a hydraulic press was used to increase the material's density. A compacted anode with a fiber volume fraction of 0.54 is shown in Figure 3.1b. Compared to a slurry electrode of the same composition (Figure 3.1c), the electrospun material contained large interfiber void spaces which allow for complete electrolyte penetration throughout the porous structure. The presence of

interfiber voids in the electrode mat is important for battery operation; electrolyte intrusion between the fibers ensures rapid Li^+ transport throughout the entire electrode during charge and discharge.

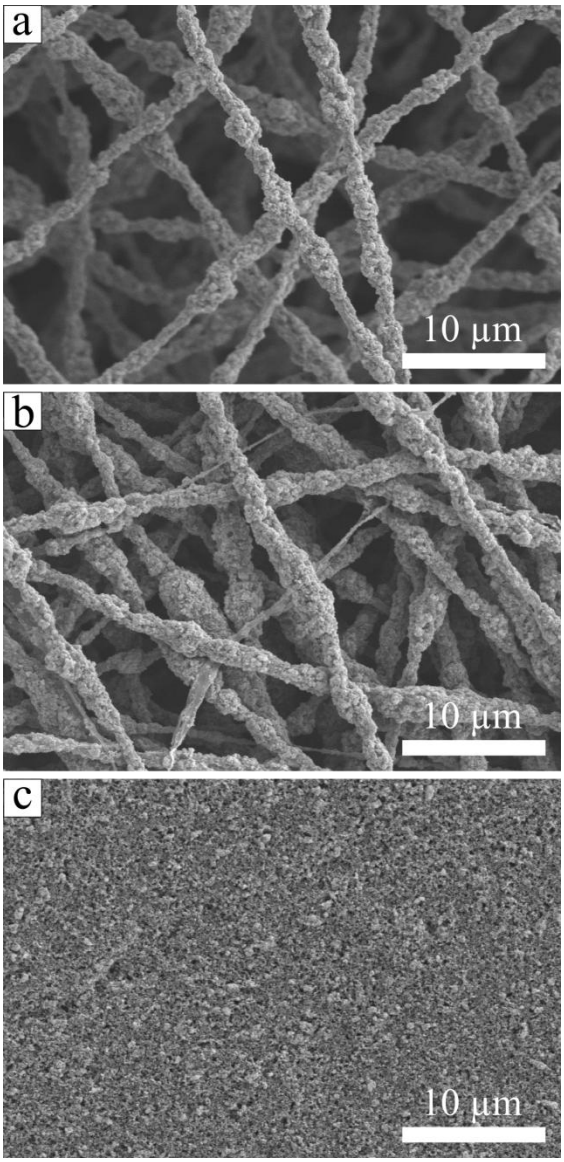

Figure 3.1. SEM images of TiO_2/C/PAA anodes. (a) An as-spun electrospun mat, (b) a compacted electrospun man with a 0.54 fiber volume fraction and (c) a conventional slurry cast anode.

The electrospun composites were characterized as LIB anodes using cyclic voltammetry (CV) and galvanostatic charge/discharge experiments. Representative cyclic voltammograms shown in Figure 3.2a exhibit peaks at 2.17 and 1.66 V vs. Li/Li^+, which correspond to TiO_2 anatase lithiation and delithiation, respectively.[40] Some peak shifting was observed during the first few scans, as has been reported by others, but the voltammograms stabilized after 10 cycles.[40] Forward and reverse peak currents were within ~ 5 % of one another, indicating good reversibility of the lithiation reaction. The galvanostatic charge/discharge curves shown in Figure 3.2b exhibit lithiation/delithiation potential plateaus which correlate well with the CV peaks. During the first delithiation cycle, the capacity of an electrospun anode (as averaged over numerous samples) was 73 ± 5 mAh g^{-1} (i.e., 183 mAh $g_{TiO_2}^{-1}$). An irreversible capacity loss of 35 % during the first cycle is attributed to anatase structural defects which trap Li inside TiO_2 interstitial spaces.[20, 41] Ortiz et al.[20] reported a similar irreversible capacity loss of 29 % for a TiO_2 nanotube anode. Despite this initial loss, the electrospun material exhibited excellent stability with a reversible capacity of 62 mAh g^{-1} after 50 cycles. The voltammograms and charge/discharge curves agree well with those reported by others for TiO_2-based anodes, which indicates: (i) the electrospinning process did not adversely affect fundamental lithiation/delithiation properties of TiO_2 and (ii) there was sufficient carbon powder in the fibers for electron access to all TiO_2 nanoparticles.[40, 42] The gravimetric capacity of the electrospun anode was lower than other systems reported in the literature (typically > 100 mAh g^{-1}) due to the low titania content of the fibers (40 wt %). The electrode composition in this study (TiO_2/C/PAA weight ratio of 40/25/35) was required to obtain well-formed fibers with good electrical conductivity. At least 25 wt % polymer

binder was required to form continuous fibers during electrospinning. Likewise, ~ 15 wt % carbon black was needed for electron transport throughout the electrode.

Figure 3.2c shows the long-term performance of an electrospun TiO_2/C/PAA electrode over several hundred cycles. At a 0.5 C charge/discharge rate, the material demonstrated superb stability with 95 % capacity retention and a coulombic efficiency exceeding 99 % after 450 cycles. In comparison, current graphite anodes showed a capacity loss of ~ 65 % under similar testing conditions.[43] The electrospun anode was also physically stable in a battery environment. Figure 3.3 shows a post-mortem SEM image of an anode fiber mat after 50 charge/discharge cycles at 0.1 C; the fibers and interfiber voids were well-maintained during cycling (compare Figure 3.3 with the initial mat in Figure 3.1b). In general, there was no change in the fiber mat morphology after up to 510 cycles.

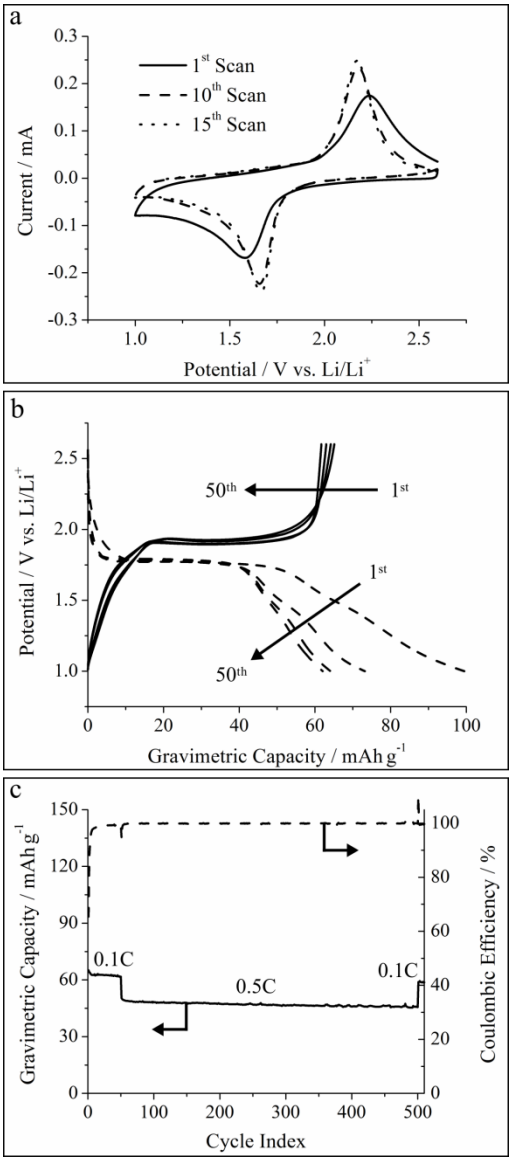

Figure 3.2. (a) Cyclic voltammograms, (b) charge/discharge curves collected at 0.1 C during the 1st, 2nd, 10th and 50th cycles, and (c) long-term performance over 510 cycles for electrospun TiO_2/C/PAA anodes.

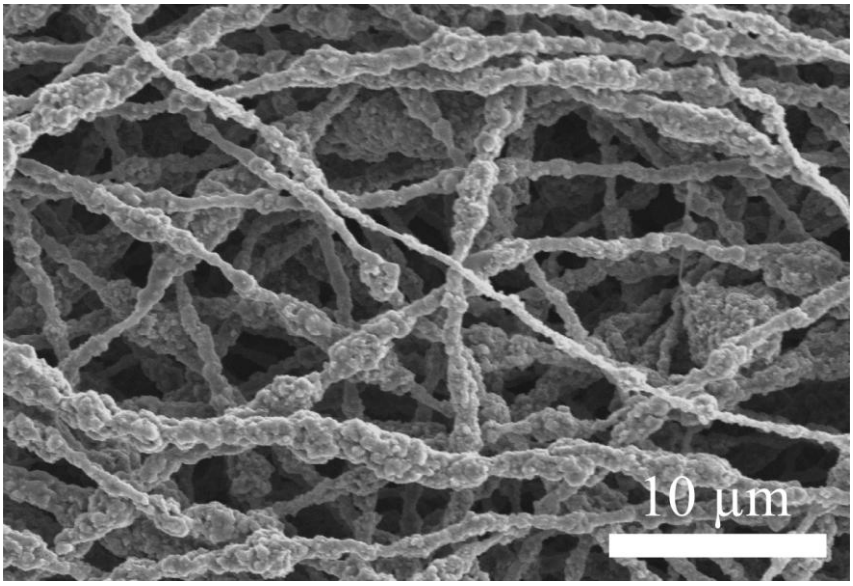

Figure 3.3. SEM of an electrospun anode fiber electrode after 50 charge/discharge cycles at 0.5 C.

In addition to long-term stability, LIB anodes must possess good rate capabilities for fast recharging. The effect of C-rate on capacity retention (i.e., capacity normalized with respect to that measured at 0.1 C) for an electrospun and a conventional slurry cast anode was assessed at two different mass loading ranges: low loading (1.4 – 2.6 mg cm^{-2}) and high loading (20.1 – 21.9 mg cm^{-2}). With a low mass loading (Figure 3.4a), both the fiber and slurry anodes had reversible capacities ~ 73 mAh g^{-1} at 0.1 C and similar capacity losses up to 5 C. Battery capacity losses at higher currents are a well-known phenomena and are due to internal resistance together with activation and concentration overpotential losses.[44] Since both morphologies demonstrated similar performance declines with increasing C-rate, Li^+ transport in the electrolyte is not likely rate limiting at the low material loadings. However, at a higher loading of 20.1 – 21.9 mg cm^{-2}, significant differences between the electrospun and slurry cast

systems were apparent, as shown in Figure 3.4b. Both electrodes again attained capacities ~ 73 mAh g^{-1} at 0.1 C, but the slurry cast electrode lost 92 % of this capacity at 5 C. In contrast, the electrospun material demonstrated dramatically improved performance and a 4-fold higher capacity retention at 5 C (31 % vs. 7.9 %). Slow Li^+ transport throughout the interior of the thick anode (i.e., high mass loading) is undoubtedly limiting the performance of the slurry cast anode. This limitation was not seen for the fibrous anode where complete electrolyte intrusion into the interfiber void space provided: (i) a large 3D electrode/electrolyte interfacial area and (ii) short Li^+ transport pathways between the electrolyte and TiO_2 nanoparticles in the radial fiber direction. Interestingly, both the low and high loading electrospun anodes maintained the same capacity retention up to 2 C. This behavior indicates that the 3D interfiber voids promoted effective Li^+ transport throughout the anode. The unique morphology of the electrospun electrodes provides superior rate capabilities at high loadings compared to a conventional slurry cast system.

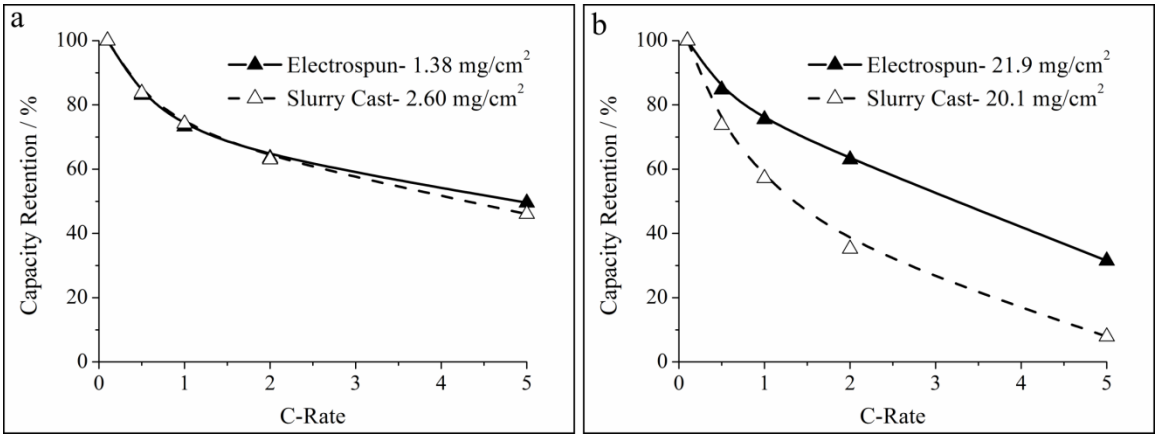

Figure 3.4. Normalized capacity vs. C-rate for different electrospun and slurry cast electrodes. (a) Low mass loading, and (b) high mass loading. Capacities are normalized with respect to the capacity at 0.1 C.

To further investigate the effect of material loading on anode performance, particle/polymer electrospinning was used to prepare ultra-thick electrodes with high areal capacities. The investigation of thick slurry cast LIB anodes (> 100 μm) has thus far been limited due to difficulties in making such electrodes (e.g., material cracking and poor adhesion to the current collector) when conventional techniques are employed.[45, 46] For an electrospun fiber anode, these limitations are circumvented; multiple fiber mats can be easily stacked to create an anode of any desired areal loading. The areal capacity dependence on C-rate for electrospun anodes of four thicknesses (50, 600, 1,000 and 1,400 μm, corresponding to areal capacities of 0.099, 1.5, 2.9, and 3.9 mAh cm^{-2}, respectively) is shown in Figure 3.5. Note that the 50 and 600 μm samples are the same as those represented in Figure 3.4. All electrodes in Figure 3.5 exhibited a gravimetric capacity of ~ 73 mAh g^{-1} at 0.1 C with no capacity fade during cycling. For the 1,400 μm thick fiber anode (54.1 mg cm^{-2} loading), a remarkably high capacity of 2.5 mAh cm^{-2} was achieved at 1 C (vs. 3.9 mAh cm^{-2} at 0.1 C). These areal capacities are comparable to those of commercial graphite anodes (2.5 – 3.5 mAh cm^{-2}).[27] A steeper decline in capacity with C-rate was observed for the 1.0 and 1.4 mm thick electrodes due to a higher ohmic potential drop within the electrode. This observation indicates a tradeoff between energy and power densities for thick electrodes with high mass loadings.

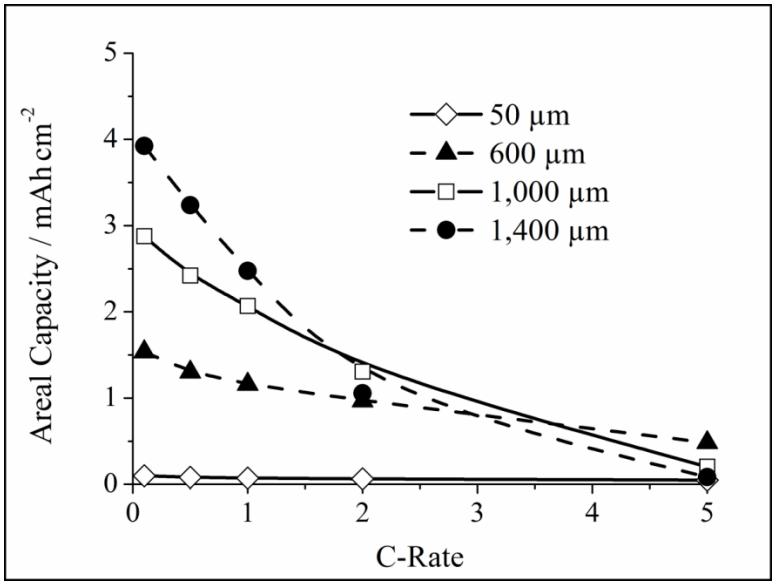

Figure 3.5. Areal capacity as a function of C-rate for electrospun anodes of different thicknesses (50 µm = 1.38 mg cm^{-2}, 600 µm = 21.9 mg cm^{-2}, 1.0 mm = 40.2 mg cm^{-2}, and 1.4 mm = 54.1 mg cm^{-2}).

The performance of the ultra-thick electrospun anodes is superior to other electrodes of comparable thickness, as reported in the literature. For example, Wang et al.[45] prepared a 1.2 mm thick anode by depositing a carbon layer onto 3D Cu foam. This material attained a high areal capacity of 17 mAh cm^{-2} at 0.05 C but showed a steady capacity fade upon cycling at 0.5 C. Evanoff et al.[46] characterized a 1 mm thick anode containing Si coated carbon nanotubes where the capacity (3,300 mAh g^{-1}) was stable at 0.2 C, but areal capacities were not reported. This anode exhibited poor rate capabilities at 0.5 C where it lost 37 % of its low-rate capacity. Neither Wang et al.[45] nor Evanoff et al.[46] examined charge/discharge currents greater than 0.5 C. For comparison with the present study, the 1.4 mm electrospun fiber anode showed stable cycling and maintained 84 % of its capacity at 0.5 C. The superior performance of the thick

electrospun anodes is again attributed to complete electrolyte intrusion between the fibers and short Li^+ transport pathways.

The performance of an electrospun titania anode is compared to published data for anodes containing either TiO_2, commercial graphite, or Si in Figure 3.6.[6, 17, 26, 47, 48] At charge/discharge rates up to 2 C, the electrospun anodes exhibited superior performance. It is important to note that Si materials, heralded for their excellent gravimetric capacity (> 1,000 mAh g^{-1}), are often limited to very low loadings and areal capacities (< 1 mAh cm^{-2}). While the electrospun system in the present study had higher areal capacities at rates up to 2 C, it exhibited a lower 5 C capacity (0.20 mAh cm^{-2}) as compared to that of the Si/CNT nanofibers (0.63 mAh cm^{-2}) and TiO_2 nanotubes (0.26 mAh cm^{-2}). Optimizing the fiber mat composition (i.e., minimizing binder and carbon content) and/or morphology (i.e., identifying the preferred fiber diameter and fiber volume fraction) is anticipated to provide higher areal capacities at charge/discharge rates > 2 C.

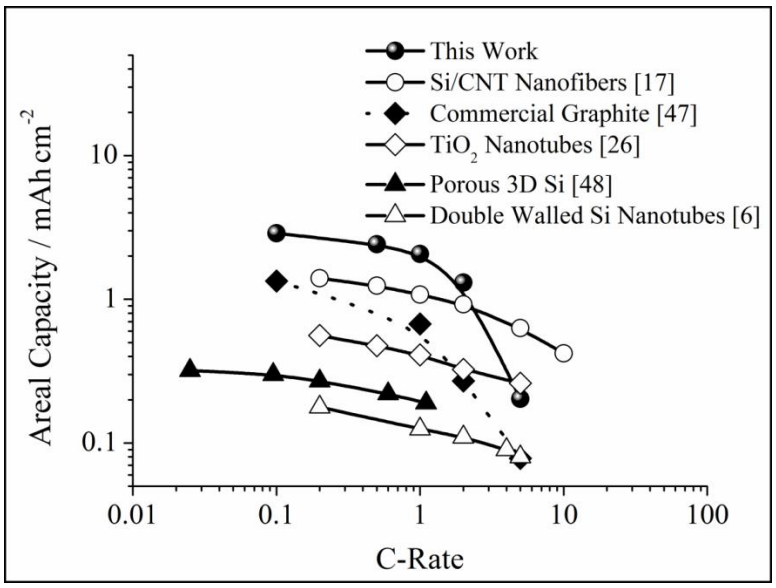

Figure 3.6. Comparison of areal capacity and rate capabilities of a particle/polymer electrospun system with several other reports in the literature.

The volumetric capacity of electrospun anodes was also considered since this measure of electrode performance is critically important for space-limited applications such as electric vehicle batteries. Table 3.1 lists the volumetric capacities of two electrospun anodes with fiber volume fractions of 0.60 and 0.87 and of one slurry cast electrode. At 0.1 C, the electrospun anode with a fiber volume fraction of 0.60 exhibited a volumetric capacity of 28.7 mAh cm^{-3} which is lower than the 47.9 mAh cm^{-3} for the slurry cast system due to the void volume between fibers in the electrospun electrode. However, since the electrospun material had superior rate capabilities, its volumetric capacity at 2 C was equal to that of a slurry cast anode (17.5 mAh $cm^{-3}$for each). A further improvement in the volumetric capacity of the electrospun anode was achieved by using a high compaction pressure to increase the mat's fiber volume fraction to 0.87. This highly compacted anode had s a 2 C volumetric capacity of 21.2 mAh cm^{-3} which

exceeds that of the slurry cast electrode. For comparison, a graphite anode report by Sivakkumar et al.[47] had a volumetric capacity of ~ 27 mAh cm^{-3} at 2 C.

Table 3.1. Volumetric capacity of electrospun and slurry cast titania-based anodes.

Anode Type[a]	Fiber Volume Fraction	Volumetric Capacity (mAh cm^{-3})			
		Theoretical[b]	0.1 C	1 C	2 C
Electrospun (low compaction)[c]	0.60	53.2	28.7	21.0	17.5
Electrospun (high compaction)	0.87	76.9	39.0	27.5	21.2
Slurry Cast	--	88.6	47.9	28.5	17.5

[a] All anodes contain 40/25/35 TiO_2/C/PAA by weight.
[b] Calculated based on 335 mAh $g_{TiO_2}^{-1}$
[c] Same electrode type as presented in Figures 3.2, 3.4, 3.5, and 3.6.

3.4 Conclusions

Particle/polymer fiber electrospinning was used for the first time to prepare high performance TiO_2-based LIB anodes. This approach utilized TiO_2 nanoparticles as a lithium host and carbon black for electronic conduction. The use of carbon black powder rather than a pyrolyzed polymer nanofiber distinguishes the anodes in this study from previous electrospun LIB electrode investigations. The method demonstrated here is robust and can be easily adapted to accommodate a variety of Li host nanoparticles and polymer binders. In the present study, composite fiber mats containing titania and carbon nanoparticles with a poly(acrylic acid) binder were fabricated and tested as LIB anodes.

Anode mats were prepared with an average fiber diameter of 1.4 μm and a fiber volume fraction of 0.50 – 0.60. The material exhibited a gravimetric capacity of 73 mAh g^{-1} at 0.1 C and showed excellent stability, with 95 % capacity retention and a

coulombic efficiency exceeding 99 % after 450 cycles. Compared to a traditional slurry cast electrode of the same composition at a material loading of 20.1 – 21.9 mg cm^{-2}, the electrospun fiber anode maintained a 4-fold higher capacity at a 5 C charge/discharge rate. Electrospun anodes with thicknesses exceeding 1 mm and areal capacities up to 3.9 mAh cm^{-2} were also prepared. Even at a 1 C charge/discharge rate, the thick anodes displayed a high capacity (2.5 mAh cm^{-2}) which is comparable to that of commercial graphite anodes. Fibrous anodes with thicknesses of 1.0 and 1.4 mm exhibited lower areal capacities at 5 C compared to thinner materials due to greater ohmic resistances, indicating a tradeoff between areal capacity and rate capabilities. Compared to TiO_2, graphite, and Si-based LIB anodes reported in the literature, the electrospun composite fibers achieved higher areal capacities at charge/discharge rates up to 2 C. A highly compacted electrospun anode with a fiber volume fraction of 0.87 had a 2 C volumetric capacity of 21.2 mAh cm^{-3} which exceeds that of a slurry cast electrode (17.5 mAh cm^{-3}).

The excellent performance of the fibrous anodes is attributed to: (i) complete electrolyte infiltration throughout the interfiber void space of an anode mat and (ii) short Li^+ transport pathways between the electrolyte and TiO_2 nanoparticles in the radial fiber direction. Further improvements in capacity at high C-rates are expected after optimizing the anode fiber mat composition (e.g., minimizing carbon and binder content while maintaining good electrical conduction and mechanical stability) and morphology (e.g., fiber diameter and fiber volume fraction).

3.5 References

[1] M. Armand, J.-M. Tarascon, *Nature* **2008**, *451*, 652.
[2] U. Kasavajjula, C. Wang, A. J. Appleby, *J. Power Sources* **2007**, *163*, 1003.
[3] C. K. Chan, H. Peng, G. Liu, K. McIlwrath, X. F. Zhang, R. A. Huggins, Y. Cui, *Nat. Nanotechnol.* **2008**, *3*, 31.
[4] C. K. Chan, R. N. Patel, M. J. O'Connell, B. A. Korgel, Y. Cui, *ACS Nano* **2010**, *4*, 1443.
[5] L.-F. Cui, Y. Yang, C.-M. Hsu, Y. Cui, *Nano Lett.* **2009**, *9*, 3370.
[6] H. Wu, G. Chan, J. W. Choi, I. Ryu, Y. Yao, M. T. McDowell, S. W. Lee, A. Jackson, Y. Yang, L. Hu, Y. Cui, *Nat. Nanotechnol.* **2012**, *7*.
[7] T. Song, J. Xia, J.-H. Lee, D. H. Lee, M.-S. Kwon, J.-M. Choi, J. Wu, S. K. Doo, H. Chang, W. I. Park, D. S. Zang, H. Kim, Y. Huang, K.-C. Hwang, J. A. Rogers, U. Paik, *Nano Lett.* **2010**, *10*, 1710.
[8] B. Hertzberg, A. Alexeev, G. Yushin, *J. Am. Chem. Soc.* **2010**, *132*, 8548.
[9] L. Xue, K. Fu, Y. Li, G. Xu, Y. Lu, S. Zhang, O. Toprakci, X. Zhang, *Nano Energy* **2013**, *2*, 361.
[10] J. Kong, W. A. Yee, Y. Wei, L. Yang, J. M. Ang, S. L. Phua, S. Y. Wong, R. Zhou, Y. Dong, X. Li, X. Lu, *Nanoscale* **2013**, *5*, 2967.
[11] X. Zhang, L. Ji, O. Toprakci, Y. Liang, M. Alcoutlabi, *Polym. Rev.* **2011**, *51*, 239.
[12] H. S. Choi, J. G. Lee, H. Y. Lee, S. W. Kim, C. R. Park, *Electrochim. Acta* **2010**, *56*, 790.
[13] N. Liu, H. Wu, M. T. McDowell, Y. Yao, C. Wang, Y. Cui, *Nano Lett.* **2012**, *12*, 3315.
[14] H. Wu, G. Yu, L. Pan, N. Liu, M. T. McDowell, Z. Bao, Y. Cui, *Nat. Commun.* **2013**, *4*.
[15] N. Liu, Z. Lu, J. Zhao, M. T. McDowell, H. W. Lee, W. Zhao, Y. Cui, *Nat. Nanotechnol.* **2014**, *9*, 187.
[16] H. Wu, G. Zheng, N. Liu, T. J. Carney, Y. Yang, Y. Cui, *Nano Lett.* **2012**, *12*, 904.
[17] Q. Xiao, Y. Fan, X. Wang, R. A. Susantyoko, Q. Zhang, *Energy Environ. Sci.* **2014**, *7*, 655.
[18] X. Su, Q. Wu, X. Zhan, J. Wu, S. Wei, Z. Guo, *J. Mater. Sci.* **2011**, *47*, 2519.
[19] C. Jiang, J. Zhang, *J. Mater. Sci. Technol.* **2013**, *29*, 97.
[20] G. F. Ortiz, I. Hanzu, T. Djenizian, P. Lavela, J. L. Tirado, P. Knauth, *Chem. Mater.* **2009**, *21*, 63.
[21] H. Lindström, S. Södergren, A. Solbrand, H. Rensmo, J. Hjelm, A. Hagfeldt, S.-E. Lindquist, *J. Phys. Chem. B* **1997**, *101*, 7710.
[22] W. Wang, M. Tian, A. Abdulagatov, S. M. George, Y. C. Lee, R. Yang, *Nano Lett.* **2012**, *12*, 655.
[23] D. Guan, J. Li, X. Gao, C. Yuan, *J. Power Sources* **2014**, *246*, 305.
[24] G. F. Ortiz, I. Hanzu, P. Lavela, J. L. Tirado, P. Knauth, T. Djenizian, *J. Mater. Chem.* **2010**, *20*, 4041.
[25] T. Yiping, T. Xiaoxu, H. Guangya, Z. Guoqu, *Electrochim. Acta* **2014**, *117*, 172.
[26] W. Wei, G. Oltean, C.-W. Tai, K. Edström, F. Björefors, L. Nyholm, *J. Mater. Chem. A* **2013**, *1*, 8160.

[27] N. Nitta, G. Yushin, *Part. Part. Syst. Char.* **2014**, *31*, 317.
[28] L. Hu, F. La Mantia, H. Wu, X. Xie, J. McDonough, M. Pasta, Y. Cui, *Adv. Energy Mater.* **2011**, *1*, 1012.
[29] A. Vu, Y. Qian, A. Stein, *Adv. Energy Mater.* **2012**, *2*, 1056.
[30] I. V. Thorat, T. Joshi, K. Zaghib, J. N. Harb, D. R. Wheeler, *J. Electrochem. Soc.* **2011**, *158*, A1185.
[31] L. Shen, X. Zhang, E. Uchaker, C. Yuan, G. Cao, *Adv. Energy Mater.* **2012**, *2*, 691.
[32] L. Ji, Y. Yao, O. Toprakci, Z. Lin, Y. Liang, Q. Shi, A. J. Medford, C. R. Millns, X. Zhang, *J. Power Sources* **2010**, *195*, 2050.
[33] Z. Lin, L. Ji, M. D. Woodroof, X. Zhang, *J. Power Sources* **2010**, *195*, 5025.
[34] L. Ji, Z. Lin, A. J. Medford, X. Zhang, *Carbon* **2009**, *47*, 3346.
[35] L. Wang, C. X. Ding, L. C. Zhang, H. W. Xu, D. W. Zhang, T. Cheng, C. H. Chen, *J. Power Sources* **2010**, *195*, 5052.
[36] B. Zhao, S. Jiang, C. Su, R. Cai, R. Ran, M. O. Tadé, Z. Shao, *J. Mater. Chem. A* **2013**, *1*, 12310.
[37] W. Zhang, P. N. Pintauro, *ChemSusChem* **2011**, *4*, 1753.
[38] M. Brodt, R. Wycisk, P. N. Pintauro, *J. Electrochem. Soc.* **2013**, *160*, F744.
[39] P. Raghavan, D.-H. Lim, J.-H. Ahn, C. Nah, D. C. Sherrington, H.-S. Ryu, H.-J. Ahn, *React. Funct. Polym.* **2012**, *72*, 915.
[40] M. G. Choi, Y.-G. Lee, S.-W. Song, K. M. Kim, *Electrochim. Acta* **2010**, *55*, 5975.
[41] A. G. Dylla, G. Henkelman, K. J. Stevenson, *Acc. Chem. Res.* **2012**, *46*, 1104.
[42] K. Hemalatha, A. S. Prakash, G. K, M. Jayakumar, *J. Mater. Chem. A* **2014**, *2*, 1757.
[43] S. R. Sivakkumar, A. G. Pandolfo, *J. Appl. Electrochem.* **2013**, *44*, 105.
[44] D. Danilov, R. A. H. Niessen, P. H. L. Notten, *J. Electrochem. Soc.* **2011**, *158*, A215.
[45] J. S. Wang, P. Liu, E. Sherman, M. Verbrugge, H. Tataria, *J. Power Sources* **2011**, *196*, 8714.
[46] K. Evanoff, J. Khan, A. A. Balandin, A. Magasinski, W. J. Ready, T. F. Fuller, G. Yushin, *Adv. Mater.* **2012**, *24*, 533.
[47] S. R. Sivakkumar, J. Y. Nerkar, A. G. Pandolfo, *Electrochim. Acta* **2010**, *55*, 3330.
[48] S. R. Gowda, V. Pushparaj, S. Herle, G. Girishkumar, J. G. Gordon, H. Gullapalli, X. Zhan, P. M. Ajayan, A. L. M. Reddy, *Nano Lett.* **2012**, *12*, 6060.

CHAPTER IV

HIGH PERFORMANCE C/PVDF NANOFIBER ANODES FOR LI-ION BATTERIES USING PARTICLE/POLYMER ELECTROSPINNING

Adapted from E. C. Self, R. Wycisk, P. N. Pintauro, *ChemSusChem* **2016**, *9*, 208 with permission from John Wiley and Sons.

4.1 Introduction

The demand for rechargeable batteries with high energy and power densities has never been greater. The functionality of many portable electronic devices is limited by battery size and lifetime. Similarly, electric vehicle propulsion systems require significant improvements to satisfy consumer expectations for long drive distances and short recharge times. To meet the demands of energy-hungry consumers, new battery electrodes with high capacities and long cycle life at fast charging rates must be developed.[1-3] These requirements have motivated intense research efforts to develop next-generation Li-ion battery (LIB) materials, in particular replacement materials/morphologies for the graphite anode. One approach is the use of 3D electrodes containing engineered void spaces to enhance Li^+ transport rates for high capacities at fast charge/discharge rates.[4-9]

Battery researchers largely focus on preparing new electrodes with high gravimetric capacity, but this metric alone is insufficient to assess a material's applicability for consumer devices. An electrode's volumetric capacity is another

important measure for applications, such as electric vehicle propulsion, where battery space is limited. Likewise, electrodes must have high areal capacities to limit the amount of inactive components (e.g., current collectors and separators) that contribute to the overall battery size and weight.[10-12] Some noteworthy studies[4, 13] on LIB cathodes focused on areal and/or volumetric capacities, but these metrics are unreported for most systems. Because gravimetric, areal, and volumetric capacities are important and complementary measures of battery performance, all three should be measured and examined to fully assess the strengths and weaknesses of new electrode materials and designs.

Particle/polymer electrospinning is an attractive technology for preparing 3D nanofiber electrodes with high gravimetric, areal, and volumetric capacities. The present paper is the latest installment by Pintauro and coworkers on the use of polymer/ particle electrospun nanofiber mats for fuel cell and LIB electrodes.[11, 14-16] We recently reported on the preparation and characterization of electrospun fiber mats containing titania nanoparticles, carbon black, and poly(acrylic acid) (henceforth referred to as TiO_2/C/PAA) as LIB anodes as described in Chapter III.[11] Compared to published data for anodes containing either TiO_2, commercial graphite, or Si, the electrospun TiO_2/C/PAA fibers exhibited superior areal capacities at fast charge/discharge rates (e.g., 1.3 mAh cm^{-2} at 2 C). Furthermore, densely packed titania fiber anodes with a fiber volume fraction of 0.87 showed a 21 % higher volumetric capacity at 2 C compared to a slurry cast anode of the same composition (21.2 and 17.5 mAh cm^{-3}, respectively). The excellent performance of the electrospun titania-based anodes was attributed to: (i) a large electrode/electrolyte interfacial area for enhanced reaction kinetics, (ii) a 3D

nanofiber network containing interfiber voids for good electrolyte infiltration, and (iii) short Li^+ transport pathways between the electrolyte and the active material in the radial fiber direction.

Although the TiO_2/C/PAA fiber anodes exhibited high areal and volumetric capacities at fast charge/discharge rates, the material had a relatively low gravimetric capacity (e.g., 70 mAh g^{-1} at 0.1 C) owing to the low theoretical capacity of titania (335 mAh g^{-1} for $LiTiO_2$) and the low titania content in the fibers; only 40 wt % of the electrode was TiO_2, with 25 wt % inactive carbon particles for electrical conduction. To address these limitations, we present results for particle/polymer electrospun nanofiber anodes containing carbon nanoparticles distributed throughout a poly(vinylidene fluoride) (PVDF) binder. The use of carbon as an active material eliminates the need for conductive additives and thus allows for high active material loadings in the fiber (65 wt % vs. 40 wt % for TiO_2/C/PAA). Additional advantages of carbon nanofiber anodes over titania include the high theoretical capacity of carbon (372 mAh g^{-1}) and a low operating potential (0.015 – 1.5 V *vs.* Li/Li^+, as compared to 1.0 – 2.6 V vs. Li/Li^+ for titania).

Previous reports on electrospun carbon nanofiber anodes for LIBs utilized high temperature processing to convert a polymer nanofiber mat into an electronically conductive carbon fiber network. Zhang et al.[17] electrospun poly(acrylonitrile) (PAN) nanofibers followed by high temperature pyrolysis to create a carbon nanofiber mat that exhibited a high gravimetric capacity of 555 mAh g^{-1} at ~ 0.18 C and 260 mAh g^{-1} at ~ 3.6 C. Similarly, Wu et al.[18] characterized carbon nanofiber anodes prepared from electrospun PAN, where the polymer was carbonized at different temperatures. These

materials exhibited moderately high capacities ranging from 250 – 450 mAh g^{-1} and excellent cycle life (more than 500 cycles at 0.27 C without significant capacity fade). Unfortunately, the volumetric capacity of such carbon fiber anodes was not discussed in these and other published papers, but it is reasonable to assume that the fiber volume fraction was < 0.25, which is far too low for practical battery use. As-spun polymeric nanofiber mats typically have a fiber volume fraction in the range of 0.01 – 0.25,[19-21] that furthers decrease after fiber pyrolysis.

Composite nanofiber electrodes prepared using particle/ polymer electrospinning are fundamentally different from and offer several key advantages over pyrolyzed carbon nanofiber electrodes. Whereas pyrolyzed carbon nanofibers are usually brittle and fracture easily,[22-24] particle/polymer nanofiber mats are flexible and mechanically robust owing to the presence of the polymer binder.[25] Thus, composite nanofiber mat electrodes can be used in flexible battery architectures, and they can be mechanically compacted under high pressure without fracture to increase the fiber volume fraction and volumetric storage capacity. Particle/polymer electrospinning is also a robust platform that can be used to prepare novel nanostructured electrodes from new active materials and binders as they are developed. This cannot be said of pyrolyzed fiber mats, where the primary electrode component will always be carbon. The goal of the present study was to prepare particle/polymer nanofiber anodes with high gravimetric, areal, and volumetric capacities at fast charge/discharge rates (e.g., ≥ 1 C) and long cycle life. High areal capacities were achieved through the use of thick electrodes (thicknesses up to 820 μm), and the volumetric capacity of the electrospun anodes was increased by mechanically compacting the mats up to a fiber volume fraction of 0.80. Compared with traditional

slurry cast electrodes, electrospun nanofiber mats are inherently porous with an interfiber void space that does not disappear upon mat compaction and that is highly uniform throughout the material. This void volume provides facile electrolyte intrusion and efficient Li^+ transport throughout thick, densely-packed electrodes to achieve high volumetric and areal capacities at fast charge/discharge rates.

4.2 Experimental

Anode slurries were prepared by mixing carbon nanoparticles (either Vulcan XC-72R, Fuel Cell Store or activated carbon, US Research Nanomaterials, Inc.) and poly(vinylidene fluoride) (PVDF, HSV-900, Arkema) with a solvent containing 7/3 dimethylformamide/acetone (w/w). The C/PVDF weight ratio in all electrodes was 65/35. Anodes were prepared by either conventional slurry casting or electrospinning a nanofiber mat. The slurry cast anodes were cast onto copper foil (9 μm, MTI Corp.) and dried at ambient conditions. Nanofiber mat anodes were prepared using a rotating drum electrospinning apparatus as shown in Figure 4.1. Mats of uniform fiber volume fraction with a narrow fiber diameter distribution were collected on an aluminum foil substrate at the following conditions: (i) 0.75 mL h^{-1} solution flow rate, (ii) 15 kV bias voltage, and (iii) 8.0 cm spinneret-to-collector distance. All electrospinning was performed in room temperature air at 30 % relative humidity. As-spun mats were typically 100 μm thick and had a fiber volume fraction < 0.25. Anode thickness was controlled by stacking multiple as-spun mats, and the fiber volume fraction was increased by mechanically compacting mats at a pressure of 1 – 90 MPa for 40 s. Thin anodes (< 100 μm) were prepared from a single compacted nanofiber mat, whereas thicker electrodes were prepared by stacking

multiple as-spun mats followed by compaction to ensure good interfiber mat contact. The morphologies of nanofiber and slurry cast anodes were assessed using scanning electron microscopy (Hitachi S4200 SEM) after gold sputtering for 90 s.

To determine the active material loading in the fibers after electrospinning, thermogravimetric analyses (TGA) were performed on Vulcan XC-72R powder, PVDF powder, and C/PVDF nanofiber mats. Each sample was heated under nitrogen atmosphere to 750 °C at a rate of 10 °C min^{-1}, followed by a 4 h constant temperature hold at 750 °C. A simple mass balance was used to determine the carbon loading in a fiber mat, where the TGA mass loss of the C/PVDF fibers (30.5 %) was given by the sum of mass losses for carbon and PVDF powders (3.1 and 73.5 %, respectively). The fiber volume fraction of an electrospun mat was calculated as the ratio of the measured mat density to the density of a hypothetical/idealized mat containing no interfiber voids. To estimate the density of the latter, an SEM image of a reference nanofiber mat was processed using ImageJ such that the interfiber voids were represented by white pixels and the electrospun fibers were black pixels. The fiber volume fraction of the reference mat was then determined as the fraction of black pixels in this image. The reference mat was highly compacted to minimize depth of field errors when visually determining fiber volume fraction. From the apparent fiber volume fraction and the measured density of the reference mat, the extrapolated density of a nanofiber mat with no interfiber void space was found to be 0.91 ± 0.03 g cm^{-3}. From the densities of carbon black and PVDF and the known composition of electrospun fibers, a zero porosity mat should have a density of 1.79 g cm^{-3}. From these two density calculations, the internal porosity of an electrospun fiber was estimated to be 0.49.

CR2032 half cells were constructed in an argon-filled glovebox using an electrospun or slurry cast anode disk (10 mm in diameter) and a Li metal counter/reference electrode. The electrolyte was 1.0M LiPF6 in a mixture of ethylene carbonate, dimethyl carbonate, and diethyl carbonate (1/1/1 by volume, MTI Corp.). Two sheets of Celgard 2500 soaked in the electrolyte were used as a membrane separator. Several drops of electrolyte were added to completely fill the cell volume. Cells were crimped at 1000 psi (6.9 MPa) and rested overnight before electrochemical characterization.

Cyclic voltammograms were collected by polarizing the cells from 0.015 – 1.5 V at a scan rate of 0.5 mV s^{-1} using a Gamry Reference 3000 potentiostat. Galvanostatic charge/discharge experiments were conducted between 0.015 – 1.5 V at current densities ranging from 0.1 – 5 C. Cells were cycled a minimum of 5 times at each current density to ensure stable performance. Charge/discharge experiments at 0.1 C were performed on an 8 channel battery tester (5 V/1 mA, MTI Corp.). A Gamry Reference 3000 potentiostat was used for charge/discharge cycling at high rates (0.5 – 5 C). Potentiostatic electrochemical impedance spectroscopy was performed with a 10 mV AC amplitude over a frequency range of $1x10^6$ – 0.1 Hz. A modified Randles circuit[26] was fit to experimental data using the simplex method in Gamry Echem Analyst software. At least two coin cells were tested for each sample to assess the reproducibility of these experiments. The electrochemical performance of each sample was reproducible within approximately 15 – 20 % among independent coin cell tests. Select cells were disassembled after cycling, and the anodes were rinsed with diethyl carbonate before post-mortem SEM imaging.

C-rates are based on the theoretical capacity of graphite (i.e., 1 C = 372 mA g_C^{-1}). Except where otherwise indicated, capacities are normalized to the entire composite anode (i.e., total amounts of carbon and PVDF). Areal capacities are calculated based on the anode's geometric footprint. All potentials are referenced vs. Li/Li^+.

4.3 Results and Discussion

Nanofiber mat anodes were prepared using a rotating drum electrospinning apparatus illustrated in Figure 4.1. A scanning electron microscopy (SEM) image of an electrospun nanofiber mat containing Vulcan XC-72R carbon black nanoparticles and a PVDF binder is shown in Figure 4.2. All anodes in this study contained carbon nanoparticles and PVDF binder (C/PVDF) in a 65/35 weight ratio. This composition produced well-formed nanofibers (no beading) with a random orientation and a uniform particle distribution. To precisely determine the active material loading in the fibers, thermogravimetric analyses were performed on: (i) carbon powder, (ii) PVDF powder, and (iii) C/PVDF nanofibers. From the resulting thermogravimetric curves, the calculated carbon loading in the fibers was found to be 61 wt %, which is in good agreement with the nominal 65 wt % used during ink preparation. The mat in Figure 4.2 had a fiber volume fraction of 0.18 and an average fiber diameter of 910 nm (typical for all mats made in the present study). The fiber volume fraction was increased by application of an appropriate hydraulic pressure for 40 s. A plot of experimental pressure vs. fiber volume fraction is shown in Figure 4.3, and compacted C/PVDF nanofiber mats with fiber volume fractions of 0.39 and 0.80 are shown in Figure 4.4a and b, respectively. The highly compacted sample in Figure 4.4b showed merging of individual fibers, but all

electro spun samples retained some interfiber void space after mechanical compaction. For comparison, a slurry cast anode of the same composition as the electrospun nanofiber mats (65/35 C/PVDF by weight) had a dense structure with essentially no visible voids (see Figure 4.4c).

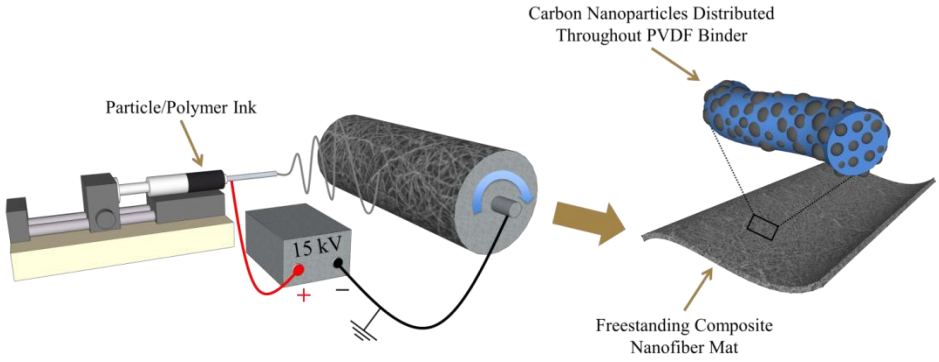

Figure 4.1. Electrospinning apparatus used to produce a particle/polymer nanofiber mat.

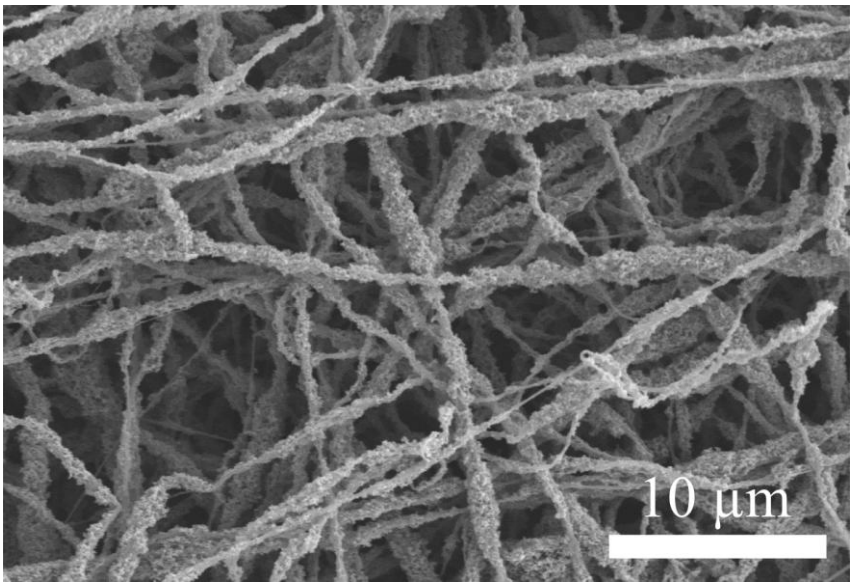

Figure 4.2. SEM image of an as-spun C/PVDF nanofiber anode with a fiber volume fraction of 0.18.

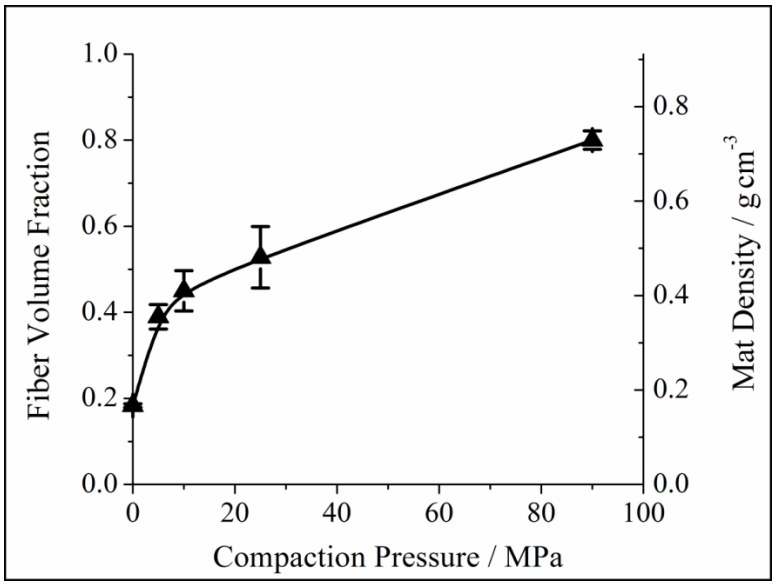

Figure 4.3. The effect of applied compaction pressure on fiber volume fraction and mat density. Error bars represent the standard deviation of at least three samples.

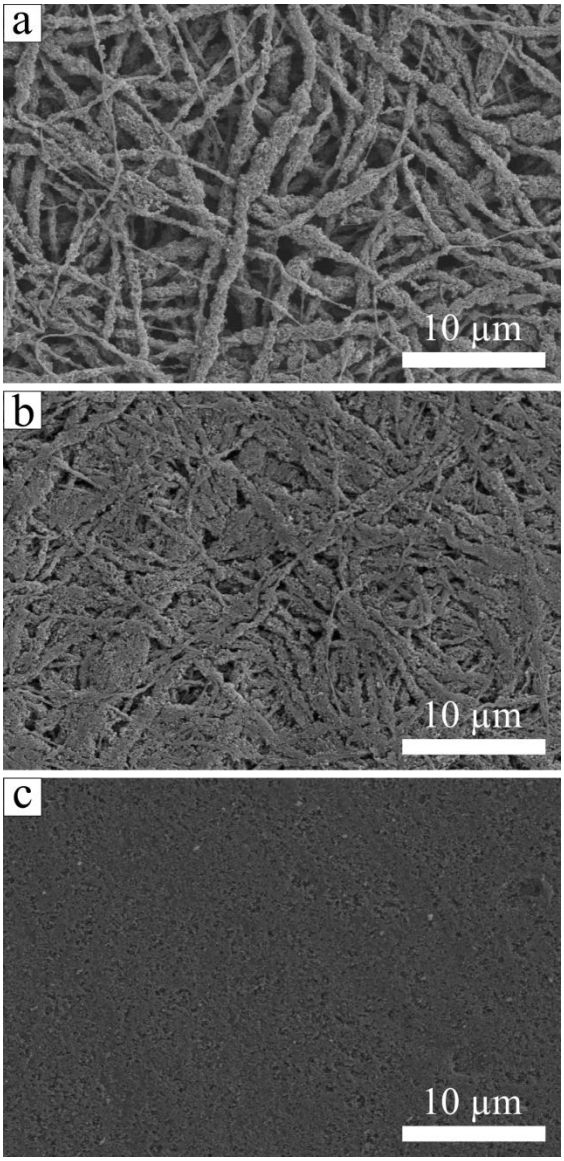

Figure 4.4. SEM images of electrospun C/PVDF nanofiber anodes with fiber volume fractions of (a) 0.39 and (b) 0.80 and (c) a slurry cast C/PVDF anode.

Cyclic voltammograms of a C/PVDF nanofiber anode are shown in Figure 4.5a. During initial scans, slight peak shifting occurred, but the voltammograms stabilized after 15 cycles with no changes during subsequent scans. A sloping baseline with a small peak (0.8 V) during lithiation and two broad peaks (0.3 and 1.0 V) during delithiation can be

seen, which is consistent with Takei et al.[27] who characterized carbon black anodes. Integrating the forward and reverse scans yields a coulombic efficiency of 98.0 %, which indicates good chemical reversibility of the lithiation reaction. Similar voltammograms were observed for electrospun anodes with fiber volume fractions ranging from 0.18 – 0.80 and for a slurry cast C/PVDF anode. The sloping baselines in the voltammograms of Figure 4.5a could be the result of a bulky electrical double layer at the electrode's surface. To determine the double layer capacitance of the nanofiber anodes, a Nyquist plot was generated through an electrochemical impedance experiment, and the results were fitted with a modified Randles circuit,[26] as shown in Figure 4.5b. The calculated double-layer capacitance was 4.8 mF, which is a typical value for LIB anodes.[28, 29] This result shows that no bulky electrical double layer is present, and the nanofiber anodes undergo electrochemical lithiation/ delithiation as expected.

The charge/discharge curves shown in Figure 4.6a provide further insights into the fundamental electrochemical characteristics of C/PVDF nanofiber anodes. The sloping profiles over 0.015 – 1.5 V indicate that lithiation/delithiation processes occurred over a wide potential range compared to graphite (typically < 0.5 V vs. Li/Li^+). Sloping charge/discharge curves for nongraphitized carbon anodes were reported by several groups[30-38] and are attributed to a distribution of site energies in the active material.[39] For the electrospun anodes, the shapes of the charge and discharge curves did not change with fiber volume fractions in the 0.18 – 0.80 range. These curves also match those reported by Tran et al.[40] who characterized several slurry cast carbon black anodes. At 0.1 C, the gravimetric capacity of the nanofiber anodes was 166 mAh g^{-1}, which corresponds to a carbon active material capacity of 255 mAh g^{-1}. This value is within the

range of capacities for various carbon blacks reported in the literature (197 – 346 mAh g^{-1})[40, 41] and is similar to but a bit lower than that achieved with carbon fiber anodes (e.g., ~ 290 mAh g^{-1} for a pyrolyzed electrospun PAN mat[17] when cycled between 0 – 1.5 V at ~ 0.18 C and ~ 200 mAh g^{-1} for a carbon fiber anode grown by chemical vapor deposition).[42] As expected, at higher charge/discharge rates, the C/PVDF nanofiber anode capacity decreased with greater separation between the lithiation and delithiation curves, owing to a combination of activation, ohmic, and concentration overpotentials within the cell.[43] Figure 4.6b shows the capacity is stable at charge/discharge rates up to 5 C.

Figure 4.6c shows the long-term performance of a C/PVDF nanofiber anode over several hundred cycles at 0.1 C. A low first cycle coulombic efficiency (30.3 %) is attributed to the formation of a solid-electrolyte interface (SEI) layer. Similar irreversible capacity losses for carbon black anodes were reported by several groups.[41, 44, 45] Despite this initial loss, the nanofiber anode had improved efficiencies during subsequent cycles (e.g., during the 2^{nd}, 10^{th}, and 50^{th} cycle, the coulombic efficiencies were 82.1, 96.3, and 99.4 %, respectively). The anode also exhibited outstanding electrochemical stability with 91.7 % capacity retention after 510 cycles at 0.1 C. Likewise, the nanofiber structure was physically stable in a battery environment; initial and post-mortem SEM images of an electrospun anode are shown in Figures 4.7a and 4.7b, respectively. Although an SEI layer was deposited on the fibers, the interfiber voids were wellmaintained during cycling.

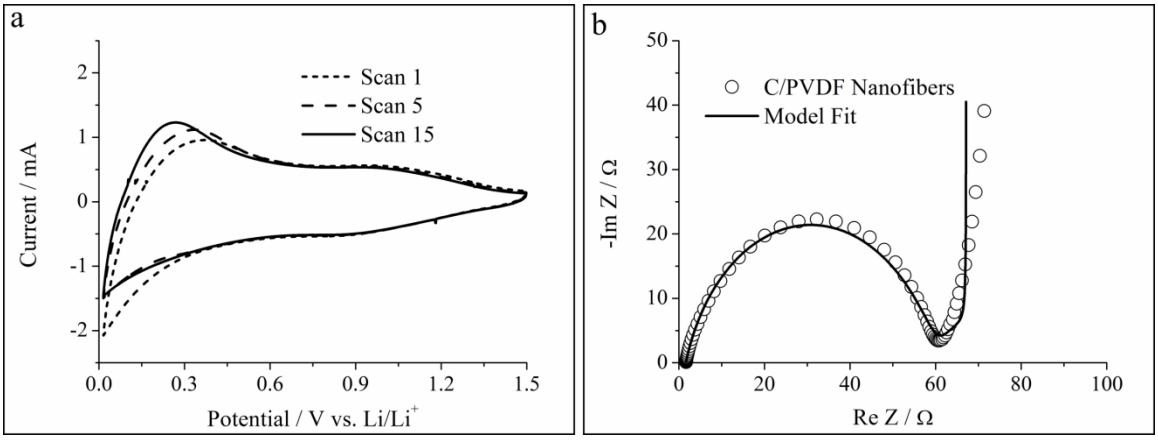

Figure 4.5. Electrochemical characterization of C/PVDF nanofiber anodes. (a) Cyclic voltammograms collected at a scan rate of 0.5 mV s^{-1} and (b) Nyquist plot showing experimental data and the fit for an equivalent circuit model.[26]

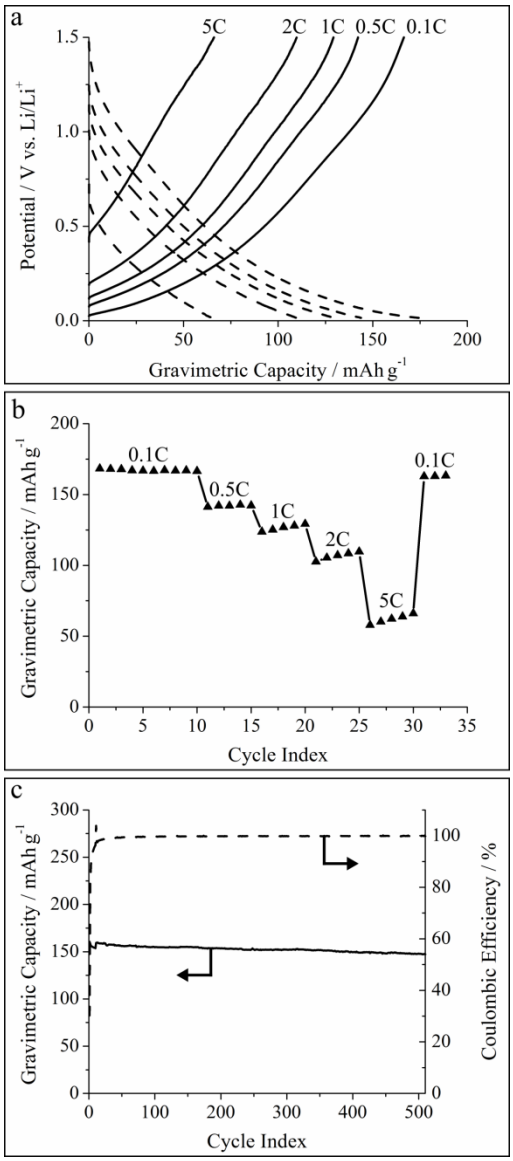

Figure 4.6. Electrochemical characterization of C/PVDF nanofiber anodes. (a) Charge/discharge curves at current densities corresponding to 0.1 – 5 C, (b) cycling stability at 0.1 – 5 C, and (c) long-term performance over 510 cycles at 0.1 C.

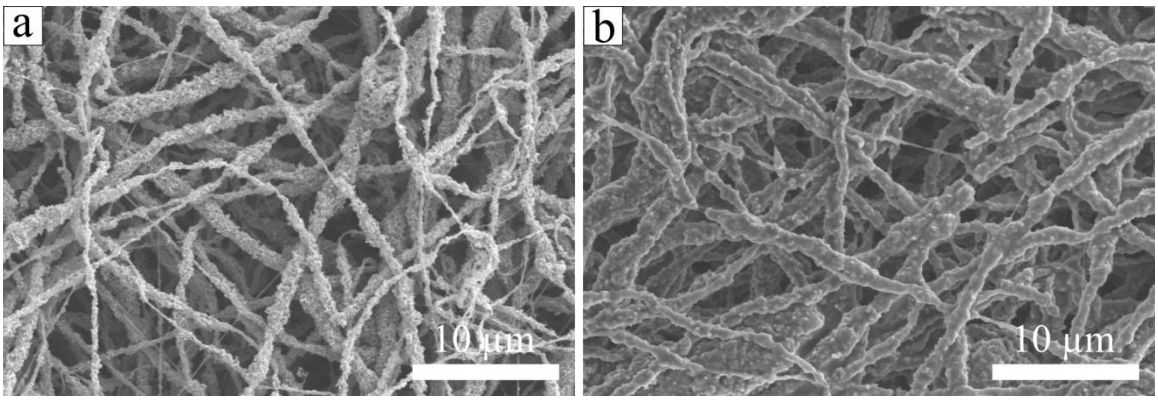

Figure 4.7. SEM images of a C/PVDF nanofiber anode containing a fiber volume fraction of 0.25 (a) before cycling and (b) after 510 cycles at 0.1 C.

Electrode performance metrics based on the electrode footprint and volume are underemphasized in the literature despite their importance for practical battery applications. Thus, a primary motivation of the current study was to evaluate how anode thickness and fiber volume fraction of a nanofiber mat affect performance. Figure 4.8a shows the dependence of volumetric capacity at 0.1 C on fiber volume fraction for five electrospun C/PVDF anodes. Nanofiber mats with a fiber volume fraction of 0.25 exhibited a very low volumetric capacity of 36 mAh cm^{-3} owing to the large interfiber void space. Volumetric capacity increased linearly with fiber volume fraction, which indicates that active material utilization was similar for all electrodes at a low charge/discharge rate. A highly compacted mat with a fiber volume fraction of 0.79 had a high volumetric capacity of 102 mAh cm^{-3} at 0.1 C, which is considerably higher than that of a slurry cast anode of the same composition (79 mAh cm^{-3}).

Figure 4.8b shows the effect of charge/discharge rate on the volumetric capacity of: (i) electrospun C/PVDF mats with a fiber volume fraction of 0.34. 0.61, or 0.79; (ii) a slurry cast C/PVDF anode of the same composition (shown in Figure 4.4c); and (iii) a

slurry cast graphite anode reported by Sivakkumar et al.[46] where the graphite particle size is larger than the carbon particles used in the present study (31 μm vs. 40 nm). The effect of fiber volume fraction on volumetric capacity is pronounced for nanofiber mats, up to a charge/discharge rate of ~ 2 C. The volumetric capacity at 2 C of a nanofiber electrode with a fiber volume fraction of 0.79 (55 mAh cm^{-3}) was twice that of the graphite anode and 67 % higher than that of the C/ PVDF slurry cast anode. As shown in Figure 4.8c, a highly compacted nanofiber anode also had excellent cycling stability, with 94 % capacity retention over 100 cycles at 2 C. The sharp peak around cycle 50 was caused by temporarily removing the cell from the battery tester. The excellent performance of C/ PVDF nanofiber anodes is attributed to the presence of intraand interfiber voids, which allow for electrolyte penetration and efficient Li^+ transport throughout the 3D fiber mat. Compared to conventional slurry cast anodes, the electrospun nanofiber anodes contain short Li^+ transport pathways from the liquid electrolyte to the carbon nanoparticles in the radial fiber direction.

In addition to high volumetric capacity, anodes must have high areal capacities at fast charge/discharge rates. Thick electrodes with high areal capacities are desired to reduce the amount of inactive components in a full cell (e.g., current collectors, separators, etc.). Figure 4.8d shows the areal capacity at charge/discharge rates up to 5 C for: (i) electrospun anodes with a fiber volume fraction of 0.34, 0.61, or 0.79 (thicknesses of 340, 190, and 140 μm, respectively); (ii) a slurry cast C/PVDF anode of the same composition (200 μm); and (iii) a slurry cast graphite anode reported by Sivakkumar et al.[46] (100 μm). All electrodes were prepared such that they had areal capacities of ~ 1.5 mAh cm^{-2} at 0.1 C. Nanofiber mats with fiber volume fractions of 0.61

and 0.79 exhibited similar areal capacities of 0.77 and 0.79 mAh cm^{-2} at 2 C. The electrospun anode with a fiber volume fraction of 0.34 had the best rate capabilities of all samples tested, with a reversible capacity of 1.12 mAh cm^{-2} at 2 C. In comparison, the slurry cast C/PVDF and graphite anodes had significantly lower capacities at 2 C (0.67 and 0.27 mAh cm^{-2}, respectively).

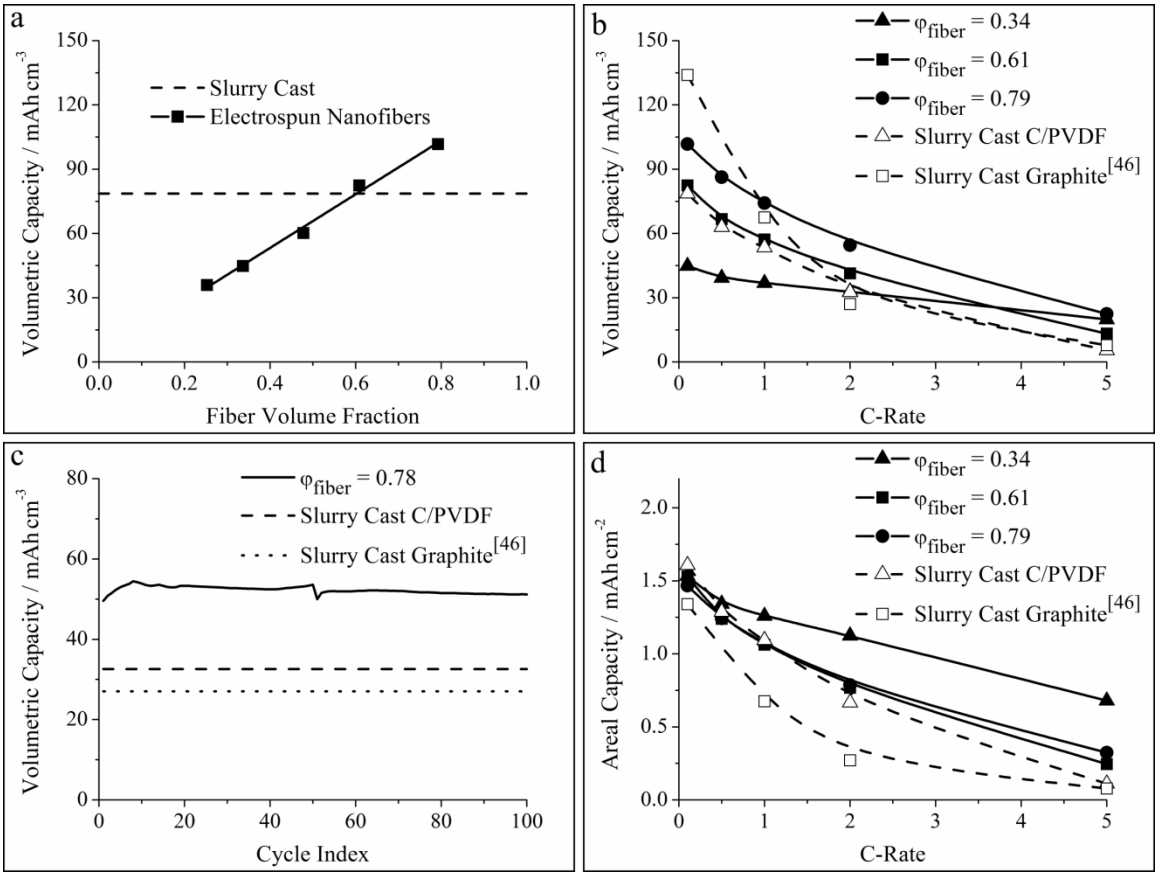

Figure 4.8. (a) Volumetric capacity at 0.1 C as a function of fiber volume fraction in the anode, (b) volumetric capacity at charge/discharge rates up to 5 C for electrospun and slurry cast anodes, (c) cycling stability at 2 C for a C/PVDF nanofiber anode, and (d) Areal capacity at charge/discharge rates (C-rate) up to 5 C for nanofiber and slurry cast anodes. φ_{fiber} refers to fiber volume fraction in (b) – (d).

It is known that the capacity of a carbon anode at high charge/discharge rates can be improved by utilizing smaller carbon particles. Thus the performance of a conventional slurry cast electrode containing a high surface area activated carbon (1400 m^2 g^{-1}, as compared to 254 m^2 g^{-1} for Vulcan XC-72R used in the previously discussed electrodes) was compared to that of a nanofiber anode containing Vulcan carbon. Figure 4.9 shows the areal capacity up to 5 C for: (i) C/PVDF slurry cast anodes, containing either Vulcan XC-72R or activated carbon as the active material and (ii) electrospun nanofibers containing Vulcan XC-72R with a fiber volume fraction of 0.34. All electrodes contained 65 wt % active material and 35 wt % PVDF binder. Whereas all three anodes exhibited similar areal capacities at 0.1 C (~ 1.5 mAh cm^{-2}), the electrospun material had the best rate capabilities at 2 C, with a capacity of 1.12 mAh cm^{-2}. The very poor performance of the activated carbon anode is attributed to its greater thickness and density (270 μm and 0.70 g cm^{-3}, respectively) relative to the Vulcan XC-72R slurry cast anode (200 μm and 0.52 g cm^{-3}, respectively). Thus, the activated carbon anode contained longer and more tortuous transport pathways that inhibited Li^+ diffusion/migration throughout the electrode's pores at fast charge/discharge rates. These results demonstrate that high surface area active materials do not necessarily improve the rate capabilities of slurry cast anodes, especially for thick electrodes where Li^+ transport in the electrolyte is rate limiting. In comparison, electrospun mats exhibit outstanding performance owing to the intra- and inter-fiber void space that cannot be emulated with traditional slurry cast materials. The results in Figures 4.8 and 4.9 suggest that an electrode's rate capabilities are controlled by Li^+ transport rates in the electrolyte phase throughout the void volume in a porous electrode. This conclusion is consistent

with our previous study on electrospun titania-based anodes[11] and indicates that composite nanofiber electrodes offer significant advantages over conventional slurry cast electrode materials. The results also show that high areal and volumetric capacities can be achieved with a relatively low gravimetric capacity anode material (like C/PVDF with 161 mAh g^{-1}) by preparing thick, densely packed nanofiber mats.

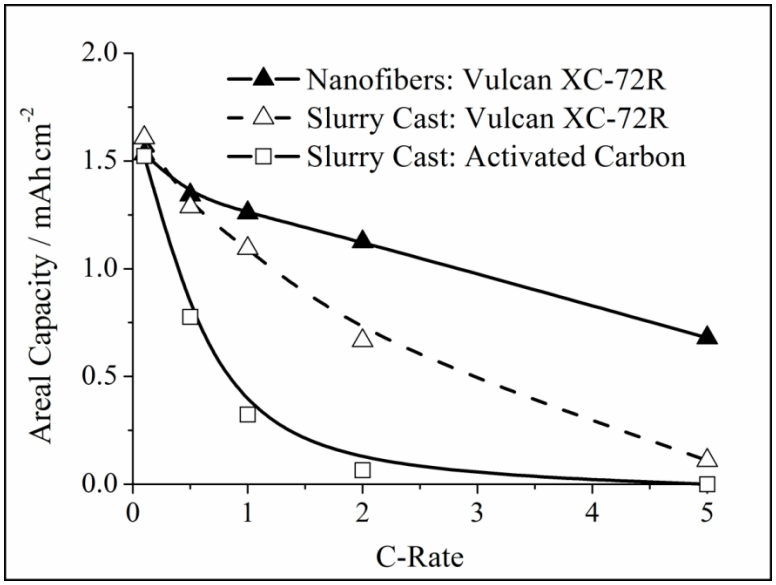

Figure 4.9. Rate capabilities of a nanofiber anode (fiber volume fraction = 0.34) compared to slurry cast anodes containing either Vulcan XC-72R or high surface area activated carbon as the active material. All anodes contained 65 wt % carbon nanoparticles and 35 wt % PVDF binder.

To investigate the effects of Li^+ transport rates on the rate capabilities of 3D electrospun anodes, the performance of nanofiber mats of different thicknesses was evaluated. Stacking of multiple electrospun mats was employed to expedite anode fabrication on a lab scale. For commercial manufacturing, electrospinning thick mats in a

single step using a roll-to-roll process might be more desirable (and cost effective), but the electrode performance of the two systems should be identical for a given mat thickness and fiber volume fraction. Four electrospun anodes each with a fiber volume fraction ~ 0.60 and a thickness ranging from 40 – 510 μm were characterized. Figure 4.10a shows that areal capacity at 0.1 C scaled linearly with anode thickness, indicating similar active material utilization for all samples at slow charge/discharge rates. The thicker electrodes, however, had lower capacities at high charge/discharge rates (as shown in Figure 4.10b, where the areal capacity of a 510 μm anode at 2 C was only 0.17 mAh cm^{-2} vs. 0.77 mAh cm^{-2} for a 190 μm anode). The lower capacity of the thick electrodes at fast charge/discharge rates is attributed to slower Li^+ ion transport, where Li^+ transport to the back of the anode (at points farthest from the separator) is rate limiting, even for nanofiber anodes with an interfiber void fraction of 0.40. Thus, Li^+ ions do not have adequate time to reach all active material sites before the cutoff potential is reached, resulting in lower active material utilization for thicker electrodes.[11, 12] This conclusion is consistent with a report by Fongy et al.[13] who studied the effects of electrode thickness and porosity on the rate capabilities of LiFePO4 cathodes. One must consider both fiber mat thickness and fiber volume fraction when optimizing areal capacity at fast charge/ discharge rates. To prove this point, two thick electrospun anodes with different fiber volume fractions were prepared and characterized. In these experiments, the fiber volume fraction was either 0.42 or 0.63, and the thickness was either 820 or 510 μm, respectively. Note that the more porous anode had to be made thicker to achieve the same carbon loading. As shown in Figure 4.10c, both anodes had similar areal capacities at 0.1 C (~ 4 mAh cm^{-2}), but the more porous nanofiber anode had

higher capacities at charge/discharge rates ≥ 0.5 C. At 2 C, the areal capacity of the anode with a fiber volume fraction of 0.42 was 4-times greater than that of the anode with a fiber volume fraction of 0.63 (0.70 vs. 0.17 mAh cm^{-2}).

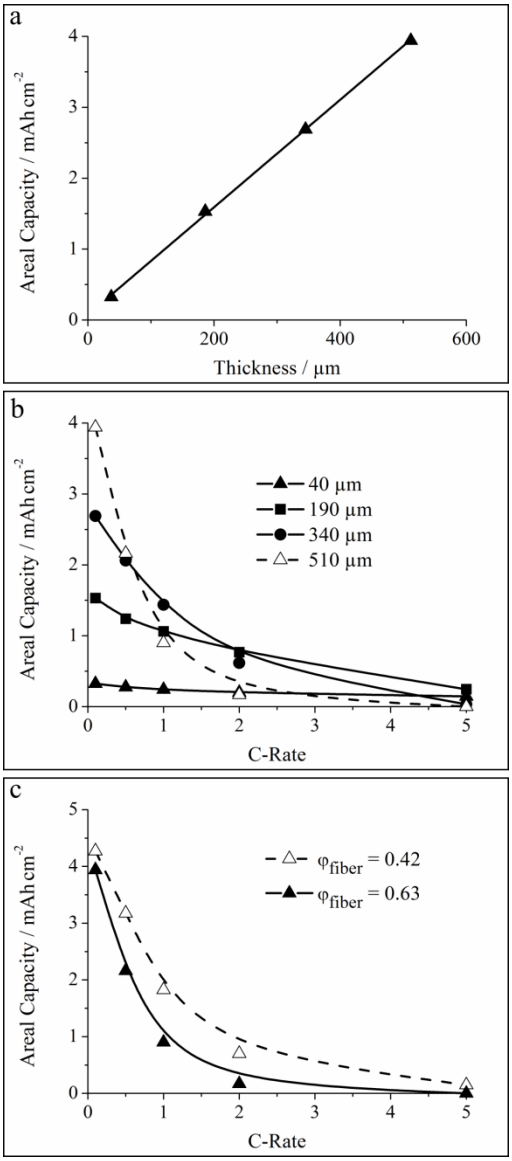

Figure 4.10. (a) Areal capacity at 0.1 C as a function of anode thickness for electrospun anodes containing fiber volume fractions of 0.59 – 0.66, (b) rate capabilities of electrospun anodes containing fiber volume fractions of 0.59 – 0.66 and thicknesses up to 510 µm, and (c) rate capabilities of thick electrospun anodes containing fiber volume fractions (φ_{fiber}) of 0.42 and 0.63 and thicknesses of 820 and 510 µm, respectively.

4.4 Conclusions

Particle/polymer electrospinning is used to prepare high performance anodes containing carbon nanoparticles and a poly(vinylidene fluoride) binder (C/PVDF) for LIBs. By utilizing electronically conductive carbon nanoparticles as the Li host, high active material loadings (65 wt %) and high gravimetric capacities (161 mAh g^{-1} at 0.1 C, 1 C = 372 mA g_C^{-1}) were achieved. The nanofiber anodes exhibited excellent electrochemical stability with 91.7 % capacity retention after 510 cycles at 0.1 C. Furthermore, the nanofiber morphology was structurally stable during charge/discharge processes, and the interfiber voids were well-maintained during cycling.

Whereas anodes produced using many nanofabrication schemes (e.g., nanowires, carbon nanofibers, etc.) are restricted to low areal and/or volumetric capacities, particle/polymer electrospinning does not have these limitations. Mechanical compaction was used to increase the fiber volume fraction and volumetric capacity of the nanofiber mats. At a 0.1 C charge/discharge rate, a highly densified nanofiber mat with a fiber volume fraction of 0.79 exhibited a volumetric capacity of 102 mAh cm^{-3}. Furthermore, highly compacted electrospun anodes had excellent rate capabilities with a stable volumetric capacity of 55 mAh cm^{-3} at 2 C which is 67 % greater than that of a slurry cast C/PVDF anode (33 mAh cm^{-3}) and twice that of a graphite anode (27 mAh cm^{-3}).

Particle/polymer electrospinning was also used to prepare thick anodes with high areal capacities, up to 4.3 mAh cm^{-2} at 0.1 C. The rate capabilities of thick electrodes were significantly improved by increasing the interfiber void volume in the nanofiber mat. An anode containing a fiber volume fraction of 0.42 had a 4-fold higher areal

capacity at 2 C as compared to an anode mat with a volume fraction of 0.63 (0.70 and 0.17 mAh cm^{-2}, respectively).

Particle/polymer electrospinning is a robust platform for the preparation of high performance LIB anodes with high gravimetric, volumetric, and areal capacities. The method can accommodate new active materials and polymer binders as they are developed. The excellent performance of the C/PVDF nanofiber anodes is attributed to the intra- and interfiber void space, which allows for good electrolyte uptake and efficient Li^+ transport from the electrolyte to active material nanoparticles in the radial fiber direction. The results show that proper electrode design on the micron-scale level can enhance Li^+ transport rates and improve the performance of a LIB.

4.5 References

[1] P. N. Pintauro, *Polym. Rev.* **2015**, *55*, 201.
[2] M. Armand, J.-M. Tarascon, *Nature* **2008**, *451*, 652.
[3] G. Liu, H. Zheng, A. S. Simens, A. M. Minor, X. Song, V. S. Battaglia, *J. Electrochem. Soc.* **2007**, *154*, A1129.
[4] S. K. Martha, J. O. Kiggans, J. Nanda, N. J. Dudney, *J. Electrochem. Soc.* **2011**, *158*, A1060.
[5] X.-L. Huang, R.-Z. Wang, D. Xu, Z.-L. Wang, H.-G. Wang, J.-J. Xu, Z. Wu, Q.-C. Liu, Y. Zhang, X.-B. Zhang, *Adv. Funct. Mater.* **2013**, *23*, 4345.
[6] H.-G. Wang, S. Yuan, D.-L. Ma, X.-B. Zhang, J.-M. Yan, *Energy Environ. Sci.* **2015**, *8*, 1660.
[7] X. L. Huang, D. Xu, S. Yuan, D. L. Ma, S. Wang, H. Y. Zheng, X. B. Zhang, *Adv. Mater.* **2014**, *26*, 7264.
[8] H. G. Wang, D. L. Ma, Y. Huang, X. B. Zhang, *Chem. Eur. J.* **2012**, *18*, 8987.
[9] S. Yuan, X. L. Huang, D. L. Ma, H. G. Wang, F. Z. Meng, X. B. Zhang, *Adv. Mater.* **2014**, *26*, 2273.
[10] N. Nitta, G. Yushin, *Part. Part. Syst. Char.* **2014**, *31*, 317.
[11] E. C. Self, R. Wycisk, P. N. Pintauro, *J. Power Sources* **2015**, *282*, 187.
[12] M. Singh, J. Kaiser, H. Hahn, *J. Electrochem. Soc.* **2015**, *162*, A1196.
[13] C. Fongy, A. C. Gaillot, S. Jouanneau, D. Guyomard, B. Lestriez, *J. Electrochem. Soc.* **2010**, *157*, A885.
[14] W. Zhang, P. N. Pintauro, *ChemSusChem* **2011**, *4*, 1753.
[15] M. Brodt, R. Wycisk, P. N. Pintauro, *J. Electrochem. Soc.* **2013**, *160*, F744.
[16] M. Brodt, T. Han, N. Dale, E. Niangar, R. Wycisk, P. Pintauro, *J. Electrochem. Soc.* **2014**, *162*, F84.
[17] B. Zhang, Y. Yu, Z.-L. Xu, S. Abouali, M. Akbari, Y.-B. He, F. Kang, J.-K. Kim, *Adv. Energy Mater.* **2014**, *4*, 1301448.
[18] Y. Wu, M. V. Reddy, B. V. Chowdari, S. Ramakrishna, *ACS Appl. Mater. Interfaces* **2013**, *5*, 12175.
[19] X.-H. Qin, D.-P. Xin, *Fiber Polym.* **2010**, *11*, 632.
[20] H. Hou, D. H. Reneker, *Adv. Mater.* **2004**, *16*, 69.
[21] A. Park, F. Turley, R. Wycisk, P. Pintauro, *J. Electrochem. Soc.* **2015**, *162*, F560.
[22] E. Zussman, X. Chen, W. Ding, L. Calabri, D. A. Dikin, J. P. Quintana, R. S. Ruoff, *Carbon* **2005**, *43*, 2175.
[23] S. N. Arshad, M. Naraghi, I. Chasiotis, *Carbon* **2011**, *49*, 1710.
[24] M. Faccini, G. Borja, M. Boerrigter, D. Morillo Martín, S. Martìnez Crespiera, S. Vázquez-Campos, L. Aubouy, D. Amantia, *J. Nanomater.* **2015**, *2015*, 1.
[25] S. H. Kim, S. Y. Jeon, P. J. Yoo, L. S. Pu, J. Y. Lee, *Fiber Polym.* **2014**, *14*, 1975.
[26] J. Bisquert, G. Garcia-Belmonte, P. Bueno, E. Longo, L. O. S. Bulhões, *J. Electroanal. Chem.* **1998**, *452*, 229.
[27] K. Takei, N. Terada, K. Kuma, T. Iwahori, T. Uwai, T. Miura, *J. Power Sources* **1995**, *55*, 191.
[28] L. Li, A. R. Raji, J. M. Tour, *Adv. Mater.* **2013**, *25*, 6298.
[29] M. V. Reddy, G. Prithvi, K. P. Loh, B. V. Chowdari, *ACS Appl. Mater. Interfaces* **2014**, *6*, 680.

[30] L. Ji, Y. Yao, O. Toprakci, Z. Lin, Y. Liang, Q. Shi, A. J. Medford, C. R. Millns, X. Zhang, *J. Power Sources* **2010**, *195*, 2050.
[31] X.-B. Cheng, Q. Zhang, H.-F. Wang, G.-L. Tian, J.-Q. Huang, H.-J. Peng, M.-Q. Zhao, F. Wei, *Catal. Today* **2015**, *249*, 244.
[32] M. Kim, D. Y. Kim, Y. Kang, O. O. Park, *RSC Adv.* **2015**, *5*, 3299.
[33] R. Mei, X. Song, Y. Hu, Y. Yang, J. Zhang, *Electrochim. Acta* **2015**, *153*, 540.
[34] S. Petnikota, N. K. Rotte, M. V. Reddy, V. V. Srikanth, B. V. Chowdari, *ACS Appl. Mater. Interfaces* **2015**, *7*, 2301.
[35] K. R. Saravanan, N. Kalaiselvi, *Carbon* **2015**, *81*, 43.
[36] Z. Sun, X. Song, P. Zhang, L. Gao, *RSC Adv.* **2015**, *5*, 3657.
[37] S. Wang, Y. Xing, C. Xiao, X. Wei, H. Xu, S. Zhang, *RSC Adv.* **2015**, *5*, 7959.
[38] H. Zhang, X. Sun, X. Zhang, H. Lin, K. Wang, Y. Ma, *J. Alloys Compd.* **2015**, *622*, 783.
[39] J. R. Dahn, R. Fong, M. J. Spoon, *Phys. Rev. B* **1990**, *42*, 6424.
[40] T. D. Tran, J. H. Feikert, *J. Electrochem. Soc.* **1995**, *142*, 3297.
[41] D. Molina Piper, S.-B. Son, J. J. Travis, Y. Lee, S. S. Han, S. C. Kim, K. H. Oh, S. M. George, S.-H. Lee, C. Ban, *J. Power Sources* **2015**, *275*, 605.
[42] H. Kim, X. Huang, X. Guo, Z. Wen, S. Cui, J. Chen, *ACS Appl. Mater. Interfaces* **2014**, *6*, 18590.
[43] D. Danilov, R. A. H. Niessen, P. H. L. Notten, *J. Electrochem. Soc.* **2011**, *158*, A215.
[44] L. Fransson, T. Eriksson, K. Edström, T. Gustafsson, J. O. Thomas, *J. Power Sources* **2001**, *101*, 1.
[45] F. La Mantia, R. A. Huggins, Y. Cui, *J. Appl. Electrochem.* **2012**, *43*, 1.
[46] S. R. Sivakkumar, J. Y. Nerkar, A. G. Pandolfo, *Electrochim. Acta* **2010**, *55*, 3330.

CHAPTER V

$LiCoO_2$-BASED FIBER CATHODES FOR ELECTROSPUN FULL CELL LI-ION BATTERIES

Adapted from E. C. Self, E. C. McRen, R. Wycisk, P. N. Pintauro, *Electrochim. Acta* **2016**, *214*, 139 with permission from Elsevier.

5.1 Introduction

Despite their extraordinary commercial success, Li-ion batteries (LIBs) do not meet the performance expectations of many end users, especially when these batteries limit the functionality of portable electronic devices and electric vehicle propulsion systems.[1-3] New electrode materials and designs must be developed to produce LIBs that can be recharged quickly while providing high energy density and long cycle life. To this end, researchers have largely focused their efforts on developing battery electrodes with high gravimetric capacity, but such studies often miss an important point that an electrode's areal and volumetric capacities at high C-rates are critical for most practical battery applications. Normalizing electrode performance only with respect to mass conceals important limitations when thin electrodes with low densities of active material are utilized.

Electrodes with high areal capacities are desired to increase the ratio of active material to inactive components (e.g., current collectors, separators, etc.) in a cell; similarly, high volumetric capacities allow batteries of a given size to store more

energy.[4-7] High areal and volumetric capacities can be achieved at slow charge/discharge rates with thick, highly densified slurry cast electrodes, but such electrodes often exhibit poor performance at high C-rates due to Li^+ transport limitations in the electrode depth direction.[8-11] To fully assess the applicability of new LIB electrode materials for practical devices, gravimetric, areal, and volumetric capacities must all be evaluated at both slow and fast charge/discharge rates.

The present manuscript represents the latest installment by Pintauro and coworkers on the use of electrospun particle/polymer nanofiber mat electrodes for fuel cells and batteries.[6, 7, 12-14] We previously reported on the preparation and characterization of two fiber mat LIB anodes containing either: (i) titania nanoparticles, carbon powder, and poly(acrylic acid) (TiO_2/C/PAA)[6] (Chapter III) or (ii) carbon powder and poly(vinylidene fluoride) (C/PVDF)[7] (Chapter IV). These studies showed that thick nanofiber electrodes with a high fiber volume fraction (defined as the ratio of the measured mat density to the density of a mat containing no interfiber voids) could be prepared with high areal and volumetric capacities at fast charge/discharge rates, where the capacity was stable over several hundred cycles. For example, a 1.0 mm thick TiO_2/C/PAA anode exhibited an areal capacity of 1.3 mAh cm^{-2} at 2 C. Likewise, a C/PVDF anode exhibited a stable volumetric capacity of 55 mAh cm^{-3} at 2 C, which is twice that of a conventional slurry cast graphite anode.[15] The excellent performance of the electrospun fiber mats is attributed to: (i) a large electrode/electrolyte interfacial area, (ii) short Li^+ transport pathways between the electrolyte and active material in the radial fiber direction, and (iii) good electrolyte infiltration throughout the intra- and interfiber void space of the fiber mat. Our published work on electrospun particle/polymer battery

electrodes has thus far focused on the anode[6, 7], whereas the present paper deals with an electrospun fiber mat cathode containing $LiCoO_2$ and carbon powder in a poly(vinylidene fluoride) (PVDF) binder.

Slurry cast $LiCoO_2$ cathodes are widely used in commercial LIBs due to their high energy density and good cycle life.[1, 16] Electrospun cathodes with a carefully engineered void space (i.e., intra- and interfiber porosity) could improve $LiCoO_2$ cathode performance in the same way a fiber morphology improved carbon and titania-based anodes, especially at high C-rates where performance is limited by Li^+ transport.[16, 17] Several groups[18-23] have reported on the use of electrospun $LiCoO_2$ cathodes where the fibers were prepared through sol-gel chemistry and high temperature pyrolysis. The $LiCoO_2$ nanofiber cathodes were tested as either freestanding nanofiber mats[18-21] or in slurry cast electrodes[22, 23] containing a mixture of $LiCoO_2$ nanofibers, carbon powder, and polymer binder. In general, the performance of these $LiCoO_2$ nanofiber cathodes in LIB half cells was very good, with reversible capacities of 127 – 182 mAh g^{-1} at low C-rates (e.g., 0.07 – 0.25 C) and 85 – 108 mAh g^{-1} at high C-rates (1.5 – 10 C). The areal and volumetric capacities of these cathodes were not discussed, but scanning electron microscopy (SEM) images showed the electrospun mats had very low fiber volume fractions (< 0.25), suggesting that freestanding fiber mat electrodes had low volumetric energy densities.

In the present paper, we improve upon the performance of previous work on electrospun and slurry cast $LiCoO_2$ cathodes by utilizing a particle/polymer electrospun fiber mat cathode which contains: (i) a high loading of $LiCoO_2$ nanoparticles, (ii) carbon powder for electrical conduction, and (iii) a PVDF binder. The polymer binder is retained

in the fibers after electrode fabrication which allows the mats to be compacted to high fiber volume fractions. The binder also absorbs some electrolyte which provides fast Li^+ transport in the radial fiber direction. The $LiCoO_2$/C/PVDF nanofiber cathodes were characterized in half cells using a Li metal counter/reference electrode and in full cells containing an electrospun nanofiber anode prepared with carbon powder and PVDF. The full cell results represent the first ever use of a paired electrospun particle/polymer cathode and anode in a LIB.

5.2 Experimental

$LiCoO_2$ nanoparticles were synthesized from a Co_3O_4 nanoparticle precursor using a sonochemical method adapted from the literature.[24, 25] A dispersion containing Co_3O_4 nanoparticles (10 – 50 nm, US Research Nanomaterials, Inc.) and $LiOH{\cdot}H_2O$ (Sigma-Aldrich) in methanol was prepared, where the Co_3O_4/LiOH molar ratio was 1/20 and the total solids content was 15 wt %. A Co_3O_4/LiOH molar ratio of 1/20 was used to ensure complete conversion of Co_3O_4 to $LiCoO_2$. The dispersion was stirred for 10 min followed by sonication for 60 minutes. Co_3O_4/LiOH particles were collected by centrifugation and then heated in air for 3 h at 700 °C to form $LiCoO_2$ nanoparticles via a solid-state reaction. After heating, the $LiCoO_2$ nanoparticles were washed several times with deionized water and methanol. Co_3O_4 and $LiCoO_2$ particle size was assessed using transmission electron microscopy (FEI Tecnai Osiris TEM). The crystal structure of Co_3O_4 and $LiCoO_2$ nanoparticles was determined by x-ray diffraction (XRD, Scintag XGEN-4000) and Raman spectroscopy (Renishaw inVia Raman microscope with a

532 nm wavelength laser source). Rietveld refinement[26] of the XRD pattern for $LiCoO_2$ was performed with FullProf Suite software[27] using a least squares fitting model.

Cathode inks were prepared by mixing the $LiCoO_2$ nanoparticles with carbon black (Vulcan XC-72R, Fuel Cell Store) and poly(vinylidene fluoride) (PVDF, HSV-900, Arkema Inc.) in a solvent containing 7/3 dimethylformamide/acetone (w/w). The ratio of $LiCoO_2$/C/PVDF in the cathodes was fixed at 70/10/20 unless otherwise indicated. Cathodes were prepared by either conventional slurry casting or electrospinning a fiber mat. The slurry cast cathodes were cast onto aluminum foil and dried at ambient conditions. Fiber mat cathodes were prepared using a single needle spinneret and the custom rotating drum electrospinning apparatus described in Chapter IV.[7] Mats were spun onto an aluminum foil substrate at the following conditions: (i) 0.75 mL h^{-1} solution flow rate, (ii) 15 kV bias voltage, (iii) 8.0 cm spinneret-to-collector distance, and (iv) 60 – 75 % relative humidity. The morphologies of electrospun and slurry cast cathodes were assessed using scanning electron microscopy (Hitachi S4200 SEM) after gold sputtering for 90 s.

Thick, densely packed $LiCoO_2$/C/PVDF fiber mat cathodes were prepared by stacking multiple as-spun mats followed by mechanically compacting the mats on a hydraulic press at a pressure of 1 – 20 MPa for 40 s. The fiber volume fraction of an electrospun mat was calculated as the ratio of the measured mat density to the density of a hypothetical mat containing no interfiber voids. The density of the latter was determined to be 1.71 ± 0.02 g cm^{-3} based on analysis of SEM images as described in Chapter IV.[7] This experimentally determined density is lower than the theoretical density of a zero porosity mat (3.25 g cm^{-3}) which was calculated using the fiber

composition and the densities of $LiCoO_2$, carbon black, and PVDF. Thus, the internal porosity of an electrospun fiber was estimated to be 0.47.

CR2032 half cells were constructed in an argon-filled glovebox using an electrospun or slurry cast cathode disk (10 mm in diameter, dried overnight at 150 °C under vacuum) and a Li metal counter/reference electrode. The electrolyte was 1.0 M $LiPF_6$ in a mixture of ethylene carbonate, dimethyl carbonate, and diethyl carbonate (1:1:1 by volume, MTI Corp.). Two sheets of Celgard 2500 soaked in the electrolyte were used as a membrane separator. Several drops of electrolyte were added to completely fill the cell volume. Cells were crimped at 1,000 psi and rested for at least 2 h before electrochemical characterization.

The half cells were characterized using cyclic voltammetry by polarizing the cells from 2.75 – 4.20 V at a scan rate of 0.1 mVs^{-1} using a Gamry Reference 3000. Galvanostatic charge/discharge experiments were conducted between 2.75 – 4.20 V at current densities ranging from 0.1 – 2 C. Cells were cycled a minimum of 5 times at each current density to ensure stable performance. Charge/discharge experiments at 0.1 C were performed on an 8 channel battery tester (5 V/1 mA, MTI Corp.). A Gamry Reference 3000 was used for charge/discharge cycling at high rates (0.5 – 2 C). Selected cells were disassembled after cycling, and the cathodes were rinsed with diethyl carbonate before post-mortem SEM image analysis was performed. C-rates reported for the half cells are based on a theoretical capacity of 274 mAh $g_{LiCoO_2}^{-1}$. Except where otherwise indicated, half cell capacities are normalized with respect to the entire composite cathode (i.e., total amounts of $LiCoO_2$, carbon, and PVDF).

CR2032 full cells containing a $LiCoO_2$/C/PVDF nanofiber cathode and C/PVDF nanofiber anode were assembled and evaluated. Electrospun C/PVDF anodes were prepared as previously reported.[7] The full cells contained the same electrolyte and separator as used in half cells. To minimize the irreversible capacity loss in the full cells, the $LiCoO_2$/C/PVDF cathodes and C/PVDF anodes were preconditioned in half cells for 10 cycles at 0.1 C, as has been done in other studies.[28-37] Full cells were also prepared with slurry cast electrodes of the same $LiCoO_2$/C/PVDF and C/PVDF compositions as the nanofiber mats. The cathode/anode mass ratio in all full cells was ~ 1.90 to ensure good capacity matching of the electrodes (N/P capacity ratios of 0.91 ± 0.03).

Full cells were characterized using galvanostatic charge/discharge cycling between 2.50 – 4.20 V at 0.1 – 2 C. C-rates for the full cells were based on the measured capacity of the cathode. Full cell capacities were normalized with respect to both electrodes (i.e., the combined amounts of the $LiCoO_2$/C/PVDF cathode and C/PVDF anode). During the self-discharge experiments, the full cells were charged to 4.20 V at 0.1 C, rested at open-circuit for 1 week, and then discharged to 2.50 V at 0.1 C.

At least two coin cells were tested for each sample to assess the reproducibility of the half cell and full cell experiments in this study. The electrochemical performance of each sample was reproducible within approximately 15 – 20 % among independent coin cell tests.

5.3 Results and Discussion

The desired $LiCoO_2$ particle size for electrospun fibers is < 1 μm, but since such nanoparticles were not commercially available, they were synthesized from a Co_3O_4

precursor using a procedure from the literature.[24, 25] Figure 5.1a shows a transmission electron microscopy (TEM) image of the as-received Co_3O_4 nanoparticles which ranged in size from 10 – 90 nm. After mixing with LiOH and heating in air at 700 °C for 3 h, the Co_3O_4 was converted into $LiCoO_2$ nanoparticles with diameters ranging from 270 – 980 nm (Figure 5.1b) which were acceptable for electrospinning. As an alternative synthesis method, $LiCoO_2$ nanoparticles were also prepared using a sol-gel reaction as described in Appendix A. However, these sol-gel derived particles had an undesired fused structure which was not suitable for electrospinning and thus were not further investigated in the present study.

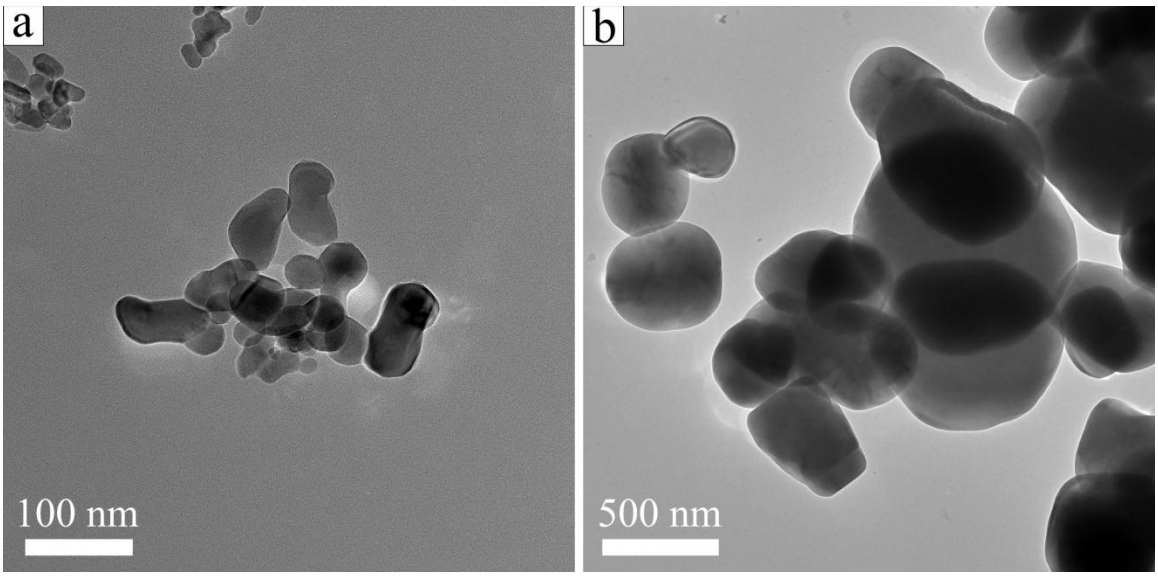

Figure 5.1. TEM images of (a) as-received Co_3O_4 nanoparticles and (b) synthesized $LiCoO_2$ nanoparticles.

The crystal structure of $LiCoO_2$ particles was determined using x-ray powder diffraction (XRD) and Raman spectroscopy. XRD patterns of the as-received Co_3O_4 and

synthesized $LiCoO_2$ nanoparticles are shown in Figure 5.2a. The diffractogram of $LiCoO_2$ contained well-defined peaks characteristic of a trigonal $R\bar{3}m$ structure which is consistent with: (i) previous reports on $LiCoO_2$ electrodes[38, 39] and (ii) the $LiCoO_2$ JCPDS powder diffraction file. The $LiCoO_2$ diffraction pattern contained no peaks at 2θ values of 31° or 56°, indicating complete conversion of Co_3O_4. Figure 5.2b shows the results of a Rietveld refinement[26] performed on the $LiCoO_2$ XRD pattern. Good agreement between the experimental data and fitted model were obtained (χ^2 = 1.473); the calculated unit cell parameters, a = b = 2.8189 Å and c = 14.0854 Å, are consistent with previous reports on $LiCoO_2$.[40, 41] Raman spectra of the Co_3O_4 and $LiCoO_2$ nanopowders, shown in Figure 5.2c, also confirmed the presence of the desired $LiCoO_2$ crystal structure. The two bands at 472 and 585 cm^{-1} for $LiCoO_2$ correspond to the Raman modes E_g and A_{1g}, respectively.[42-44] The absence of a large band at 676 cm^{-1} confirmed complete conversion of the Co_3O_4 into $LiCoO_2$.

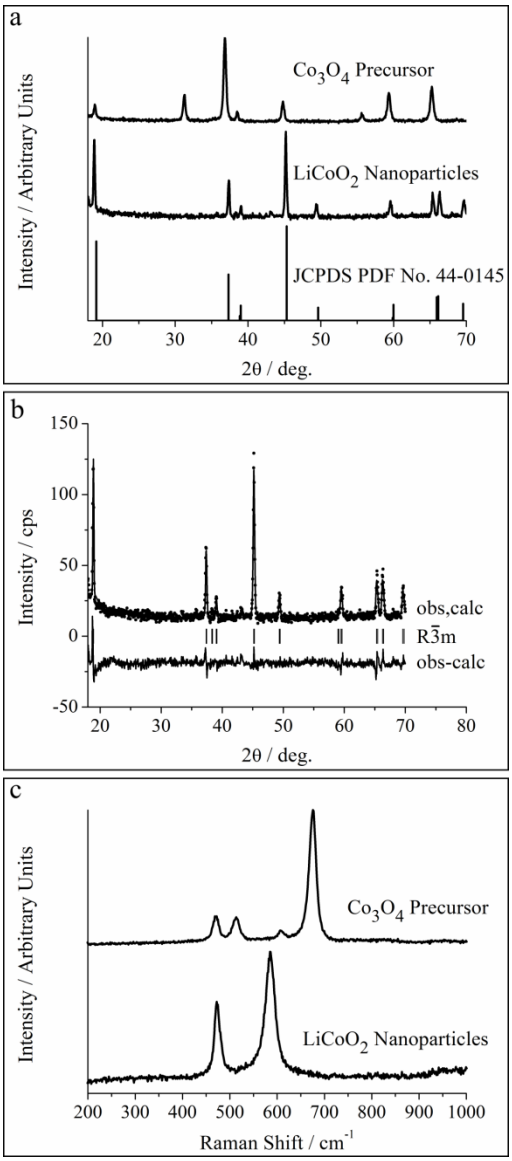

Figure 5.2. (a) XRD patterns for the as-received Co_3O_4 and synthesized $LiCoO_2$ nanoparticles, (b) Rietveld refinement of the XRD pattern for the $LiCoO_2$ nanoparticles, and (c) Raman spectra for Co_3O_4 and $LiCoO_2$ nanoparticles.

A number of electrospun fiber mat cathodes containing $LiCoO_2$ nanoparticles, carbon black, and poly(vinylidene fluoride) (PVDF) with a fixed fiber composition ($LiCoO_2$/C/PVDF weight ratio of 70/10/20) were fabricated. A scanning electron

microscopy (SEM) image of an as-spun fiber mat with a fiber volume fraction of 0.25 and an average fiber diameter of 1.3 μm is shown in Figure 5.3a. The fiber volume fraction of the mat was increased by application of an appropriate hydraulic pressure (1 – 20 MPa) for 40 s. Top down SEM images of compacted $LiCoO_2$/C/PVDF fiber mats with fiber volume fractions of 0.65 and 0.85 are shown in Figures 5.3b and 5.3c, respectively. The highly compacted sample in Figure 5.3c shows merging of individual fibers, but all electrospun samples retained some interfiber void space after compaction. For comparison, a slurry cast cathode of the same composition as the electrospun fiber mats (70/10/20 $LiCoO_2$/C/PVDF by weight) had a dense structure with few visible voids, as shown in Figure 5.3d.

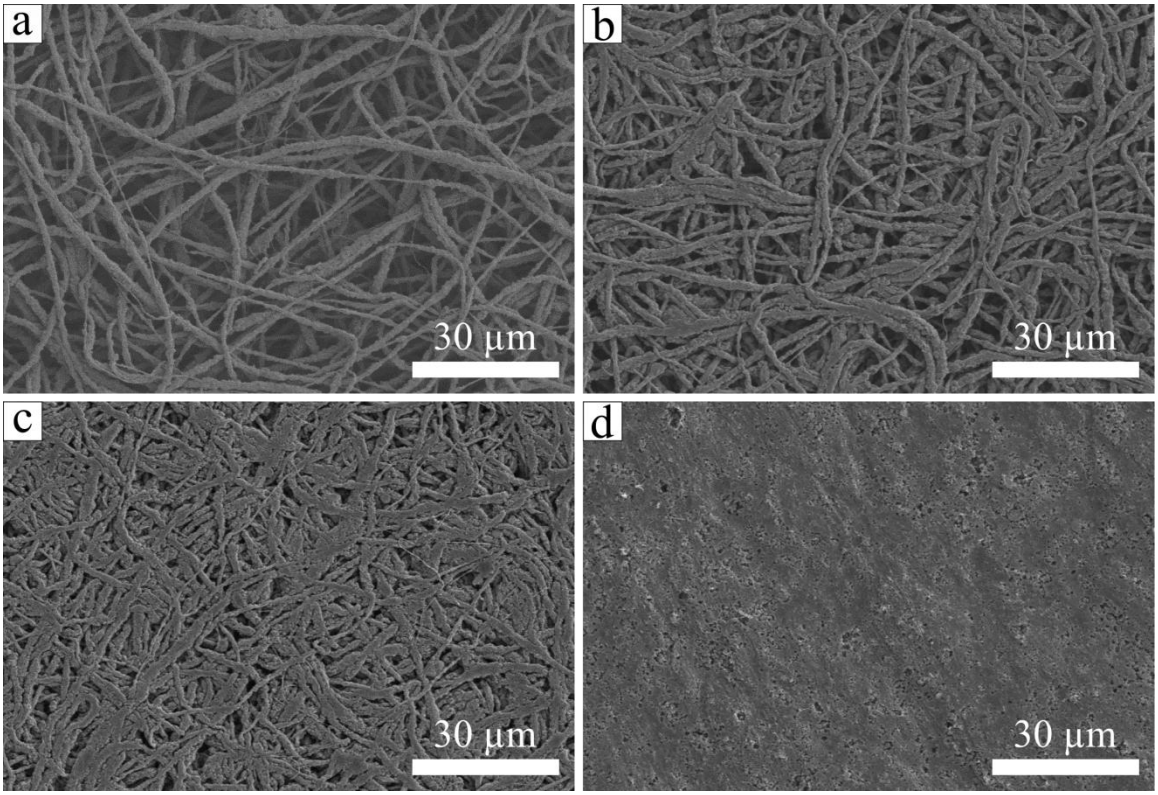

Figure 5.3. SEM images of $LiCoO_2$/C/PVDF cathodes. (a) An as-spun fiber mat with a fiber volume fraction of 0.25, compacted fiber mats with fiber volume fractions of (b) 0.65 and (c) 0.85, and (d) a slurry cast cathode. All electrodes contained $LiCoO_2$/C/PVDF in a 70/10/20 weight ratio.

A cyclic voltammogram (CV) of an electrospun $LiCoO_2$/C/PVDF fiber mat cathode with a fiber volume fraction of 0.24 in a half cell is shown in Figure 5.4a. The peaks at 3.99 and 3.82 V vs. Li/Li^+ correspond to delithiation and lithiation of the $LiCoO_2$ active material, respectively. Integrating the anodic and cathodic scans yielded a coulombic efficiency of 97 %, indicating good chemical reversibility of the lithium storage reaction. The shape of this voltammogram is consistent with previous reports on $LiCoO_2$ cathodes.[45, 46] Thus, the synthesized $LiCoO_2$ nanoparticles undergo

delithiation/lithiation redox reactions as expected, and electrospinning does not alter the fundamental electrochemical properties of $LiCoO_2$.

Charge/discharge curves at 0.1 – 2 C for an electrospun $LiCoO_2$/C/PVDF fiber mat cathode in a half cell are shown in Figure 5.4b. Voltage plateaus near 3.9 V vs. Li/Li^+ correspond to delithiation/lithiation of the $LiCoO_2$ active material.[39, 47-50] At 0.1 C, the reversible capacity of the electrospun fibers was 90 mAh g^{-1} (corresponding to 128 mAh $g_{LiCoO_2}^{-1}$ when normalized to the active material mass) which agrees well with previous studies on $LiCoO_2$ cathodes, where reported capacities range from 110 – 140 mAh $g_{LiCoO_2}^{-1}$.[39, 47-50] At higher C-rates, the electrospun fibers exhibited lower capacities and greater separation between the charge and discharge curves due to activation, ohmic, and concentration overpotentials within the cell. Appendix B compares the rate capabilities of the electrospun $LiCoO_2$/C/PVDF fiber mat cathodes with that of the TiO_2/C/PAA[6] and C/PVDF[7] anodes described in Chapters III and IV, respectively. Overall the results in Appendix B demonstrate that the rate capabilities of particle/polymer fiber mat anodes and cathodes are insensitive to the active material and polymer binder used. Figure 5.4c shows the capacity of the $LiCoO_2$/C/PVDF fiber mat cathode at 0.1 C was fully recovered after cycling at high C-rates. Furthermore, the electrospun cathode exhibited outstanding cycling stability with 78 % capacity retention after 200 cycles at 0.5 C, as shown in Figure 5.4d. The fiber mat cathode was also physically stable in the battery environment with no visible difference in the fiber structure before and after cycling (see Figure 5.5). Overall, the performance shown in Figure 5.4 was representative of electrospun mats with fiber volume fractions in the range of 0.24 – 0.85.

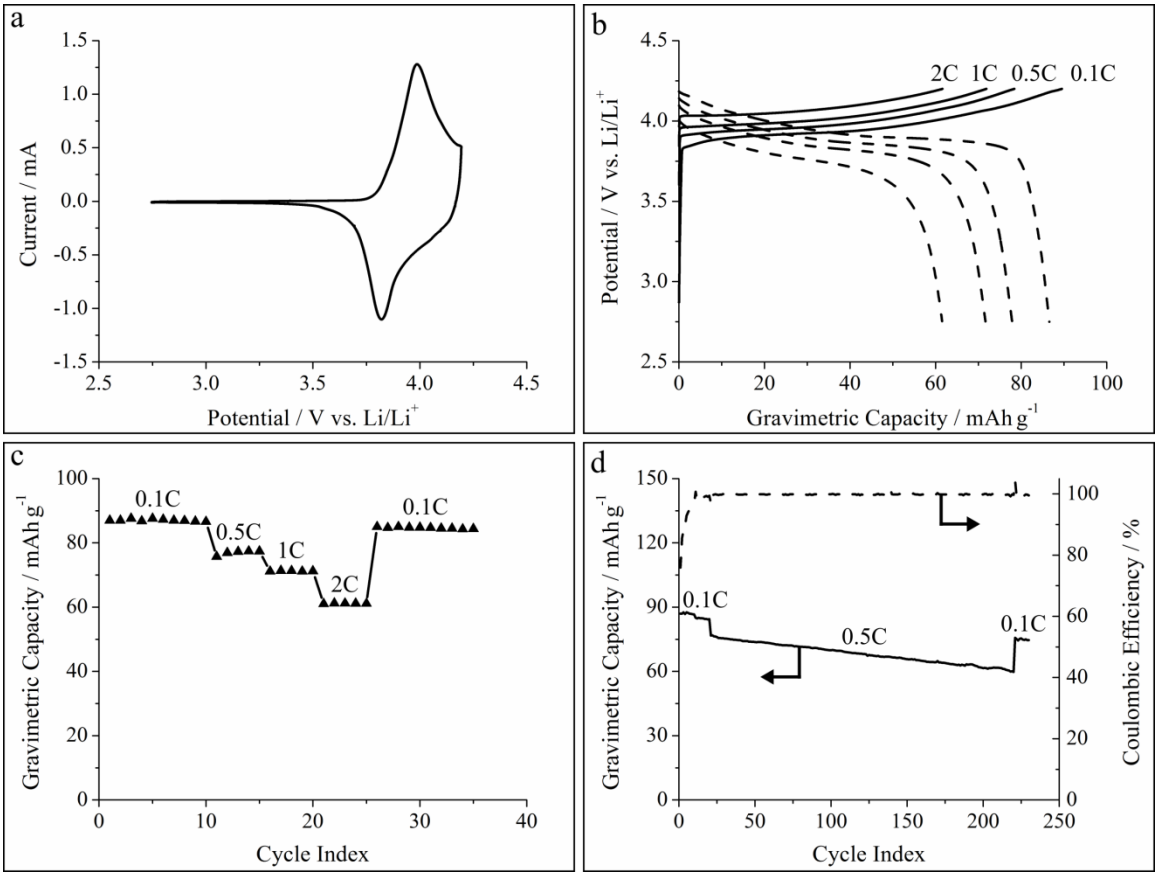

Figure 5.4. Fundamental electrochemical characterization of an electrospun $LiCoO_2$/C/PVDF fiber cathode. (a) Cyclic voltammogram, (b) charge/discharge curves collected at 0.1 – 2 C, (c) cycling stability at 0.1 – 2 C, and (d) long-term cycling stability at 0.1 – 0.5 C.

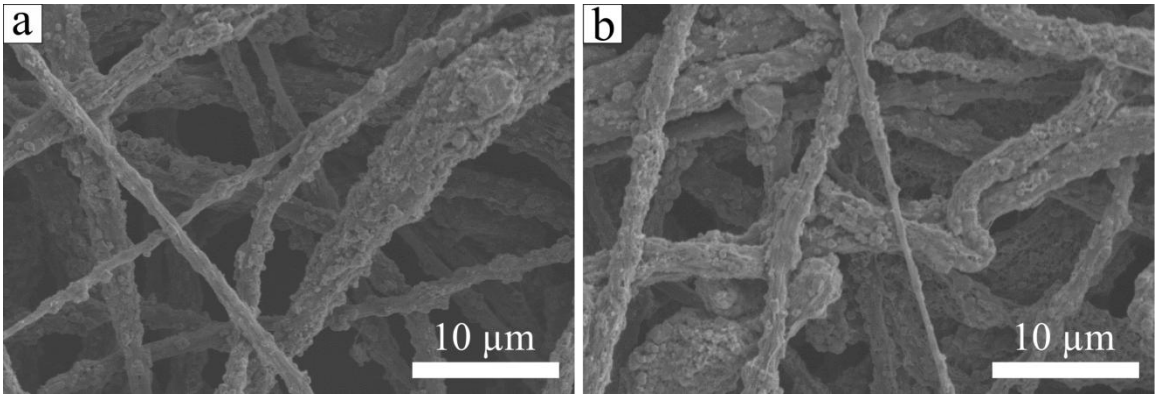

Figure 5.5. SEM images of a $LiCoO_2$/C/PVDF fiber mat cathode (a) before cycling and (b) after 100 cycles at 0.1 C.

The performance of the $LiCoO_2$/C/PVDF fiber mats was compared to other electrospun $LiCoO_2$ cathodes in the literature. Mizuno et al.[22] reported on the preparation and characterization of electrospun $LiCoO_2$ nanofibers as active materials in a slurry cast electrode containing $LiCoO_2$ nanofibers, carbon black, and poly(tetrafluoroethylene) binder. The material had a high gravimetric capacity of 135 mAh $g_{LiCoO_2}^{-1}$ at 0.18 C, but the capacity faded significantly during cycling, retaining only 108 mAh $g_{LiCoO_2}^{-1}$ after 30 cycles (corresponding to a capacity fade rate of 0.67 % $cycle^{-1}$). In another study, Lu et al.[21] prepared and characterized electrospun $LiCoO_2$ nanofibers which were used as a freestanding fiber mat cathode in a half cell. The material exhibited an initial gravimetric capacity of 85 mAh $g_{LiCoO_2}^{-1}$ at 1.5 C, but the capacity faded to only 20 mAh $g_{LiCoO_2}^{-1}$ over 25 cycles (capacity fade rate of 3.0 % $cycle^{-1}$). The authors attributed the poor cycling stability of their $LiCoO_2$ nanofiber cathodes to collapse of the fiber structure during cycling. Compared to these studies, the electrospun $LiCoO_2$/C/PVDF cathodes reported here had a similar gravimetric capacity

(128 and 88 mAh $g_{LiCoO_2}^{-1}$ at 0.1 C and 2 C, respectively) and superior cycle life (capacity fade rate of 0.11 % $cycle^{-1}$ over 200 cycles at 0.5 C). The excellent performance of the electrospun particle/polymer fiber cathodes is attributed to the use of high quality $LiCoO_2$ nanoparticles (i.e., particles with an $R\bar{3}m$ structure, high capacity, and good cycle life, as previously discussed) and preservation of the fiber structure during cycling.

To determine how composition affects the performance of electrospun $LiCoO_2$/C/PVDF cathodes, fiber mats with a $LiCoO_2$/C/PVDF weight ratio of 40/25/35 were prepared. Representative SEM images shown in Figure 5.6a show that the mats had uniform fibers with diameters ~ 1 μm. The overall structure of the mats with 40 wt % $LiCoO_2$ was similar to that of a mat with 70 wt % $LiCoO_2$ (see Figure 5.6b).

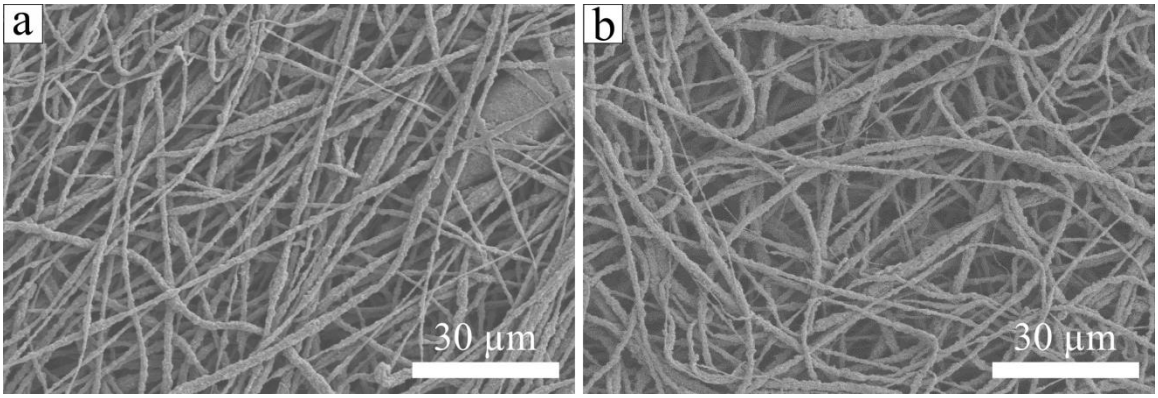

Figure 5.6. SEM images of electrospun $LiCoO_2$/C/PVDF fiber mat anodes where the $LiCoO_2$/C/PVDF weight ratio is (a) 40/25/35 and (b) 70/10/20.

The electrochemical performance of $LiCoO_2$/C/PVDF fiber mat cathodes containing 40 and 70 wt % $LiCoO_2$ were compared in half cells. Charge/discharge curves collected at 0.1 C for these fiber mats (see Figure 5.7a) show that lithiation/delithiation processes occurred at potentials ~ 3.9 V vs. Li/Li^+ which is typical for $LiCoO_2$-based

cathodes. The reversible capacity of electrodes with 40 and 70 wt % $LiCoO_2$ were 51 and 87 mAh g^{-1}, respectively, and each electrode had good active material utilization with ~ 125 mAh $g_{LiCoO_2}^{-1}$. Figure 5.7b shows the cycling stability of each electrode was excellent, with no capacity fade over 10 cycles. The gravimetric capacity of these electrodes was evaluated at charge/discharge rates ranging from 0.1 – 2 C as shown in Figure 5.7c. At all C-rates investigated, the gravimetric capacity of the cathode with 70 wt % $LiCoO_2$ was greater than that of the fiber mat with 40 wt % $LiCoO_2$, indicating that increasing the carbon content from 10 to 25 wt % did not provide any improvement in the performance of $LiCoO_2$/C/PVDF cathodes up to 2 C. Thus, the remainder of the present study focused on characterizing fiber mat cathodes with a $LiCoO_2$/C/PVDF weight ratio of 70/10/20.

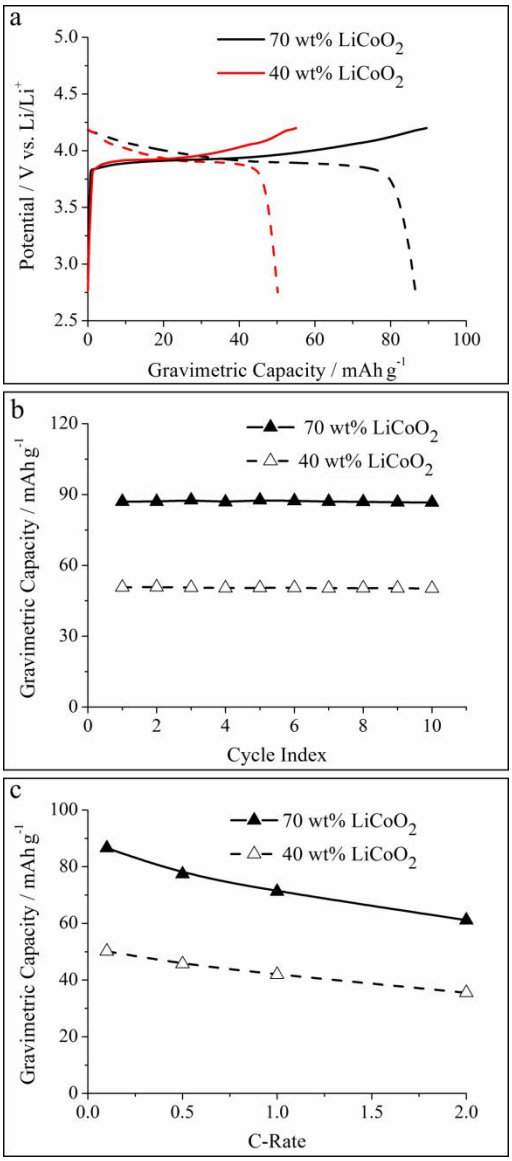

Figure 5.7. Electrochemical performance of $LiCoO_2$/C/PVDF fiber mat cathodes in half cells where the $LiCoO_2$/C/PVDF weight ratio 40/25/35 and 70/10/20. (a) Charge/discharge curves at 0.1 C, (b) Cycling stability over 10 cycles at 0.1 C, and (c) Gravimetric capacity at 0.1 – 2 C.

The performance of a fiber mat cathode (130 μm thick, fiber volume fraction of 0.60) with a $LiCoO_2$/C/PVDF weight ratio of 70/10/20 was evaluated and compared to

that of a slurry cast cathode (120 μm thick) of the same composition in half cell tests. Figure 5.8a shows the gravimetric capacity of the electrospun and slurry cast cathodes at charge/discharge rates ranging from 0.1 – 2 C; the performance in Figure 5.8a was representative for samples tested in triplicate. At 0.1 C the electrospun and slurry cast cathodes exhibited similar gravimetric capacities ~ 80 mAh g^{-1} (114 mAh $g_{LiCoO_2}^{-1}$) indicating good active material utilization at a slow charge/discharge rate. The electrospun cathode exhibited excellent rate capabilities with reversible capacities of 71 and 61 mAh g^{-1} at 1 C and 2 C, respectively, compared to 53 mAh g^{-1} at 1 C and 0.25 mAh g^{-1} at 2 C for the slurry cast cathode. It should be noted that the performance of the slurry cast cathode prepared in the present study (see Figure 5.8a) was similar to that reported by Stephenson et al.[51] for an electrode containing $LiCoO_2$/C/PVDF in a 91/6/3 weight ratio, where the capacity at 2.5 C was 15 mAh g^{-1}. Compared to the slurry cast electrodes, the excellent performance of the electrospun cathode is attributed to the small fiber diameter and the intra/interfiber void space of the mat which allowed for electrolyte infiltration throughout the electrode, a large electrode/electrolyte interfacial area, and efficient Li^+ transport between the electrolyte and active material nanoparticles.

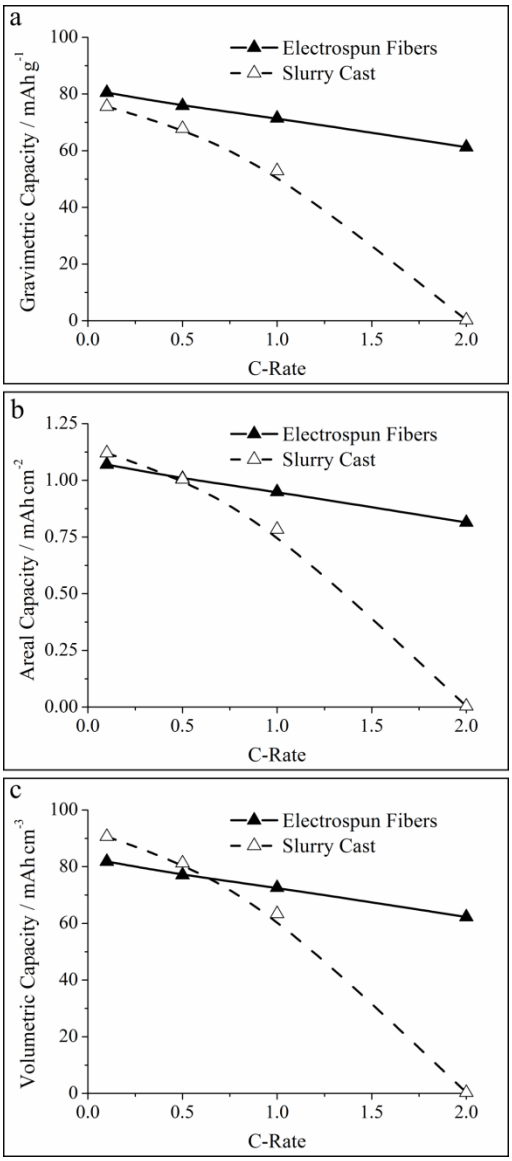

Figure 5.8. Rate capabilities of electrospun and slurry cast $LiCoO_2$/C/PVDF cathodes. (a) Gravimetric (b) areal, and (c) volumetric capacities at 0.1 – 2 C. All electrodes contained $LiCoO_2$/C/PVDF in a 70/10/20 weight ratio.

Areal and volumetric capacities, which are important for battery design and electrode assessment, were determined at 0.1 – 2 C for an electrospun mat (130 µm thick, fiber volume fraction of 0.60) and a slurry cast cathode (120 µm thick) of the same

composition. The results are shown in Figures 5.8b and 5.8c. At a 0.1 C charge/discharge rate, both electrodes had an areal capacity of ~ 1.1 mAh cm^{-2}. The electrospun cathode retained a high capacity of 0.95 and 0.81 mAh cm^{-2} at 1 C and 2 C, respectively, whereas the slurry cast cathode had very poor rate capabilities at high C-rates, with an areal capacity of only 0.78 mAh cm^{-2} at 1 C and essentially no reversible capacity at 2 C (0.004 mAh cm^{-2}). Similarly, there was only a slight decrease in volumetric capacity of the electrospun cathode as the charging rate was increased from 0.1 C to 1 C and 2 C (82 , 73, and 62 mAh cm^{-3}, respectively) as shown in Figure 5.8c. In comparison, the volumetric capacity of a slurry electrode was high at 0.1 C (91 mAh cm^{-3}) but decreased significantly at higher C-rates (e.g., 0.30 mAh cm^{-3} at 2 C).

The results in Figures 5.4, 5.7, and 5.8 were collected for half cells containing a $LiCoO_2$/C/PVDF cathode and Li metal counter/reference electrode. Half cells provide a convenient and reliable way to characterize individual electrodes, but Li metal anodes cannot be utilized in consumer devices due to Li dendrite formation.[52, 53] To evaluate a more practical and relevant LIB device, full cells containing a $LiCoO_2$/C/PVDF cathode and a carbon powder/PVDF anode (C/PVDF[7], described in Chapter IV) were prepared and characterized.

Figure 5.9a shows typical charge/discharge curves at 0.1 – 2 C for a full cell containing an electrospun $LiCoO_2$/C/PVDF cathode (fiber volume fraction of 0.86 and thickness of 180 μm) and electrospun C/PVDF fiber mat anode (fiber volume fraction of 0.56 and thickness of 280 μm). The sloping profiles of the charge/discharge curves are due to the wide operating potential of the C/PVDF anode[7] where lithiation/delithiation processes occur from 0.015 – 1.5 V vs. Li/Li^+. At 0.1 C, the initial gravimetric capacity

of the full cell was 49 mAh g^{-1} (normalized to the combined mass of the cathode and anode) which corresponded well to the theoretical capacity Q_{total} (51 mAh g^{-1}) calculated using equation 5.1:

$$\frac{1}{Q_{total}} = \frac{1}{Q_{cathode}} + \frac{1}{Q_{anode}} \tag{5.1}$$

where $Q_{cathode}$ and Q_{anode} are the effective gravimetric capacities of the cathode and anode, taking into account the active and inactive components of the electrodes (80 and 140 mAh g^{-1} for the cathode and anode, respectively). Good agreement between the measured capacity and theoretical capacity indicates that the anode and cathode active materials were well-utilized in the cell. After storing the full cell with electrospun electrodes for 168 h at open-circuit, 87 % of the discharge capacity was retained. Such a self-discharge rate is typical for LIBs; Du Pasquier et al.[54] reported that a battery containing a $LiCoO_2$ cathode and $Li_4Ti_5O_{12}$ anode retained 93 % of its discharge capacity after 200 h of storage at open-circuit.

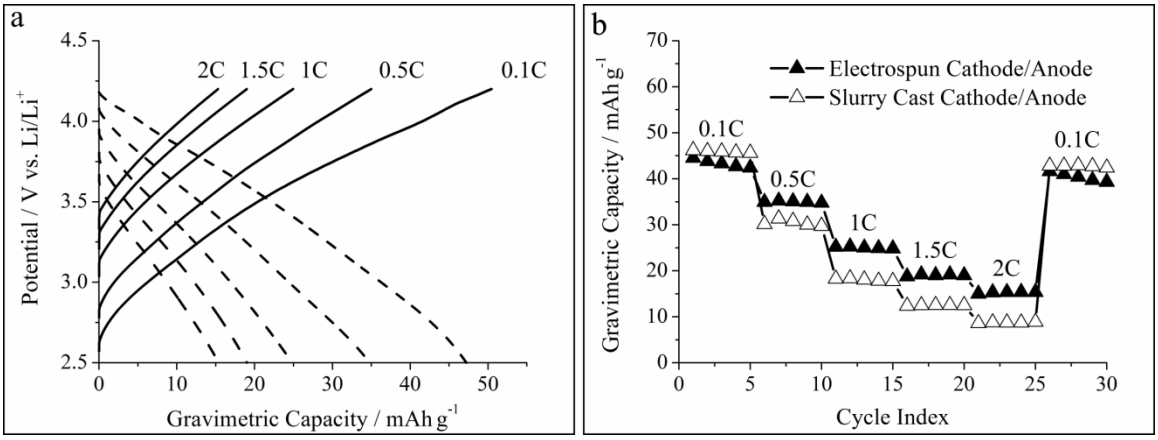

Figure 5.9. Electrochemical characterization of full cells containing a $LiCoO_2$/C/PVDF cathode and C/PVDF anode. (a) Charge/discharge curves at 0.1 – 2 C for a full cell with an electrospun cathode/anode and (b) cycling stability at 0.1 – 2 C for full cells containing either electrospun electrodes or slurry cast electrodes.

The performance of a full cell containing an electrospun $LiCoO_2$/C/PVDF cathode and electrospun C/PVDF anode was compared to that of a full cell prepared with slurry cast electrodes of the same composition. Gravimetric capacities of the electrospun and slurry cast cells at 0.1 – 2 C are shown in Figure 5.9b. Both cells exhibited similar capacities of ~ 44 mAh g^{-1} at 0.1 C, but the electrospun battery had superior rate capabilities with a 73 % higher capacity at 2 C (15.4 mAh g^{-1} for the fiber electrodes vs. 8.9 mAh g^{-1} for the slurry cast full cell). The data in Table 5.1 show that the full cell with electrospun electrodes also had higher areal and volumetric capacities at 1 C and 2 C compared to that of the slurry cast full cell. Furthermore, the capacity at 0.1 C was fully recovered in both cells after cycling at rates varying between 0.5 – 2 C as shown in Figure 5.9b.

Table 5.1. Areal and volumetric capacities of full cells containing $LiCoO_2$/C/PVDF cathodes and C/PVDF anodes.

Full Cell	Areal Capacity (mAh cm^{-2})			Volumetric Capacity (mAh cm^{-3})		
	0.1 C	1 C	2 C	0.1 C	1 C	2 C
Electrospun Cathode + Anode	1.76	1.03	0.64	37.7	22.1	13.7
Slurry Cast Cathode + Anode	1.75	0.68	0.34	38.6	15.0	7.5

Only two other literature reports have characterized full cells containing an electrospun cathode and anode. Aravindan and Jayaraman et al.[55] prepared electrospun $LiMn_2O_4$ nanofibers (for the cathode) and electrospun TiO_2 nanofibers (for the anode) using sol-gel chemistry and high temperature processing. The authors reported a gravimetric capacity of 100 mAh g^{-1} and an energy density of 220 Wh kg^{-1}, but these values were normalized only to the mass of the active cathode material. For a more meaningful comparison with data in the present paper, the overall mass of both sol-gel fiber electrodes was used to re-calculate an effective gravimetric capacity of 50 mAh g^{-1} and energy density of 111 Wh kg^{-1} for the electrospun $LiMn_2O_4/TiO_2$ full cell. The same group[56] also reported on a full cell containing an electrospun $LiMn_2O_4$ cathode and electrospun $TiNb_2O_7$ anode with an effective gravimetric capacity of 58 mAh g^{-1}, areal capacity ~ 0.5 mAh cm^{-2}, and an effective energy density of 139 Wh kg^{-1} at 0.52 C. For comparison, the full cell of the present study with an electrospun $LiCoO_2$/C/PVDF cathode and C/PVDF anode had a comparable gravimetric capacity of 42 mAh g^{-1} and energy density of 144 Wh kg^{-1} at 0.1 C but a much higher areal capacity (up to 1.76 mAh cm^{-2}, as per Table 5.1).

5.4 Conclusions

Particle/polymer electrospinning was used to prepare fiber mat cathodes for LIBs, where the fibers contained 70 wt % $LiCoO_2$ nanoparticles, 10 wt % carbon powder, and 20 wt % poly(vinylidene) binder ($LiCoO_2$/C/PVDF). The fiber cathode exhibited a high gravimetric capacity of 90 mAh g^{-1} (128 mAh $g_{LiCoO_2}^{-1}$) and good cycling stability (only 0.11 % capacity fade $cycle^{-1}$ which is superior to previous reports on electrospun $LiCoO_2$ electrodes).

Thick, densely packed $LiCoO_2$/C/PVDF fiber mats were prepared for high areal and volumetric capacity cathodes. The areal and volumetric capacities at 0.1 C of a 130 μm thick electrospun mat cathode with a fiber volume fraction of 0.60 were 1.1 mAh cm^{-2} and 82 mAh cm^{-3}, respectively. Electrospun cathodes also exhibited excellent rate capabilities, with capacity retentions of 89 % at 1 C and 76 % at 2 C, vs. a slurry cast electrode of the same composition which had a capacity retention of 70 % at 1 C and essentially no reversible capacity at 2 C.

Full cells containing an electrospun cathode ($LiCoO_2$/C/PVDF) and electrospun anode (C/PVDF) were also prepared and characterized. The full cells had a high gravimetric capacity (42 mAh g^{-1}) and energy density (144 Wh kg^{-1}) at 0.1 C. Notably, the areal and volumetric capacities of the electrospun full cell were 1.03 mAh cm^{-2} and 22.1 mAh cm^{-3} at 1 C. This performance was significantly better than that of a full cell containing slurry cast electrodes of the same composition (0.68 mAh cm^{-2} and 15.0 mAh cm^{-3} at 1 C) and full cells reported in the literature containing electrospun electrodes prepared through sol-gel chemistry (e.g., ~ 0.5 mAh cm^{-2} at 0.52 C).

The results in this paper show that particle/polymer fiber electrospinning is a robust platform for the preparation of LIB electrodes with high gravimetric, areal, and volumetric capacities at fast charge/discharge rates. Electrodes can be prepared with high particle content, and the polymer binder is retained in the final electrode structure. The excellent performance of the $LiCoO_2$/C/PVDF fiber cathodes reported here is attributed to the intra- and interfiber void space which allows for good electrolyte infiltration throughout the electrode mat, a large electrode/electrolyte interfacial area, and short Li^+ transport pathways between the electrolyte and active material in the radial fiber direction. The presence of a polymer binder in the fibers is also beneficial, making the electrode mechanically flexible and allowing for some electrolyte uptake into the fibers for better Li^+ ion transport. Overall these results demonstrate that incorporating nanoscale active materials into 3D electrospun fiber mats improves battery performance compared to conventional materials.

5.5 References

[1] J.-M. Tarascon, M. Armand, *Nature* **2001**, *414*, 359.
[2] M. Armand, J.-M. Tarascon, *Nature* **2008**, *451*, 652.
[3] P. N. Pintauro, *Polym. Rev.* **2015**, *55*, 201.
[4] N. Nitta, G. Yushin, *Part. Part. Syst. Char.* **2014**, *31*, 317.
[5] S. J. Kim, M. Naguib, M. Zhao, C. Zhang, H.-T. Jung, M. W. Barsoum, Y. Gogotsi, *Electrochim. Acta* **2015**, *163*, 246.
[6] E. C. Self, R. Wycisk, P. N. Pintauro, *J. Power Sources* **2015**, *282*, 187.
[7] E. C. Self, E. C. McRen, P. N. Pintauro, *ChemSusChem* **2016**, *9*, 208.
[8] C. Fongy, A. C. Gaillot, S. Jouanneau, D. Guyomard, B. Lestriez, *J. Electrochem. Soc.* **2010**, *157*, A885.
[9] S. K. Martha, J. O. Kiggans, J. Nanda, N. J. Dudney, *J. Electrochem. Soc.* **2011**, *158*, A1060.
[10] M. Singh, J. Kaiser, H. Hahn, *J. Electrochem. Soc.* **2015**, *162*, A1196.
[11] X. Zhang, T. W. Verhallen, F. Labohm, M. Wagemaker, *Adv. Energy Mater.* **2015**, *5*, 1500498.
[12] W. Zhang, P. N. Pintauro, *ChemSusChem* **2011**, *4*, 1753.
[13] M. Brodt, R. Wycisk, P. N. Pintauro, *J. Electrochem. Soc.* **2013**, *160*, F744.
[14] M. Brodt, T. Han, N. Dale, E. Niangar, R. Wycisk, P. Pintauro, *J. Electrochem. Soc.* **2014**, *162*, F84.
[15] S. R. Sivakkumar, J. Y. Nerkar, A. G. Pandolfo, *Electrochim. Acta* **2010**, *55*, 3330.
[16] S. Kalluri, K. H. Seng, Z. Guo, H. K. Liu, S. X. Dou, *RSC Advances* **2013**, *3*, 25576.
[17] H.-G. Wang, S. Yuan, D.-L. Ma, X.-B. Zhang, J.-M. Yan, *Energy Environ. Sci.* **2015**, *8*, 1660.
[18] Z.-W. Fu, J. Ma, Q.-Z. Qin, *Solid State Ionics* **2005**, *176*, 1635.
[19] Y. Gu, D. Chen, X. Jiao, *J. Phys. Chem. B* **2005**, *109*, 17901.
[20] Y. Gu, D. Chen, X. Jiao, F. Liu, *J. Mater. Chem.* **2007**, *17*, 1769.
[21] H.-W. Lu, L. Yu, W. Zeng, Y.-S. Li, Z.-W. Fu, *Electrochem. Solid-State Lett.* **2008**, *11*, A140.
[22] Y. Mizuno, E. Hosono, T. Saito, M. Okubo, D. Nishio-Hamane, K. Oh-ishi, T. Kudo, H. Zhou, *J. Phys. Chem. C* **2012**, *116*, 10774.
[23] Y. Ou, J. Wen, H. Xu, S. Xie, J. Li, *J. Phys. Chem. Solids* **2013**, *74*, 322.
[24] H. Yang, J.-H. Pee, H. T. Kim, Y. Kim, *J. Ceram. Process. Res.* **2012**, *13*, 319.
[25] J.-P. Park, J.-Y. Park, C.-H. Hwang, M.-H. Choi, J.-E. Kim, K.-M. Ok, I.-W. Shim, *Bull. Korean Chem. Soc.* **2010**, *31*, 327.
[26] H. M. Rietveld, *J. Appl. Cryst.* **1969**, *2*, 65.
[27] J. Rodríguez-Carvajal, *Physica B* **1993**, *192*, 55.
[28] F. Bonino, S. Brutti, P. Reale, B. Scrosati, L. Gherghel, J. Wu, K. Müllen, *Adv. Mater.* **2005**, *17*, 743.
[29] A. Caballero, L. Hernan, J. Morales, *ChemSusChem* **2011**, *4*, 658.
[30] I. R. M. Kottegoda, Y. Kadoma, H. Ikuta, Y. Uchimoto, M. Wakihara, *J. Electrochem. Soc.* **2005**, *152*, A1595.
[31] Ó. Vargas, Á. Caballero, J. Morales, *Electrochim. Acta* **2015**, *165*, 365.

[32] C. Chae, H. Park, D. Kim, J. Kim, E.-S. Oh, J. K. Lee, *J. Power Sources* **2013**, *244*, 214.
[33] J. Hassoun, F. Croce, I. Hong, B. Scrosati, *Electrochem. Commun.* **2011**, *13*, 228.
[34] R. Kataoka, T. Mukai, A. Yoshizawa, T. Sakai, *J. Electrochem. Soc.* **2013**, *160*, A1684.
[35] K.-L. Lee, J.-Y. Jung, S.-W. Lee, H.-S. Moon, J.-W. Park, *J. Power Sources* **2004**, *130*, 241.
[36] R. Verrelli, J. Hassoun, A. Farkas, T. Jacob, B. Scrosati, *J. Mater. Chem. A* **2013**, *1*, 15329.
[37] Y. Wang, Y. Wang, D. Jia, Z. Peng, Y. Xia, G. Zheng, *Nano Lett.* **2014**, *14*, 1080.
[38] S.-T. Myung, N. Kumagai, S. Komaba, H.-T. Chung, *J. Appl. Electrochem.* **2000**, *30*, 1081.
[39] O. A. Shlyakhtin, S. H. Choi, Y. S. Yoon, Y.-J. Oh, *Electrochim. Acta* **2004**, *50*, 511.
[40] Y. Shao-Horn, L. Croguennec, C. Delmas, E. C. Nelson, M. A. O'Keefe, *Nat. Mater.* **2003**, *2*, 464.
[41] J. T. Hertz, Q. Huang, T. McQueen, T. Klimczuk, J. W. G. Bos, L. Viciu, R. J. Cava, *Phys. Rev. B* **2008**, *77*, 075119.
[42] M. Inaba, Y. Inriyama, Z. Ogumi, Y. Todzuka, A. Tasaka, *J. Raman Spectrosc.* **1997**, *28*, 613.
[43] S. Tintignac, R. Baddour-Hadjean, J.-P. Pereira-Ramos, R. Salot, *Electrochim. Acta* **2012**, *60*, 121.
[44] M. Jo, Y.-S. Hong, J. Choo, J. Cho, *J. Electrochem. Soc.* **2009**, *156*, A430.
[45] B. Huang, Y.-I. Jang, Y.-M. Chiang, D. R. Sadoway, *J. Appl. Electrochem.* **1998**, *28*, 1365.
[46] E. I. Santiago, A. V. C. Andrade, C. O. Paiva-Santos, L. O. S. Bulhões, *Solid State Ionics* **2003**, *158*, 91.
[47] Y.-M. Chiang, D. R. Sadoway, Y.-I. Jang, B. Huang, H. Wang, *Electrochem. Solid-State Lett.* **1999**, *2*, 107.
[48] R. Koksbang, J. Barker, H. Shi, M. Y. Saïdi, *Solid State Ionics* **1996**, *84*, 1.
[49] M. Sathiya, A. S. Prakash, K. Ramesha, A. K. Shukla, *Materials* **2009**, *2*, 857.
[50] A. Kondo, E. Nakamura, T. Kozawa, H. Abe, M. Naito, J. Yoshida, S. Nakanishi, H. Iba, *Adv. Powder Technol.* **2014**, *25*, 1280.
[51] D. E. Stephenson, E. M. Hartman, J. N. Harb, D. R. Wheeler, *J. Electrochem. Soc.* **2007**, *154*, A1146.
[52] V. Aravindan, Y.-S. Lee, S. Madhavi, *Adv. Energy Mater.* **2015**, *5*, 1402225.
[53] J. B. Goodenough, *Acc. Chem. Res.* **2013**, *46*, 1053.
[54] A. Du Pasquier, I. Plitz, S. Menocal, G. Amatucci, *J. Power Sources* **2003**, *115*, 171.
[55] V. Aravindan, J. Sundaramurthy, P. S. Kumar, N. Shubha, W. C. Ling, S. Ramakrishna, S. Madhavi, *Nanoscale* **2013**, *5*, 10636.
[56] S. Jayaraman, V. Aravindan, P. Suresh Kumar, W. Chui Ling, S. Ramakrishna, S. Madhavi, *ACS Appl. Mater. Interfaces* **2014**, *6*, 8660.

CHAPTER VI

ELECTROSPUN PARTICLE/POLYMER SI-BASED NANOFIBER ANODES FOR LI-ION BATTERIES

6.1 Introduction

Since their commercial debut in 1991, Li-ion batteries (LIBs) have revolutionized the functionality of portable electronic devices, and the LIB industry continues to grow today due emerging applications such as electric vehicle propulsion.[1, 2] Despite the extraordinary success of LIBs, many devices are still limited by battery performance, and thus new batteries with higher energy density and long cycle life must be developed to satisfy the ever-increasing demands of consumers.[3, 4]

Si has been widely investigated as a replacement for graphite in today's LIB anodes due to its high theoretical capacity (3,600 mAh g^{-1} for $Li_{15}Si_4$ vs. 372 mAh g^{-1} for LiC_6) and low operating potential (< 0.5 V vs. Li/Li^+).[5, 6] However, Si-based anodes often exhibit poor cycling stability due to large volume changes during charging and discharging. Lithiation of Si is accompanied by a volumetric expansion exceeding 300 %, and repeated swelling and shrinking of Si during battery cycling results in capacity fade due to Si pulverization, electronic isolation of Si particles, and irreversible Li consumption associated with repeated formation and rupture of the solid-electrolyte interphase (SEI) layer.[7, 8] Although Si pulverization can be eliminated through the use of nanoscale active materials (e.g., Si nanoparticles[9-11] and Si nanowires[12-15]), effective techniques which prevent electronic isolation of Si and stabilize the SEI layer are yet to

be identified.[7, 8] Furthermore, previously reported nanoscale Si anodes typically contained low active material loadings and densities, resulting in low areal and volumetric capacities. To produce Si anodes which are suitable for commercial applications, new anode designs which can tolerate Si volumetric changes while maintaining high gravimetric, areal, and volumetric capacities over many charge/discharge cycles must be developed.

One attractive Si anode design involves the use of an electrospun nanofiber mat with interfiber voids which can accommodate the volumetric changes of Si during cycling.[16, 17] Previous studies[18-24] on electrospun Si anodes have largely been directed towards the pyrolysis of polymer fibers with embedded Si particles to create an electronically conductive Si-C nanofiber network. Freestanding Si-C nanofiber mats exhibited high gravimetric capacities (e.g., 800 – 1,600 mAh g^{-1}) and good stability over 30 – 100 cycles, but most of these studies neglected to examine carefully the anode's areal and volumetric capacities. Si areal loadings in many electrospinning studies were very low (e.g., < 0.1 mg_{Si} cm^{-2})[24, 25], and SEM images suggested that the fiber volume fraction of the mats were far too low (< 0.25) for practical battery use.

An alternative to pyrolyzed carbon fiber-based electrodes is the use of electrospun particle/polymer fiber mat electrodes, an approach that has been pursued by Pintauro and coworkers.[26-28] The preparation and characterization of several particle/polymer fiber mat LIB electrodes have been reported, including: (i) anodes containing titania nanoparticles, carbon powder, and poly(acrylic acid) (TiO_2/C/PAA)[26] (Chapter III), (ii) anodes containing carbon powder and poly(vinylidene fluoride) (C/PVDF)[27] (Chapter IV), and (iii) cathodes containing $LiCoO_2$ nanoparticles, carbon powder, and

PVDF ($LiCoO_2$/C/PVDF)[28] (Chapter V). These studies showed that fiber mats with a high material loading (e.g., 54.1 mg cm^{-2}) and high fiber volume fractions (up to 0.86) worked exceptionally well, with high areal and volumetric capacities at fast charge/discharge rates (e.g., 1.3 mAh cm^{-2} and 62 mAh cm^{-3} at 2 C). The excellent performance of electrospun particle/polymer fiber mat electrodes is attributed to: (i) a large electrode/electrolyte interfacial area, (ii) short Li^+ transport pathways between the electrolyte and active material in the radial fiber direction, and (iii) good electrolyte infiltration throughout the electrode via the intra- and interfiber void space of the mat.

Based on our encouraging prior results with electrospun particle/polymer electrodes containing moderate capacity materials[26-28], it made sense to apply the technique to high capacity Si-based anodes. A particle/polymer fiber mat containing Si nanoparticles offers several advantages over previously reported Si-C fiber anodes prepared via high temperature pyrolysis. The presence of the polymer binder ensures that particle/polymer fiber mats can be compacted under high pressure without fracturing, and thus thick, densely packed nanofiber electrodes can be created for high gravimetric, areal, and volumetric capacities.[26-28] For practical battery applications, high areal capacities are desired to reduce the amount of inactive cell components (e.g., current collectors, separators, etc.), and batteries with a high volumetric capacity allow more energy to be stored within a given space.[6, 26-28] Electrospun particle/polymer fibers can also be made with a binder that absorbs electrolyte, ensuring that Li^+ ions have access to most/all Si nanoparticles in the electrode. Furthermore, the binder in such fiber mats can be chosen to help stabilize the Si particles during charge/discharge cycling, as has been reported for

electronically conductive binders[29-32] and binders like PAA[33], carboxymethyl cellulose[34], and alginate[35] which form hydrogen bonds with the SiO_x layer on Si.

The present paper describes the preparation and characterization of two types of electrospun particle/polymer fiber mat LIB anodes including: (i) Si nanoparticles, carbon black, and PAA binder (hereafter denoted as Si/C/PAA) and (ii) Si nanoparticles and electronically conductive polymer binders (PFM and PEFM, synthesized by Gao Liu and coworkers at Lawrence Berkeley National Laboratory). Qualitative performance/composition/structure correlations are established by evaluating the performance of fiber mats with different compositions, fiber volume fractions, interfiber connectivities, thicknesses, and loadings. Electrodes are characterized both in half cells using a Li metal counter/reference electrode and in full cells prepared with an electrospun fiber mat $LiCoO_2$/C/PVDF cathode.

6.2 Experimental

This study investigated several Si-based anodes including: (i) Si nanoparticles (50 – 70 nm), carbon powder (Vulcan XC-72R, Fuel Cell Store), and poly(acrylic acid) (PAA, M_v = 450,000 g mol^{-1}, Sigma-Aldrich) (Si/C/PAA, electrospun only), (ii) Si nanoparticles and PFM, an electronically conductive polymer binder (Si/PFM, electrospun and slurry cast), and (iii) Si nanoparticles and PEFM, another conductive polymer binder (Si/PEFM, slurry cast only). 1 wt % poly(ethylene oxide) (PEO, M_v = 1 MDa) was added as a carrier polymer to facilitate the electrospinning process for fibers containing the PFM binder. Electrode inks were prepared by mixing the components in n-propanol (for Si/C/PAA), a 1/1 mixture of chlorobenzene/chloroform

(for Si/PFM), or chlorobenzene (for Si/PEFM). The Si/C/PAA electrodes contained either 15 or 40 wt % Si, and the anodes prepared with electronically conductive polymer binder contained between 35 – 67 wt % Si.

Slurry cast anodes were prepared by casting the electrode ink onto a copper foil current collector (9 μm, MTI Corp.) and drying at ambient conditions. Fiber mat anodes were created by electrospinning using a single needle spinneret and the custom-made rotating drum collector as described in Chapter IV.[27] Si/C/PAA fiber mats were spun onto an aluminum foil substrate at the following conditions: (i) 0.75 and 1.00 mL h^{-1} solution flow rates for anodes with 15 and 40 wt % Si, respectively, (ii) 8 kV bias voltage, (iii) 8.0 cm spinneret-to-collector distance, and (iv) 20 – 30 % relative humidity (rh). Si/PFM/PEO fiber mats were prepared at the following conditions: (i) solution flow rates of 0.25 – 0.50 mL h^{-1}, (ii) 5 – 6 kV bias voltage, (iii) 8.0 cm spinneret-to-collector distance, and (iv) 15 – 75 % rh. Top-down morphology of the electrospun mats was assessed using scanning electron microscopy (Hitachi S4200 and Zeiss Merlin SEMs).

Several types of Si/C/PAA anodes were prepared with 40 wt % Si. The first was an as-spun mat with a fiber volume fraction of ~ 0.30. The others were compacted and/or welded mats, which were prepared by: (i) mechanically compacting an as-spun mat on a hydraulic press at 90 MPa for 40 s to increase the fiber volume fraction and/or (ii) exposing the mat to methanol vapor for 1 h at room temperature to weld the interfiber contacts. For Si/C/PAA anodes prepared with 15 wt % Si, only a compacted/welded fiber mat was tested. The fiber volume fraction of all compacted mats was 0.80 ± 0.05 as determined by analysis of SEM images of fiber mats using ImageJ as described in

Chapter IV.[27] For Si/PFM/PEO anodes, only as-spun mats which were neither compacted nor welded were investigated.

CR2032 half cells were constructed in an argon-filled glovebox using an electrospun fiber mat (dried overnight at 70 °C under vacuum) as the working electrode and a Li metal counter/reference electrode. The electrolyte was 1.2 M $LiPF_6$ in a mixture of ethylene carbonate and diethyl carbonate (3/7 by volume, BASF Corp.). 30 wt % fluoroethylene carbonate (BASF Corp.) was added to the electrolyte to ensure formation of a stable SEI layer. Two sheets of Celgard 2500 soaked in electrolyte were used as a membrane separator, and several additional drops of electrolyte were added to completely fill the cell volume. Cells were crimped at 1,000 psi and rested overnight before electrochemical characterization. Galvanostatic charge/discharge experiments were conducted by polarizing the cells between 0.015 – 1.5 V at 0.1 – 1 C on an 8-channel battery tester (5 V/1 mA, MTI Corp.). C-rates for the half cells were calculated assuming a theoretical capacity of 3,600 mAh g^{-1} for Si and 372 mAh g^{-1} for carbon. At least two coin cells were tested for each sample to assess the reproducibility of these experiments. The electrochemical performance of each sample was reproducible within approximately 15 – 20 % among independent coin cell tests. Except where otherwise indicated, half cell capacities are normalized with respect to the entire composite anode (e.g., total amounts of Si, C, and PAA).

Selected half cells were disassembled after cycling, and the anodes were rinsed using dimethyl carbonate before conducting post-mortem analysis. Cross-sectional SEM images of pristine (i.e., uncycled) and cycled fiber mat anodes were collected using a Zeiss Merlin VP microscope (Carl Zeiss Microscopy GmbH, Oberkochen, Germany).

The cross-sectional investigations were carried out on electrodes broken into halves after freezing them in liquid nitrogen. Raman spectra of pristine and cycled fiber mat anodes were acquired using an Alpha 300 confocal Raman microscope (WITec, GmbH) with a solid-state 532 nm excitation laser, 100x objective, and a grating with 600 grooves mm^{-1}. Raman maps with a spatial resolution on the order of 1 µm and a pixel density of 9 pixels $µm^{-2}$ were collected with an integration time of 2 s per spectrum. The laser power was attenuated to 1 mW for analysis of the pristine electrode. The laser power was further reduced to 100 µW for analysis of the cycled sample to prevent crystallization of the amorphous silicon from laser-induced heating. Raman maps were analyzed using WITec Project Plus software.

A CR2032 full cell containing an electrospun Si/C/PAA anode and an electrospun $LiCoO_2$/C/PVDF cathode was assembled and tested. The $LiCoO_2$/C/PVDF fiber mat cathode was prepared using the ink formulation and electrospinning procedure described in Chapter V. The full cell contained the same electrolyte and separator as used in the half cells. To minimize the irreversible capacity loss in the full cell, the Si/C/PAA anode and $LiCoO_2$/C/PVDF cathode were preconditioned in half cells for at least 10 cycles at 0.1 C, as has been done in other studies.[28, 36-45] The anode/cathode mass ratio in the full cell was 1/13 to ensure good capacity matching of the electrodes (N/P capacity ratio of 0.89). The full cell was characterized using galvanostatic charge/discharge cycling between 2.50 – 4.20 V at 0.1 C, where the C-rate was calculated based on the measured capacity of the cathode. Full cell capacities were normalized with respect to both electrodes (i.e., the combined amounts of the Si/C/PAA anode and $LiCoO_2$/C/PVDF cathode).

6.3 Results and Discussion

6.3.1 Anodes with Poly(acrylic acid) (PAA) Binder

Freestanding fiber mats containing Si nanoparticles, carbon powder, and a poly(acrylic acid) binder (Si/C/PAA) were fabricated using electrospinning. Preparing particle/polymer fiber mats with a uniform particle distribution requires optimization of several experimental parameters (e.g., ink composition, flow rate, electric field strength, etc.), and thus appropriate ink formulation and electrospinning conditions were determined empirically rather than through a priori means. In the present study, fiber mats containing Si/C/PAA in a weight ratio of 40/25/35 were produced using n-propanol as the solvent and a fixed ink flow rate of 1.00 mL h^{-1}, applied bias voltage of 8 kV, and a spinneret-to-collector distance of 8 cm, as these conditions were used in our previous report on TiO_2-based fiber mat anodes.[26] Ink formulation and relative humidity during electrospinning were then optimized to form Si/C/PAA fiber mats. The solids content of the inks (i.e., combined amounts of Si nanoparticles, carbon powder, and PAA) was varied from 10 – 30 wt %, and 17 – 18 wt % solids was found to be optimal. Inks containing > 25 wt % solids could not be dispersed using magnetic stirring and sonication, and inks with 10 – 15 wt % solids had low viscosities which were not appropriate for electrospinning. Relative humidity (rh) during electrospinning had a significant impact on the properties of the fiber mats. Electrospinning at > 30 % rh resulted in the deposition of fibers which could not be peeled from the collector, presumably due to incomplete solvent evaporation of the fiber jet. On the other hand, freestanding fiber mats were produced by electorspinning at 20 – 30 % rh, and thus these conditions were used in the present study.

Scanning electron microscopy (SEM) images of an electrospun nanofiber mat containing Si nanoparticles, carbon black, and poly(acrylic acid) (Si/C/PAA) in a 40/25/35 weight ratio are shown in Figure 6.1. The as-spun mat had a fiber volume fraction of 0.30 and an average fiber diameter of 980 nm with some bead-on-fiber formation (see Figures 6.1a and 6.1b); these observations were typical for fiber mats prepared in this study. Compacting the mat increased the fiber volume fraction to 0.85, whereas welding the mat improved the interfiber connectivity. As shown in Figures 6.1c and 6.1d, a compacted/welded fiber mat maintained some interfiber void space, and corresponding cross-sectional SEM images presented in Figures 6.2a and 6.2b demonstrate that the fiber volume fraction was uniform throughout the mat and that the interfiber contact nodes were successfully welded. Compared to the as-spun mat, the compacted/welded mat was mechanically stiffer, confirming the presence of these fused fiber crossings. The interfiber connectivity was also assessed by measuring the electrical resistance over a 2 cm section of mat using an ohmmeter with point-type probes. The measured resistance of a compacted/welded mat was ~ 1,000 times lower than that of an as-spun mat (4 vs. 3,000 kΩ), indicating the compacted/welded fiber mat had much better interfiber connectivity.

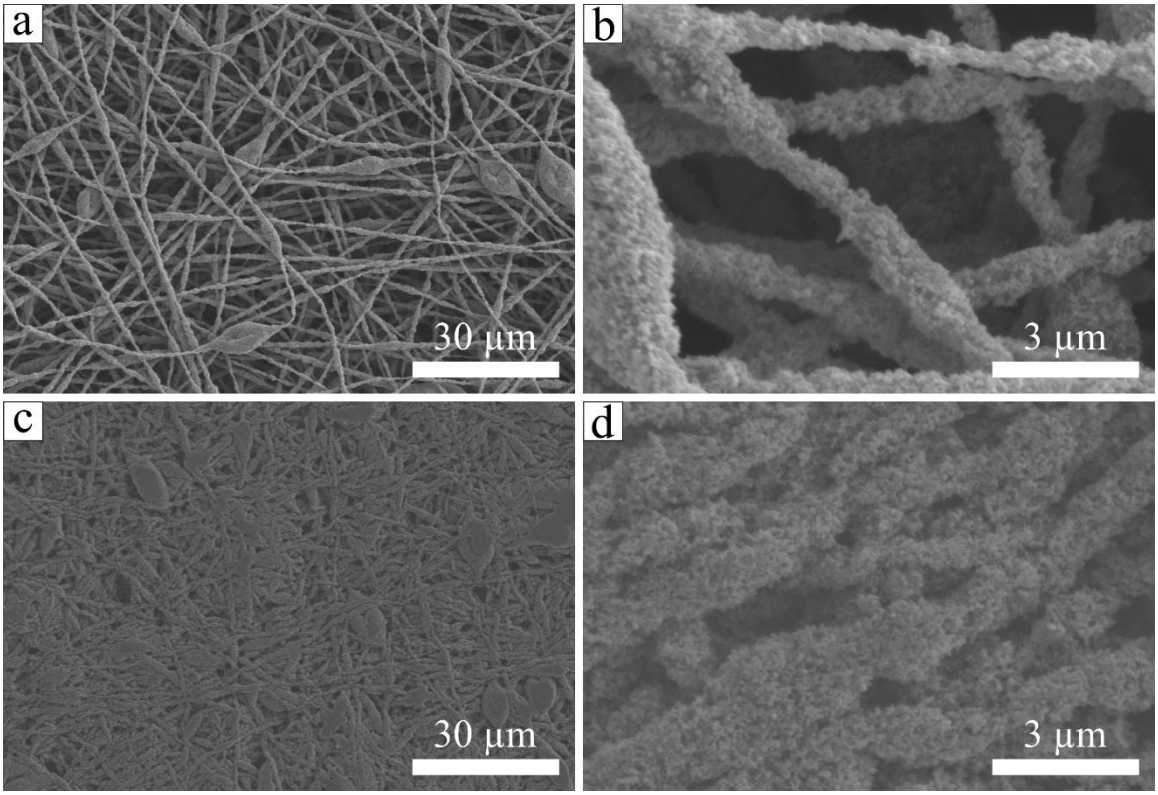

Figure 6.1. Top-down SEM images of electrospun nanofiber mats containing Si/C/PAA in a 40/25/35 weight ratio. (a,b) an as-spun fiber mat and (c,d) a compacted/welded fiber mat.

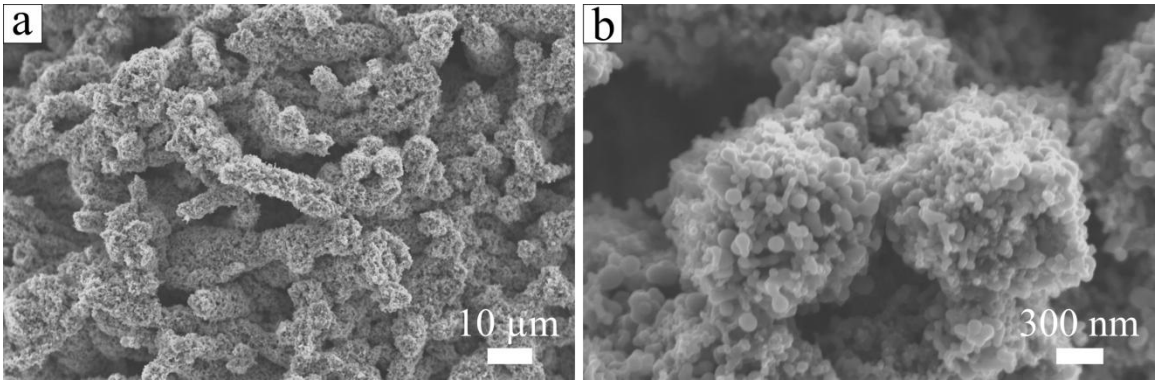

Figure 6.2. (a) Low and (b) high magnification cross-sectional SEM images of a compacted/welded fiber mat containing Si/C/PAA in a 40/25/35 weight ratio.

The performance of an as-spun nanofiber mat anode with a Si/C/PAA weight ratio of 40/25/35 was compared to that of a compacted/welded mat of the same composition. Figure 6.3a shows charge/discharge curves collected at 0.1 C for each electrode during the first two cycles. The shape of these curves are typical for Si-based anodes where lithiation and delithiation reactions occur at potentials < 0.5 V vs. Li/Li^+.[5] Both electrodes exhibited high lithiation capacities ~ 1,700 mAh g^{-1} during the first cycle, but the as-spun mat had a low reversible capacity of 1,064 mAh g^{-1} (corresponding to 2,500 mAh g_{Si}^{-1} and 67 % coulombic efficiency), suggesting some fibers in the as-spun mat were electronically isolated during the first delithiation half cycle. In comparison, the compacted/welded fiber mat anode had excellent Si utilization as evidenced by a high reversible capacity of 1,484 mAh g^{-1} (corresponding to 3,500 mAh g_{Si}^{-1} and 85 % coulombic efficiency) which was essentially unchanged during the second charge/discharge cycle.

Figure 6.3b shows the gravimetric capacity over 50 cycles at 0.1 C of four electrospun anodes with a Si/C/PAA weight ratio of 40/25/35, including: (i) an as-spun mat, (ii) a compacted (unwelded) mat, (iii) a welded (uncompacted) mat, and (iv) a compacted/welded mat. The fiber volume fractions of the uncompacted and compacted mats were approximately 0.30 and 0.85, respectively. The as-spun mat had the lowest initial capacity of 1,064 mAh g^{-1} which faded steadily to 218 mAh g^{-1} after 50 cycles. In comparison, the compacted/welded fiber mat anode showed reasonably good cycling performance with reversible capacities of 1,484 and 1,083 mAh g^{-1} during the 1^{st} and 50^{th} cycles, respectively. Mats which were only welded or only compacted showed intermediate cycling performance. These results demonstrate that mats with a fiber

volume fraction of 0.85 and welded interfiber contacts have sufficient void space for electrolyte infiltration throughout the electrode and mechanical strength to withstand the large volumetric changes of Si during cycling. Conversely, mats with a low fiber volume fraction (~ 0.30) and/or poor interfiber connectivity cannot tolerate reversible Si swelling/shrinking.

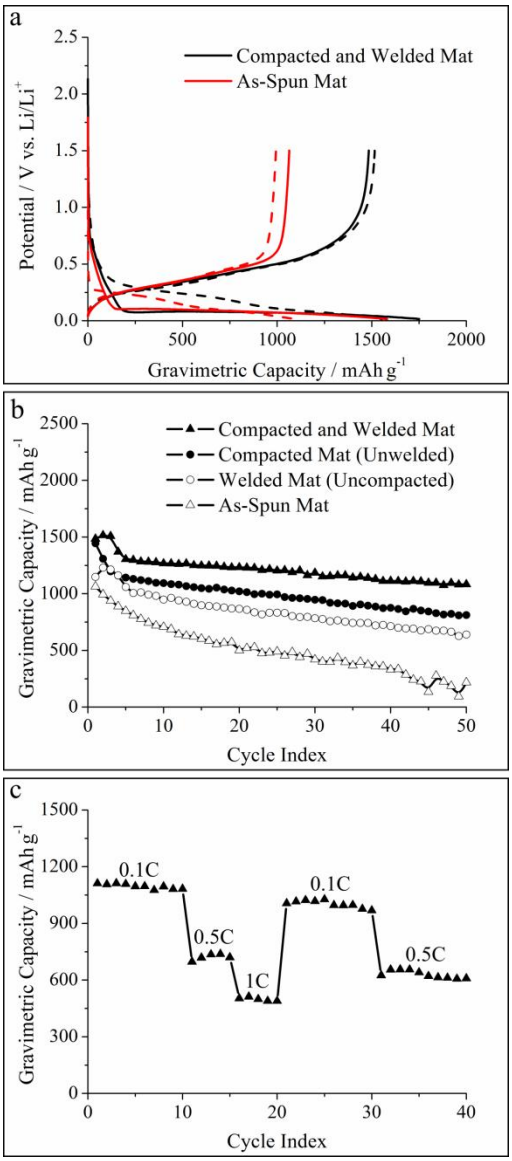

Figure 6.3. Electrochemical characterization of electrospun anodes containing Si/C/PAA in a 40/25/35 weight ratio. (a) Charge/discharge curves for the 1st and 2nd cycles (solid and dashed lines, respectively) for as-spun and compacted/welded fiber mats and (b) gravimetric capacity over 50 cycles at 0.1 C for as-spun, compacted (unwelded), welded (uncompacted), and compacted/welded fiber mats.

The gravimetric capacity of a compacted/welded Si/C/PAA fiber mat anode (prepared with 40 wt % Si, a fiber volume fraction of 0.85, and a thickness of 22 μm) at charge/discharge rates of 0.1 – 1 C over 40 cycles is shown in Figure 6.3c. This rate capability study was conducted after stabilizing the electrode for 40 cycles at 0.1 C at which point the reversible capacity was 1,113 mAh g^{-1}. Overall, the Si/C/PAA fiber had good rate capabilities with stable capacities of 722 and 489 mAh g^{-1} at 0.5 C and 1 C, respectively. The capacity at 0.1 C was fully recovered after cycling at 1 C. The good performance of the electrospun fiber mat anode at high C-rates is attributed to rapid Li^+ transport between the electrolyte and Si nanoparticles in the radial fiber direction which is a consequence of the small fiber diameter (~ 1 μm) and electrolyte penetration throughout the mat's interfiber void space. These results are consistent with our previous reports on other electrospun particle/polymer fiber mat electrodes for Li-ion batteries.[26-28]

Thick electrodes with high areal capacities are desired to reduce the amount of inactive components (e.g., current collectors, separators, etc.) in a LIB. To determine how electrode loading and thickness affect areal capacity and cycling stability, compacted/welded fiber mat anodes (Si/C/PAA weight ratio of 40/25/35) at two different loadings (0.71 and 3.49 mg cm^{-2} with thicknesses of 22 and 65 μm, respectively) were characterized over 50 cycles at 0.1 C. The thin electrode was prepared from a single layer of an electrospun mat which was compacted and welded, whereas the thick electrode with higher loading was prepared by stacking 5 individual mats followed by the compaction and welding steps. The measured densities of the thin and thick electrodes were 0.32 and 0.54 g cm^{-3}, corresponding to porosities of 82 and 70 %, respectively; these porosities

were sufficient for good electrolyte infiltration throughout the fiber mats. As shown in Figure 6.4a, the initial gravimetric capacity when normalized to the total electrode mass was essentially the same for the two mats (1,300 mAh g^{-1} at 3.49 mg cm^{-2} and 1,484 mAh g^{-1} at 0.71 mg cm^{-2}), and each anode retained ~ 70 % of its initial capacity after 50 cycles. As expected, the primary difference in the two nanofiber anodes was their areal capacities (see Figure 6.4b). Of note, the thick anode (with a loading of 3.49 mg cm^{-2}) exhibited very high areal and volumetric capacities of 4.5 mAh cm^{-2} and 750 mAh cm^{-3}, which exceed that of commercial graphite anodes (typically 3 mAh cm^{-2} and 430 mAh cm^{-3}). The excellent performance of the particle/polymer fiber mat anodes is attributed to the good binder/particle adhesion (i.e., PAA interacts with the SiO_x surface on Si nanoparticles via hydrogen bonding), the high Si loading in the fibers, a sufficient (but not excessive) interfiber porosity for electrolyte infiltration, and the presence of interfiber welds (where both welding and a high fiber volume fraction impart mechanical strength to the mat).

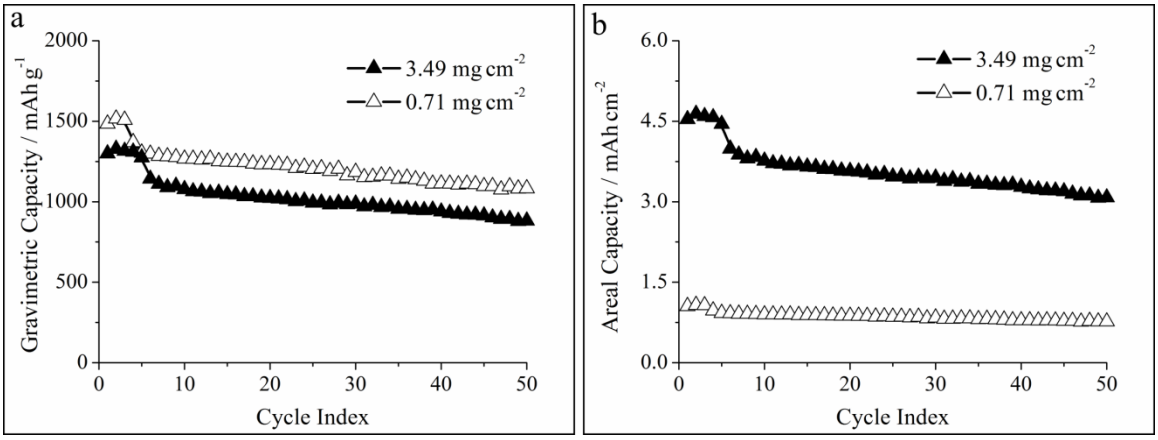

Figure 6.4. (a) Gravimetric capacity and (b) areal capacity of compacted/welded Si/C/PAA nanofiber mats over 50 cycles at 0.1 C. Electrodes at two different loadings (0.71 and 3.49 mg cm^{-2}) were characterized. The electrodes contained Si/C/PAA in a 40/25/35 weight ratio.

The performance of the compacted/welded Si/C/PAA fiber mat anodes in Figure 6.4 compare well to electrospun Si-based anodes reported in the literature. Xiao et al.[25] prepared and characterized a coaxial electrospun nanofiber mat prepared by sputtering a Si layer onto Ni-plated PVDF nanofibers. The electrode exhibited a high capacity when normalized to the Si active material (3,210 mAh g_{Si}^{-1}), but the Si loading in the fibers was only 18.1 wt %, corresponding to an effective gravimetric capacity of 581 mAh g^{-1}. Furthermore, this electrode had a very low material loading of 0.08 mg cm^{-2}, with an areal capacity of 0.046 mAh cm^{-2} which is far too low for practical battery applications. In another study, Xu et al.[22] prepared a 3D Si/C fiber anode by electrospinning poly(acrylonitrile) fibers and electrospraying Si nanoparticles., followed by high temperature pyrolysis to create an electronically conductive nanofiber network. The electrode exhibited stable performance over 100 cycles with high gravimetric and

volumetric capacities (1,600 mAh g^{-1} and 1,000 mAh cm^{-3}, respectively), but the areal capacity (2.7 mAh cm^{-2}) was lower than that of the Si/C/PAA fiber mat anodes reported here (4.5 mAh cm^{-2}).

In principle, the thickness of electrospun Si/C/PAA anodes can be further increased to achieve even higher areal capacities than those reported in Figure 6.4. Our previous studies[26-28] on electrospun particle/polymer fiber mat electrodes have demonstrated that fiber mats which are several hundred microns thick have good active material utilization at slow and fast charge/discharge rates. Extrapolating the results shown in Figure 6.4, a 200 μm thick Si/C/PAA fiber mat with a fiber volume fraction ~ 0.80 would have an extremely high areal capacity of 14 mAh cm^{-2} at 0.1 C which is an order of magnitude greater than that of state-of-the-art materials. Such electrodes were not prepared in this study, but these experiments should be the subject of future work to determine how Si/C/PAA fiber mat thickness and porosity affect electrode capacity and rate capabilities.

To determine how the structure of the electrospun Si/C/PAA anodes evolved during charge/discharge cycling, post-mortem analyses of a fiber mat electrode containing 40 wt % Si were conducted. Figure 6.5 shows Raman spectra for a pristine (i.e., uncycled) fiber mat anode and an electrode after 50 cycles at 0.1 C. The pristine electrode had a large peak near 520 cm^{-1}, associated with the presence of crystalline Si.[46-48] This peak was absent in the cycled electrode, indicating a crystalline to amorphous transformation of Si during cycling.[47] This change was mapped over a large area ~ 4.5 x 9 μm^2 as shown in Figure 6.6; these results indicate that the transformation occurred uniformly throughout the fiber mat.

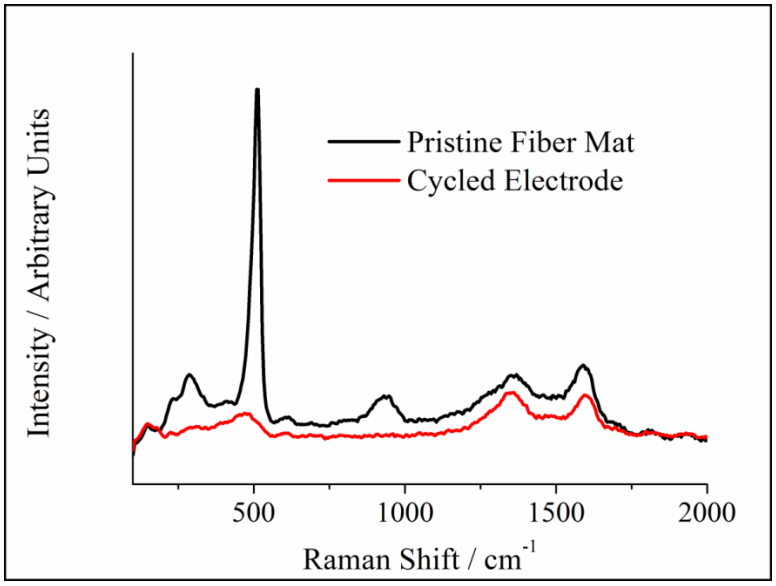

Figure 6.5. Raman spectra of Si/C/PAA fiber mat anodes before and after 50 cycles at 0.1 C. The electrodes contained Si/C/PAA in a 40/25/35 weight ratio.

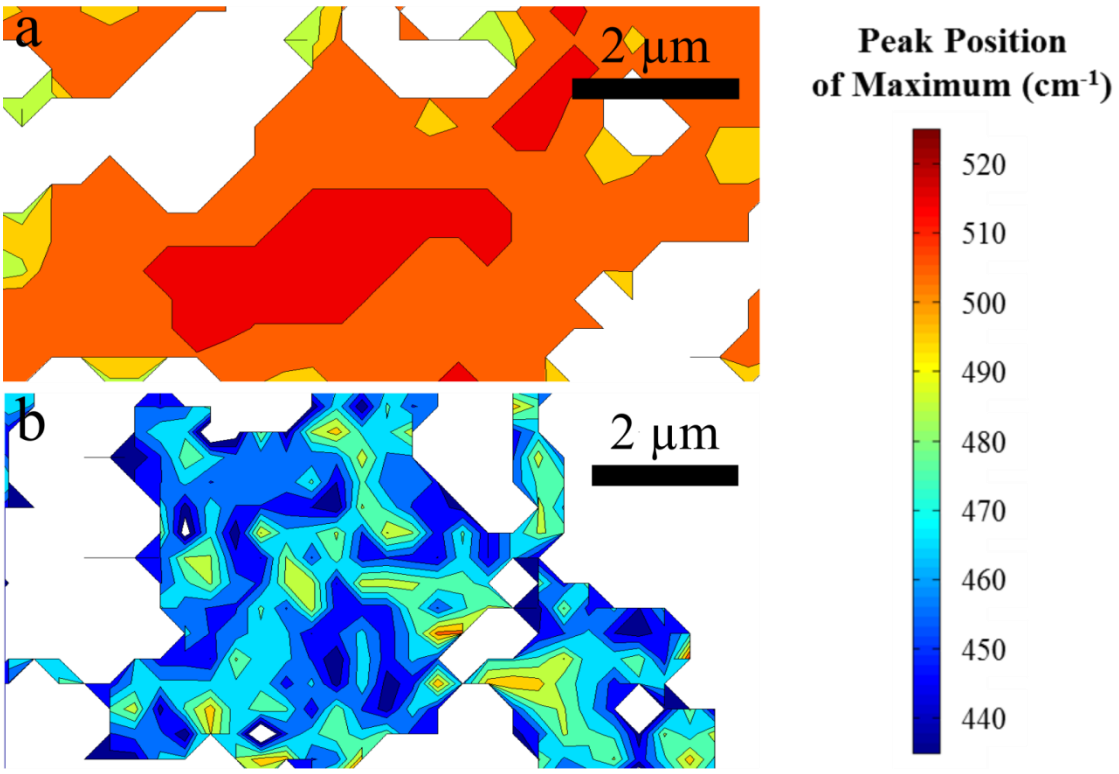

Figure 6.6. Raman maps collected over an area ~ 4.5 x 9 µm^2 showing the Raman shift of the maximum peak for Si/C/PAA fiber mat anodes (a) before cycling and (b) after 50 cycles at 0.1 C. The electrodes contained Si/C/PAA in a 40/25/35 weight ratio.

SEM images of Si/C/PAA fiber mat cross-sections taken before and after 50 charge/discharge cycles are shown in Figure 6.7. These images reveal features related to the: (i) overall electrode structure (Figures 6.7a and 6.7b), (ii) interfiber void space (Figures 6.7c and 6.7d), and (iii) individual particle structure (Figures 6.7e and 6.7f). There was a small (11 %) increase in electrode thickness, from 65 and 72 µm before/after cycling, as indicated by the low magnification images in Figures 6.7a and 6.7b. In comparison, Piper et al.[49] found that the thickness of a slurry cast anode containing Si nanoparticles, carbon black, and PVDF increased by 50 % after 20 cycles. Thus, there is visual evidence that the nanofiber mat anode was able to reversibly accommodate the

volumetric expansion/contraction of Si with minimal changes to the overall electrode structure. As presented in Figures 6.7c and 6.7d, the interfiber void space throughout the mat was also well-preserved during cycling. The high magnification image of a single fiber in Figure 6.7e shows spherical Si particles before cycling, whereas the cycled fiber (Figure 6.7f) contained irregularly shaped particles. This change in particle appearance is attributed to the formation of an SEI layer on the fiber surface that masked the particle shape and/or actual changes in particle morphology during cycling due to the formation of amorphous Si. Overall, these post-mortem SEM images demonstrate that the fiber mat anodes exhibited excellent physical stability during charge/discharge cycling in a battery environment.

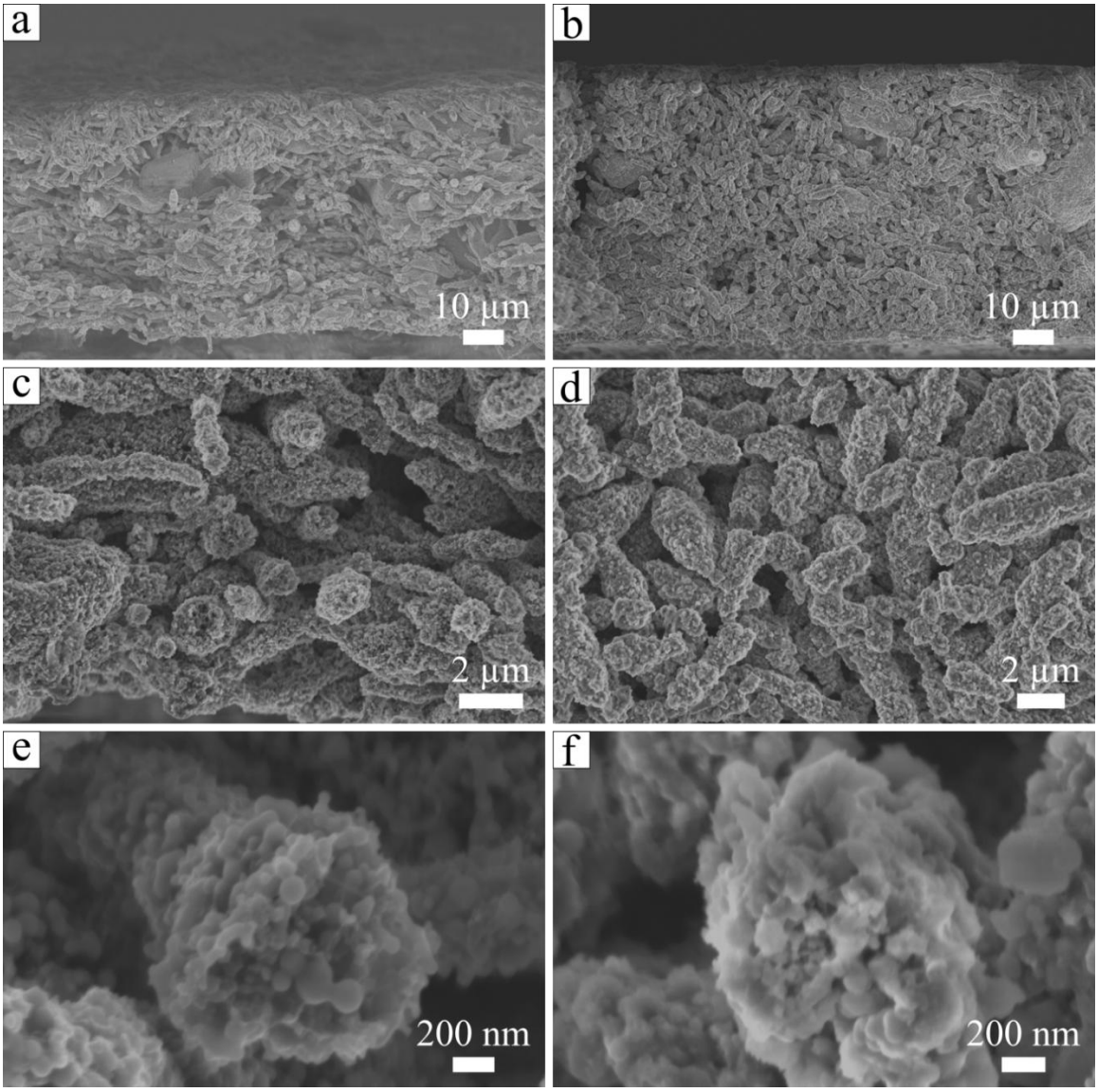

Figure 6.7. Cross-sectional SEM images of a Si/C/PAA nanofiber mat anode (a,c,e) before cycling and (b,d,f) after 50 cycles at 0.1 C. The electrodes contained Si/C/PAA in a 40/25/35 weight ratio.

The effect of Si content in the fibers on cycling performance was evaluated. A compacted/welded mat with a Si/C/PAA fiber weight ratio of 15/50/35 and a fiber volume fraction of 0.85 was prepared (see Figure 6.8), and the performance of this anode

was compared to that of a compacted/welded mat where the fibers contained 40 wt % Si. The areal loading of Si in both anodes was fixed at ~ 0.26 $mg_{Si}\ cm^{-2}$ which translates to a theoretical areal capacity of ~ 1 mAh cm^{-2}. In order to achieve this areal capacity match, the mat with 15 wt % Si was made thicker (40 µm vs. 22 µm for the anode with 40 wt % Si). As shown in Figure 6.9a, the anode with 15 wt % Si had a lower effective gravimetric capacity (582 mAh g^{-1} vs. 1,484 mAh g^{-1}) due to the lower Si content in the fibers, but both electrodes exhibited good Si utilization with reversible capacities > 3,000 mAh g_{Si}^{-1}. Figure 6.9b shows that the anode with lower Si content displayed excellent cycling stability with 90 % capacity retention after 50 cycles vs. 73 % capacity retention for the anode containing 40 wt % Si. The better cycling stability of the 15 wt % Si anode is attributed to smaller net volume changes of the fibers during charging and discharging. Overall, these results demonstrate that the lower effective gravimetric capacity of the anode containing 15 wt % Si can be offset by increasing the electrode thickness to achieve the same areal capacity as a fiber mat with a higher Si weight fraction.

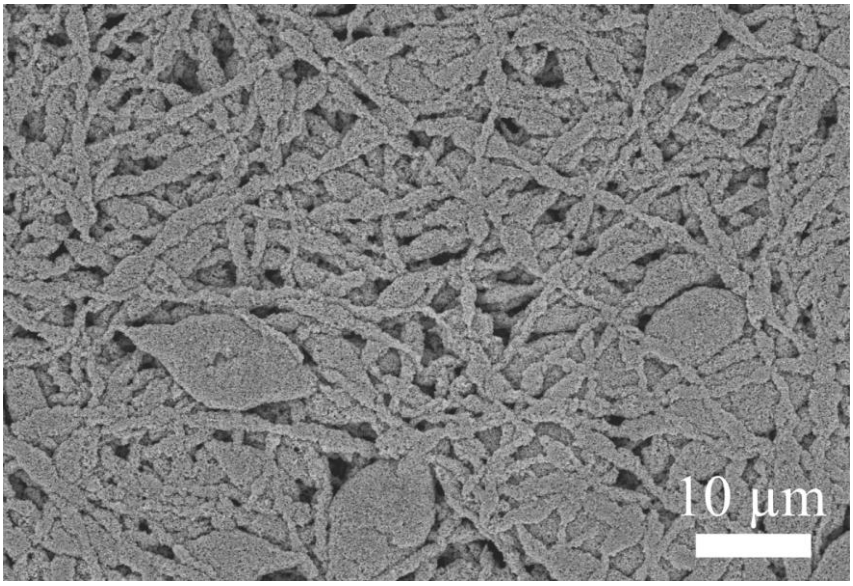

Figure 6.8. SEM image of a compacted/welded nanofiber mat with a fiber volume fraction of 0.85 and Si/C/PAA in a 15/50/35 weight ratio.

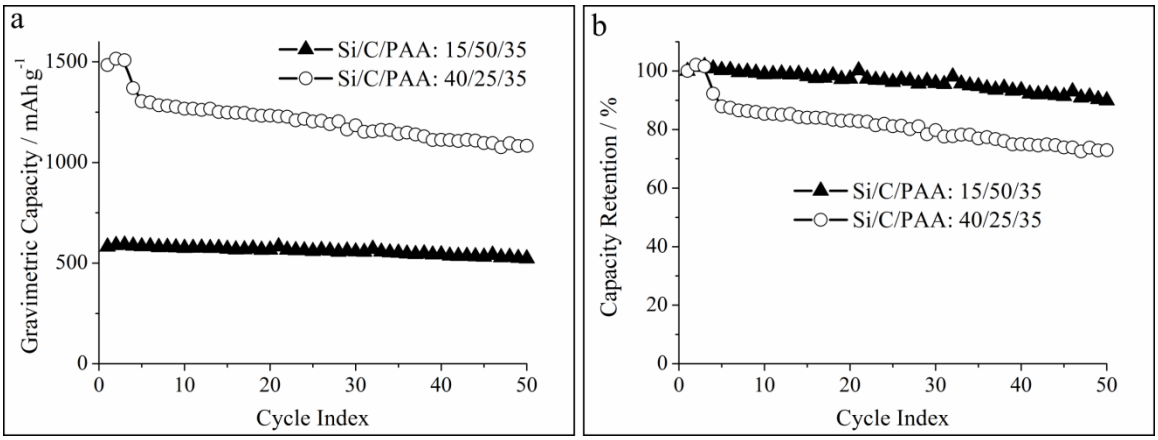

Figure 6.9. Electrochemical characterization of compacted/welded nanofiber mat anodes containing Si/C/PAA weight ratios of 40/25/35 and 15/50/35. (a) Gravimetric capacity and (b) capacity retention over 50 cycles at 0.1 C.

As an alternative to Si nanoparticle-based fiber mat anodes, electrospun fiber mats containing Si nanowires, carbon powder, and PAA binder were also prepared and

characterized. The performance of as-spun Si/C/PAA fiber mats (i.e., mats which were neither compacted nor welded) containing either Si nanowires or Si nanoparticles were compared in half cells as discussed in Appendix C. In short, these experiments showed that electrospun anodes prepared with Si nanowires had a lower reversible capacity of 432 mAh g^{-1} at 0.1 C but better cycling stability with 68 % capacity retention after 50 cycles (compared to 1,001 mAh g^{-1} and 21 % capacity retention for an as-spun anode with Si nanoparticles). The lower capacity of the Si nanowires may be due to the presence of a thick (~ 10 nm) SiO_x passive layer on the nanowire surface as determined by Jagjit Nanda and coworkers at Oak Ridge National Laboratory using x-ray photoelectron spectroscopy (results not shown). Since the Si nanowires had lower gravimetric capacities, they were not further investigated in the present study.

Most of the existing literature on Si-based anodes focuses exclusively on half cell characterizations, but electrode performance in full cells is critical for practical battery applications.[6, 8, 28] To evaluate electrode performance under more realistic testing conditions, a full cell containing an electrospun Si/C/PAA anode (with a Si/C/PAA weight ratio of 40/25/35) and an electrospun $LiCoO_2$/C/PVDF cathode[28] was prepared and characterized.

Figure 6.10a shows a typical charge/discharge curve at 0.1 C for the electrospun Si/$LiCoO_2$ full cell. During discharge, the cell had an average operating potential of 3.6 V and a reversible capacity of 75 mAh g^{-1} (normalized to the combined mass of both electrodes) which corresponds well to the theoretical capacity of 77 mAh g^{-1} based on the individual capacities of the anode and cathode. Agreement between the measured and theoretical capacities indicates good active material utilization for the Si-based anode and

$LiCoO_2$-based cathode. The areal capacity and energy density of the Si/$LiCoO_2$ cell were 2.6 mAh cm^{-2} and 270 Wh kg^{-1}, respectively, which are the highest values reported to date in the literature for any electrospun full cell (previous studies reported effective areal capacities < 1 mAh cm^{-2} and mass normalized energy densities of 100 – 150 Wh kg^{-1}).[50, 51] Figure 6.10b shows the Si/$LiCoO_2$ full cell exhibited moderate cycling stability with a reversible capacity of 53 mAh g^{-1} after 10 cycles. It should be noted that the energy density of the Si/$LiCoO_2$ cell was limited by the cathode capacity (84 mAh g^{-1} at 0.1 C); thus the use of a higher capacity cathode material (e.g., sulfur) would lead to even higher full cell energy densities.

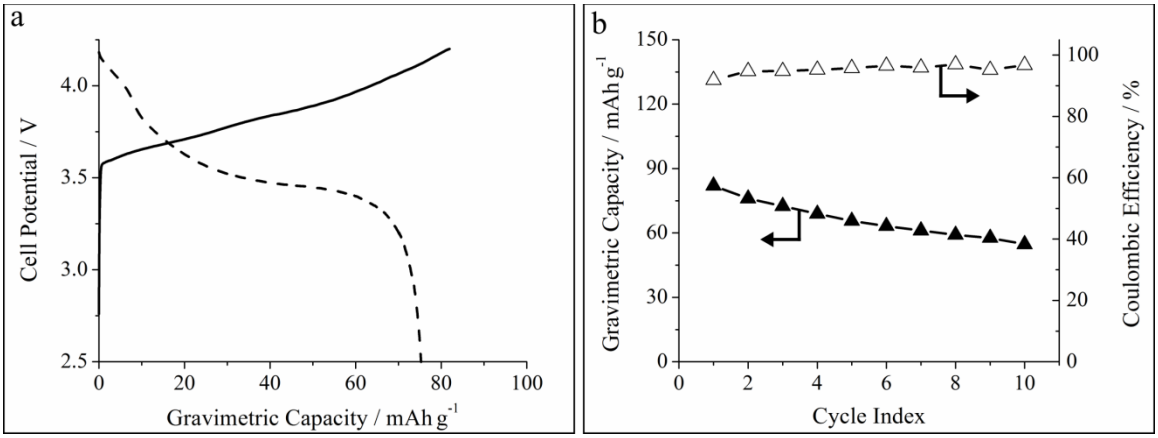

Figure 6.10. Electrochemical characterization of a full cell containing an electrospun Si/C/PAA anode and $LiCoO_2$/C/PVDF cathode. (a) Charge/discharge curve collected at 0.1 C and (b) cycling stability over 10 cycles at 0.1 C. The anode contained Si/C/PAA in a 40/25/35 weight ratio, and the cathode contained $LiCoO_2$/C/PVDF in a 70/10/20 weight ratio.

6.3.2 Anodes with Electronically Conductive Polymer Binders

Two electronically conductive polymer binders [poly(9,9-dioctylfluorene-co-fluorenone-co-methylbenzoic ester) (PFM) and poly(2,7-9,9-dioctylfluorene-co-2,7-9,9-(di(oxy-2,5,8- trioxadecane)) fluorine-co-2,7-fluorenone-co-2,5-1-methylbenzoic ester) (PEFM)] with electrical conductivities ~ 1 x 10^{-6} S m^{-1} were synthesized by Gao Liu and coworkers at Lawrence Berkeley National Laboratory as described previously.[29, 52] The structures of PFM and PEFM are shown in Figure 6.11. Electrospinning studies and electrochemical characterization of Si-based anodes containing PFM and PEFM binders were conducted at Vanderbilt.

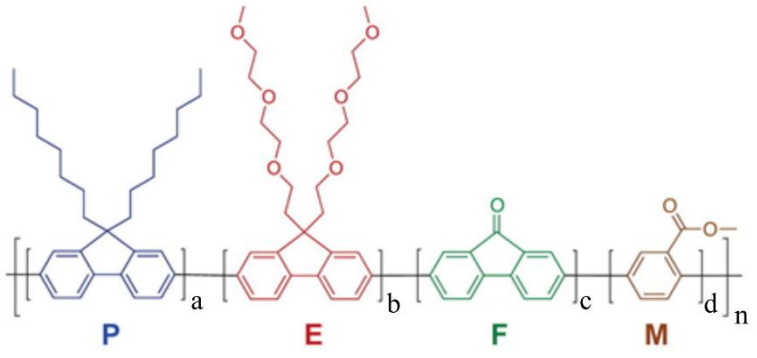

PFM a:b:c:d = 2:0:1:1
PEFM a:b:c:d = 3:1:1:1

Figure 6.11. Structure of the electronically conductive polymer binders, PFM and PEFM. Image adapted from Wu et al.[52] with permission from The American Chemical Society.

A PFM solution containing 5 wt % PFM in a chlorobenzene/chloroform solvent (1/1 by weight) was electrospun at the conditions given in Table 6.1. As shown in Figures 6.12a and 6.12b, the neat PFM fibers contained an undesirable bead-on-fiber morphology. To improve the spinnability of PFM, a poly(ethylene oxide) (PEO) carrier

polymer was utilized, and a solution containing PFM/PEO in a 99/1 weight ratio was electrospun at the conditions given in Table 6.1. PFM/PEO fibers spun at 15 % relative humidity (rh) had a smooth surface and uniform fiber diameters ~ 1.6 μm as shown in Figures 6.12c and 6.12d. In contrast, PFM/PEO fibers spun at 75 % rh (see Figures 6.12e and 6.12f) contained pores ~ 100 nm in size. The formation of surface pores at 75 % rh is attributed to the insolubility of PFM in water. During electrospinning, some water vapor adsorbed into the fibers during organic solvent evaporation from the electrospinning jet in a high humidity environment. The sorbed water resulted in phase inversion of the PFM binder and the formation of porous fibers.

Table 6.1. Electrospinning conditions for PFM and PFM/PEO solutions. All solutions contained 5 wt % polymer in a mixture of chlorobenzene/chloroform (1/1 by weight).

Fiber Composition	Flow Rate (mL h^{-1})	Bias Voltage (kV)	Distance (cm)	Relative Humidity (%)
PFM	0.25	6	8	30
PFM/PEO (99/1 w/w)	0.25	5	8	15, 75

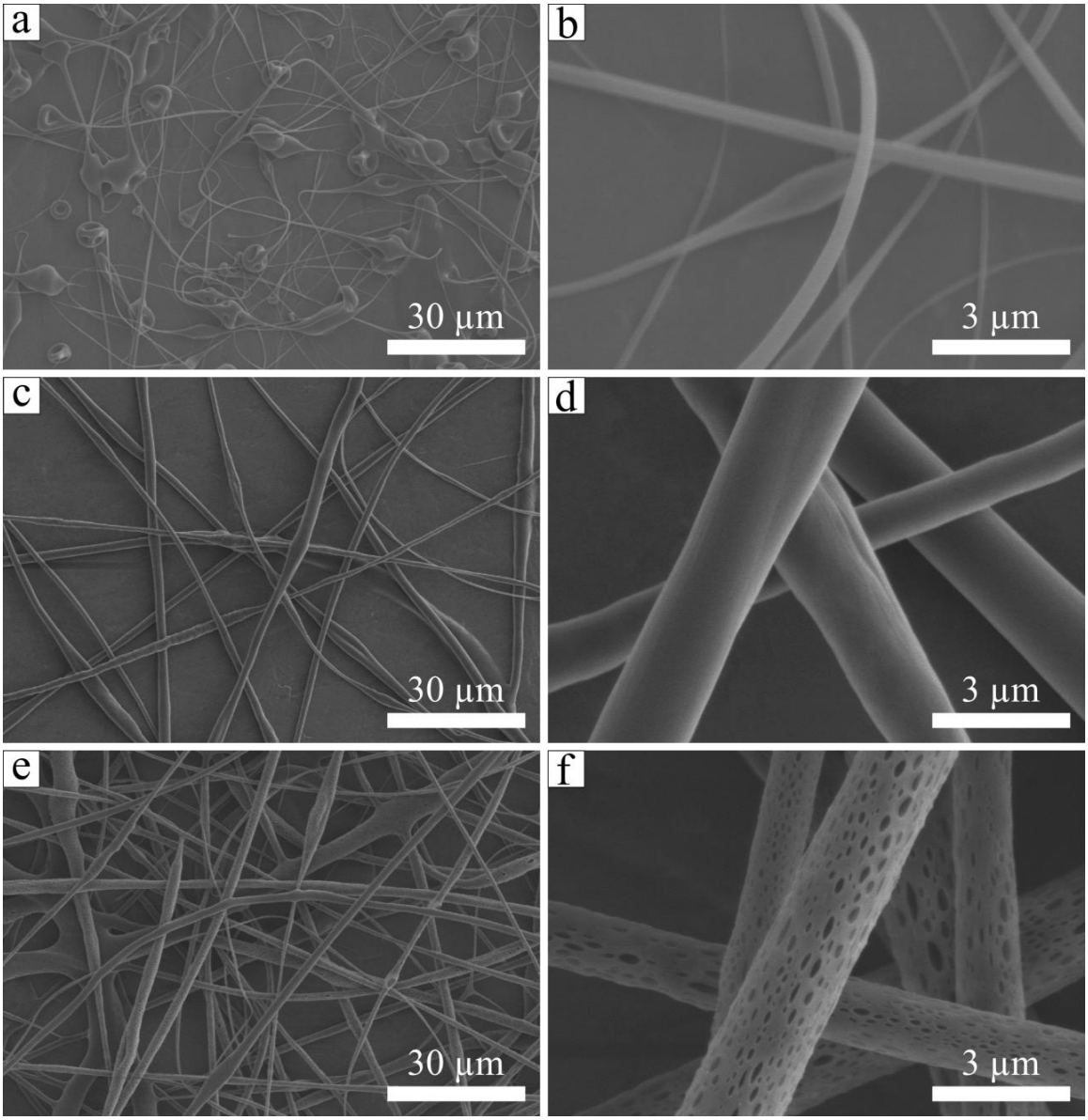

Figure 6.12. SEM images of electrospun (a,b) neat PFM fibers and (c – f) PFM/PEO fibers prepared at (c,d) 15 % rh and (e,f) 75 % rh. The PEO carrier polymer content in (b – f) was 1 wt %.

Electrospun fiber mats containing Si nanoparticles, PFM binder, and PEO carrier polymer were prepared. The solids content in the inks was 10 wt %, and two fiber compositions (Si/PFM/PEO weight ratios of 35/64/1 and 50/49/1) were investigated. The

electrospinning conditions used to form fibers containing either 35 or 50 wt % Si are listed in Table 6.2, and SEM images of the fibers are shown in Figure 6.13. The fibers containing 35 wt % Si (see Figures 6.13a and 6.13b) had a uniform particle distribution and an average fiber diameter ~ 1.5 µm. In comparison, the sample containing 50 wt % Si (see Figures 6.13c and 6.13d) exhibited a bead-on-fiber morphology with fiber diameters up to 9 µm. The rh during electrospinning had a large impact on the structure of Si/PFM/PEO fibers containing 50 wt % Si. As shown in Figure 6.14a, fibers spun at 15 % rh had a dense structure, whereas spinning at 75 % rh formed porous fibers. These observations are consistent with the experiments conducted on PFM/PEO fibers containing no Si nanoparticles discussed previously.

Table 6.2. Electrospinning conditions for inks containing Si/PFM/PEO containing 35 and 50 wt % Si.

Fiber Composition	Flow Rate (mL h^{-1})	Bias Voltage (kV)	Distance (cm)	Relative Humidity (%)
Si/PFM/PEO (35/64/1 w/w/w)	0.25	5	8	75
Si/PFM/PEO (50/49/1 w/w/w)	0.50	5	8	15, 75

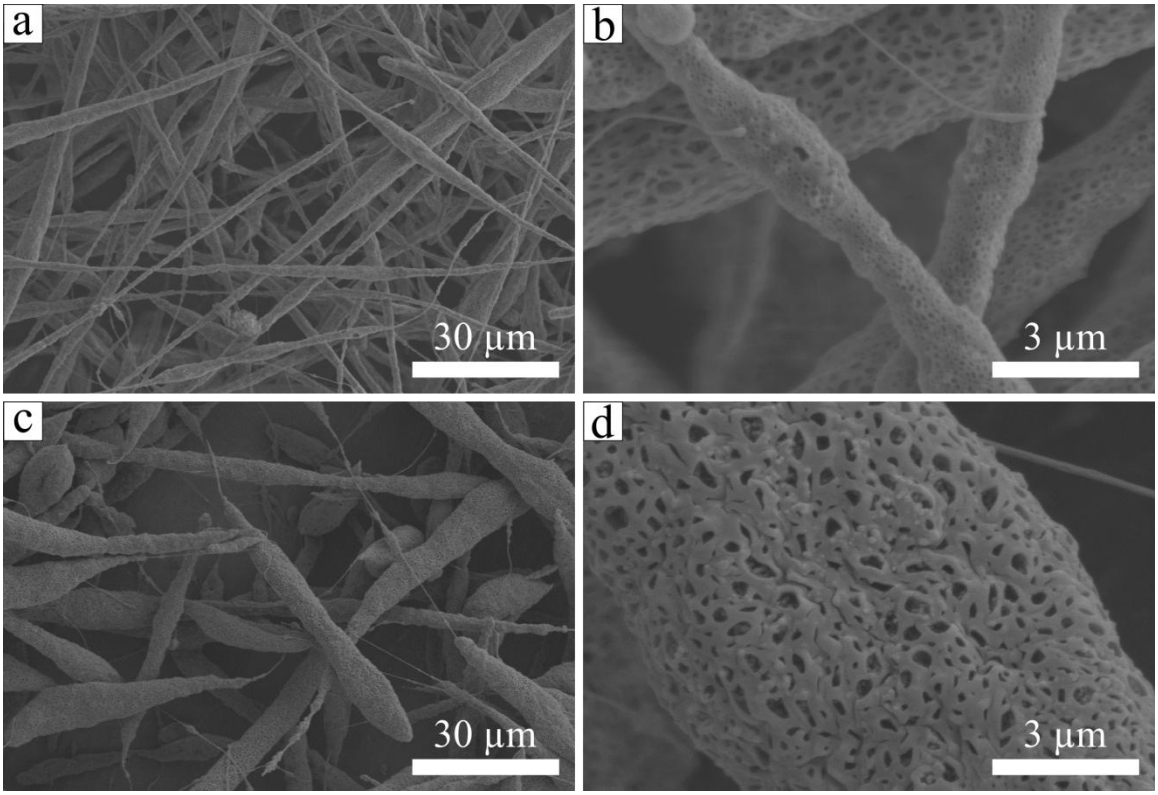

Figure 6.13. SEM images of electrospun Si/PFM/PEO fiber mats containing: (a,b) 35 wt % Si and (c,d) 50 wt % Si. All samples contained 1 wt % PEO as a carrier polymer, and electrospinning was conducted at 75 % rh.

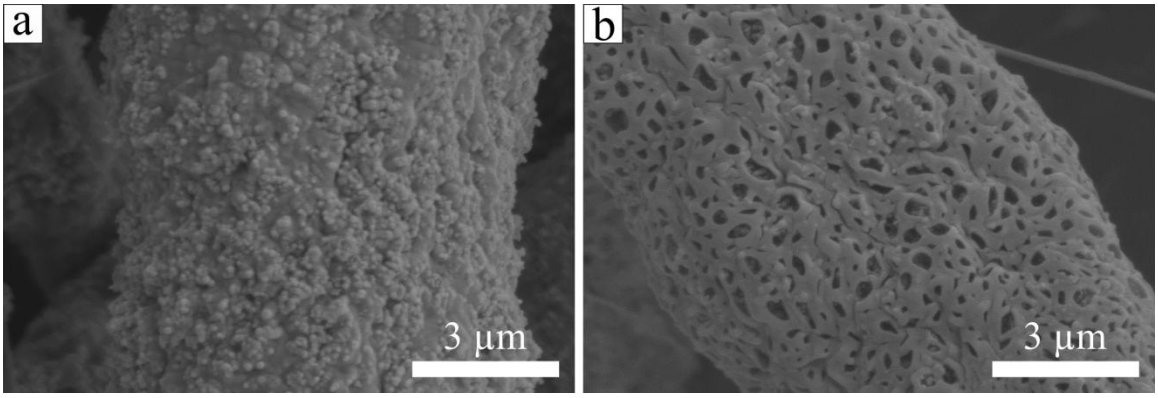

Figure 6.14. SEM images of fiber mats containing a Si/PFM/PEO weight ratio of 50/49/1 which were electrospun at (a) 15 % rh and (b) 75 % rh.

The electrochemical performance of electrospun and slurry cast anodes containing Si/PFM/PEO in a 50/49/1 weight ratio was evaluated in half cells. Typical charge/discharge curves collected at 0.1 C for these electrodes are shown in Figure 6.15. Surprisingly, all of these anodes exhibited virtually no reversible capacity (< 15 mAh g^{-1}). These observations were consistent for multiple experiments conducted at Vanderbilt and LBNL. Similar results were obtained for a Si/PFM slurry cast anode (containing no PEO polymer), indicating that PEO is not the cause of the electrodes' low capacity. Instead, it is likely that the PFM binder in these electrodes formed a thick, ionically insulating layer around the Si nanoparticles which inhibited Li^+ transport to the active material during battery cycling. One way to reduce the thickness of the polymer binder coating is to increase the Si/PFM ratio in the electrode. Thus, a series of Si/PFM slurry cast anodes with different compositions (Si/PFM weight ratios of 50/50, 55/45, 60/40, and 67/33) were prepared and characterized in half cells.

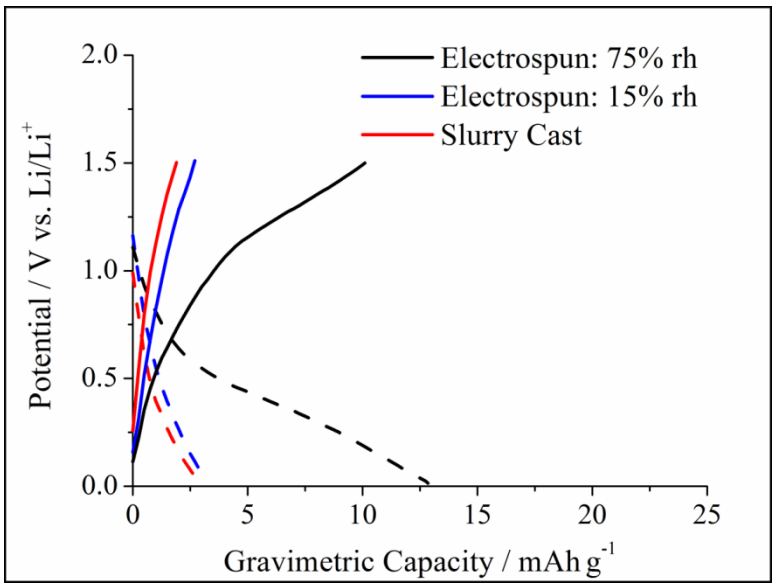

Figure 6.15. Typical charge/discharge curves collected at 0.1 C for electrospun and slurry cast anodes containing Si/PFM/PEO in a 50/49/1 weight ratio. Electrospun fiber mats were prepared at 15 % rh and 75 % rh.

Figures 6.16a and 6.16b show charge/discharge curves collected at 0.01 C for slurry cast Si/PFM anodes containing 50 – 67 wt % Si. Samples containing 50, 55, and 60 wt % Si had virtually no reversible capacity (< 15 mAh g^{-1}). In comparison, the anode with 67 wt % Si exhibited good electrochemical performance. The charge/discharge curves for the anode with 67 wt % Si show that lithiation/delithiation processes occurred at potentials < 0.5 V vs. Li/Li^+ which is expected for Si-based anodes. Figure 6.16c shows this anode had an initial gravimetric capacity of 1,898 mAh g^{-1} (corresponding to 2,800 mAh g_{Si}^{-1}) and an initial coulombic efficiency of 61 % which is attributed to: (i) formation of an SEI layer on the anode and (ii) Li doping of the PFM binder. Subsequent cycles at 0.1 C had coulombic efficiencies exceeding 98 %, and the

electrode had good cycling stability with a reversible capacity of 1,239 mAh g^{-1} after 50 cycles.

The results in Figure 6.16 demonstrate that Si/PFM anodes must contain < 40 wt % PFM to achieve good electrochemical performance. The reason for poor performance at higher PFM loadings is not yet fully understood, but it is presumed that the electrodes prepared with ≥ 40 wt % PFM had a thick polymer coating on the Si nanoparticles which made them electrochemically inaccessible even at very slow charge/discharge rates (e.g., 0.01 C). Future studies should focus on: (i) preparing electrospun Si/PFM fibers with 67 wt % Si and (ii) decreasing the fiber diameter to facilitate Li^+ transport between the electrolyte and Si nanoparticles in the radial fiber direction.

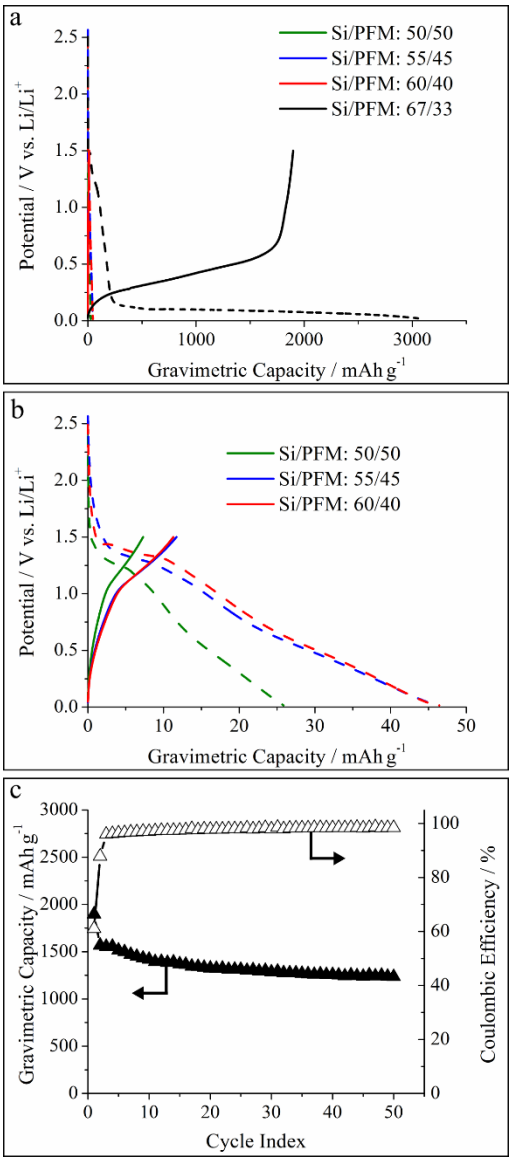

Figure 6.16. (a,b) Charge/discharge curves collected at 0.01 C for slurry cast Si/PFM anodes containing (a) 50 – 67 wt % Si and (b) 50 – 60 wt % Si. (c) Cycling stability of a Si/PFM anode with 67 wt % Si at 0.01 C for 1 cycle and 0.1 C for 50 cycles.

A second electronically conductive polymer binder (PEFM) was prepared at LBNL and sent to Vanderbilt. The performance of slurry cast Si/PEFM anodes containing 55 and 60 wt % Si was evaluated to determine the appropriate electrode

composition target for electrospun Si/PEFM fiber mat anodes to be developed in future studies.

Figure 6.17a shows charge/discharge curves collected at 0.01 C for slurry cast Si/PEFM anodes containing 55 and 60 wt % Si (45 and 40 wt % PEFM, respectively). Compared to Si/PFM slurry cast anodes which had poor performance with these binder contents, the Si/PEFM anodes with 55 and 60 wt % Si had high reversible capacities of 1,526, and 1,559 mAh g^{-1}, respectively. Figure 6.17b shows the Si/PEFM anode containing 60 wt % Si had good cycling stability with a reversible capacity of 948 mAh g^{-1} after 50 cycles at 0.1 C. These results demonstrate that the PEFM-containing anodes had better electrochemical performance at binder contents up to 45 wt % compared to that of the Si/PFM system. The superior performance of the Si/PEFM electrodes may be attributed to the presence of the binder's PEO sidechains (see Figure 6.11) which swell with battery electrolyte and thus provide better access of Li^+ to the Si active material.

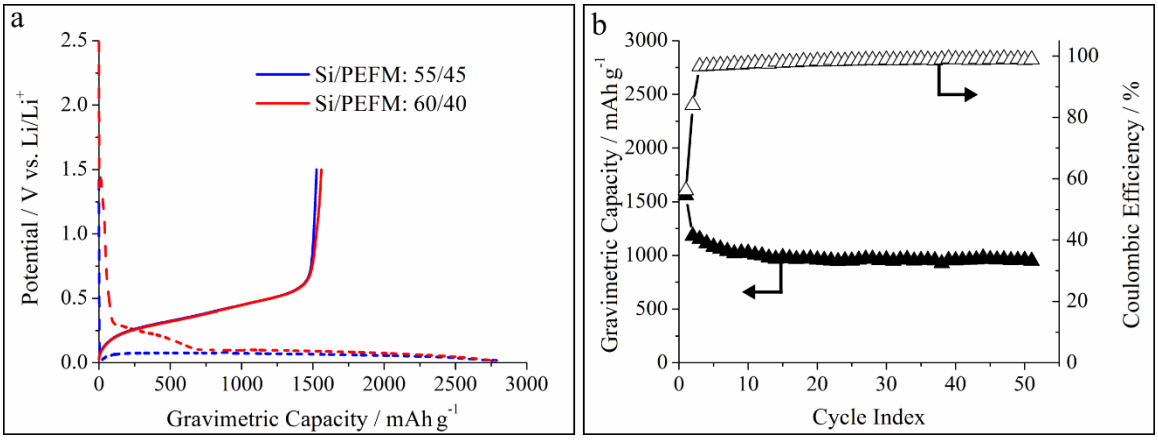

Figure 6.17. (a) Charge/discharge curves collected at 0.01 C for slurry cast Si/PEFM anodes containing 55 and 60 wt % Si. (b) Cycling stability of a Si/PEFM anode with 60 wt % Si over 1 cycle at 0.01 C and 50 cycles at 0.1 C.

6.4 Conclusions

Particle/polymer electrospinning was used to prepare fiber mat LIB anodes containing Si nanoparticles and carbon black with poly(acrylic acid) as the binder (Si/C/PAA). A compacted/welded fiber mat containing 40 wt % Si had a high gravimetric capacity of 1,484 mAh g^{-1} (3,500 mAh g_{Si}^{-1}) and good cycling stability with 73 % capacity retention after 50 cycles at 0.1 C. The anode also had good rate capabilities with a reversible capacity of 489 mAh g^{-1} at 1 C. A fiber mat anode of the same composition which was neither compacted nor welded performed poorly, with an initial capacity of 1,064 mAh g^{-1} and 20 % capacity retention after 50 cycles. Compacting and welding improved the mechanical strength of an electrospun mat, but sufficient void space remained in the electrode to accommodate the large volumetric changes of Si during charge/discharge cycling. The effect of Si content in the fibers on cycling performance was also evaluated. An electrospun Si/C/PAA fiber mat anode containing

15 wt % Si performed better than an electrospun anode prepared with 40 wt % Si. The anode with 15 wt % Si had a lower effective gravimetric capacity (582 mAh g^{-1}), but it exhibited superior cycling stability (90 % capacity retention after 50 cycles) due to smaller overall volumetric changes during cycling. Anodes containing 15 and 40 wt % Si (with thicknesses of 40 and 22 μm, respectively) were prepared with the same Si areal loading, demonstrating that the lower effective gravimetric capacity of a fiber mat anode with low Si content can be offset by utilizing a thicker electrode.

Post-mortem analyses of electrospun anodes were conducted to determine how the fiber mat structure changed during charge/discharge cycling. Raman spectroscopy showed that there was a conversion of crystalline Si to amorphous Si during cycling. Cross-sectional SEM images indicated good physical stability of the anodes in a battery environment, with preservation of the fiber mat structure and interfiber void space during cycling.

Whereas Si anodes prepared by electrospinning followed by fiber pyrolysis have low material loadings and mat densities which limit their use in practical devices, particle/polymer electrospinning can be used to prepare thick, densely packed fiber mats with high loadings for high areal and volumetric capacities. A compacted/welded nanofiber mat containing 40 wt % Si and a material loading of 3.49 mg cm^{-2} exhibited areal and volumetric capacities of 4.5 mAh cm^{-2} and 750 mAh cm^{-3}, respectively, at 0.1 C. The excellent performance of these particle/polymer nanofiber mats is ascribed to the: (i) PAA binder which interacts with the SiO_x surface on the Si nanoparticles and (ii) overall mechanical strength of the mat, which is a consequence of the high fiber volume fraction and the presence of interconnected, welded fibers. Furthermore, while

most papers in the literature have focused exclusively on characterizing electrodes in half cells, LIB full cells were built and tested using a Si/C/PAA fiber mat anode and a $LiCoO_2$/C/PVDF fiber cathode (the latter being discussed thoroughly in a prior publication[28]). The electrospun full cell exhibited a high areal capacity of 2.6 mAh cm^{-2}, high specific energy of 270 Wh kg^{-1}, and moderate cycling stability with 70 % capacity retention after 10 cycles at 0.1 C.

Si-based anodes containing electronically conductive polymer binders (PFM and PEFM, synthesized at LBNL) were also prepared and characterized. Ink formulation and electrospinning conditions to form Si/PFM/PEO fiber mats with up to 50 wt % Si were identified. Electrospun and slurry cast Si/PFM/PEO anodes containing 50 wt % Si exhibited very low reversible capacities (< 15 mAh g^{-1}) when cycled at 0.1 C. In follow-on experiments, Si/PFM slurry cast anodes containing 50 – 67 wt % Si were prepared and characterized. Whereas a Si/PFM anode containing 67 wt % Si showed a reversible capacity of 1,898 mAh g^{-1} and good cycling stability over 50 cycles, anodes prepared with 50 – 60 wt % Si had very low capacities (< 15 mAh g^{-1}). The poor performance of the electrodes with high binder content is attributed to formation of a thick, ionically insulating polymer layer on the Si nanoparticles. In comparison, slurry cast Si/PEFM anodes containing either 55 or 60 wt % Si exhibited high reversible capacities ~ 1,500 mAh g^{-1} at 0.01 C and good cycling stability with 80 % capacity retention after 50 cycles at 0.1 C. The superior performance of the Si/PEFM anodes is attributed to enhanced electrolyte sorption into the binder due to the presence of the PEO sidechains.

The experiments on slurry cast Si/PFM and Si/PEFM anodes were used to identify the composition target for electrospun fiber mat anodes containing Si nanoparticles and an electronically conductive polymer binder. For a Si/PFM system, at least 67 wt % Si should be incorporated into the fibers, whereas the Si loading of fibers with PEFM binder should at least 55 wt %.

Overall the results in the present paper demonstrate that particle/polymer electrospinning is a viable and attractive technique for the preparation of high performance porous electrodes for LIBs. The composition, thickness, fiber volume fraction, and fiber interconnectivity of electrospun mats can be easily controlled to achieve high gravimetric, areal, and volumetric capacities; this flexibility is unique to electrospun particle/polymer mats and is not possible for other electrode fabrication methods. Furthermore, the technique is compatible with a wide range of particle/polymer combinations and thus can be used to prepare nanofiber electrodes with new active materials and binders as they are developed.

6.5 References

[1] M. Armand, J.-M. Tarascon, *Nature* **2008**, *451*, 652.
[2] J.-M. Tarascon, M. Armand, *Nature* **2001**, *414*, 359.
[3] J. B. Goodenough, Y. Kim, *Chem. Mater.* **2010**, *22*, 587.
[4] J. B. Goodenough, *Acc. Chem. Res.* **2013**, *46*, 1053.
[5] U. Kasavajjula, C. Wang, A. J. Appleby, *J. Power Sources* **2007**, *163*, 1003.
[6] N. Nitta, G. Yushin, *Part. Part. Syst. Char.* **2014**, *31*, 317.
[7] H. Wu, Y. Cui, *Nano Today* **2012**, *7*, 414.
[8] J. Li, N. J. Dudney, J. Nanda, C. Liang, *ACS Appl. Mater. Interfaces* **2014**, *6*, 10083.
[9] R. C. Guzman, J. Yang, M. M.-C. Cheng, S. O. Salley, K. Y. Simon Ng, *J. Mater. Sci.* **2013**, *48*, 4823.
[10] L. Hu, H. Wu, S. S. Hong, L. Cui, J. R. McDonough, S. Bohy, Y. Cui, *Chem. Commun.* **2011**, *47*, 367.
[11] N. Liu, H. Wu, M. T. McDowell, Y. Yao, C. Wang, Y. Cui, *Nano Lett.* **2012**, *12*, 3315.
[12] C. K. Chan, H. Peng, G. Liu, K. McIlwrath, X. F. Zhang, R. A. Huggins, Y. Cui, *Nat. Nanotechnol.* **2008**, *3*, 31.
[13] C. K. Chan, R. N. Patel, M. J. O'Connell, B. A. Korgel, Y. Cui, *ACS Nano* **2010**, *4*, 1443.
[14] N. Liu, L. Hu, M. T. McDowell, A. Jackson, Y. Cui, *ACS Nano* **2011**, *5*, 6487.
[15] H. Zhou, J. Nanda, S. K. Martha, R. R. Unocic, H. M. Meyer, 3rd, Y. Sahoo, P. Miskiewicz, T. F. Albrecht, *ACS Appl. Mater. Interfaces* **2014**, *6*, 7607.
[16] L. Liu, J. Lyu, T. Li, T. Zhao, *Nanoscale* **2016**, *8*, 701.
[17] H.-G. Wang, S. Yuan, D.-L. Ma, X.-B. Zhang, J.-M. Yan, *Energy Environ. Sci.* **2015**, *8*, 1660.
[18] K. Fu, L. Xue, O. Yildiz, S. Li, H. Lee, Y. Li, G. Xu, L. Zhou, P. D. Bradford, X. Zhang, *Nano Energy* **2013**, *2*, 976.
[19] Y. Liu, K. Huang, Y. Fan, Q. Zhang, F. Sun, T. Gao, Z. Wang, J. Zhong, *Electrochim. Acta* **2013**, *102*, 246.
[20] L. Ji, X. Zhang, *Energy Environ. Sci.* **2010**, *3*, 124.
[21] L. Xue, K. Fu, Y. Li, G. Xu, Y. Lu, S. Zhang, O. Toprakci, X. Zhang, *Nano Energy* **2013**, *2*, 361.
[22] Y. Xu, Y. Zhu, F. Han, C. Luo, C. Wang, *Adv. Energy Mater.* **2015**, *5*, 1400753.
[23] Z. Favors, H. H. Bay, Z. Mutlu, K. Ahmed, R. Ionescu, R. Ye, M. Ozkan, C. S. Ozkan, *Sci. Rep.* **2015**, *5*, 8246.
[24] H. Wu, G. Zheng, N. Liu, T. J. Carney, Y. Yang, Y. Cui, *Nano Lett.* **2012**, *12*, 904.
[25] Q. Xiao, Q. Zhang, Y. Fan, X. Wang, R. A. Susantyoko, *Energy Environ. Sci.* **2014**, *7*, 2261.
[26] E. C. Self, R. Wycisk, P. N. Pintauro, *J. Power Sources* **2015**, *282*, 187.
[27] E. C. Self, E. C. McRen, P. N. Pintauro, *ChemSusChem* **2016**, *9*, 208.
[28] E. C. Self, E. C. McRen, R. Wycisk, P. N. Pintauro, *Electrochim. Acta* **2016**, *214*, 139.

[29] G. Liu, S. Xun, N. Vukmirovic, X. Song, P. Olalde-Velasco, H. Zheng, V. S. Battaglia, L. Wang, W. Yang, *Adv. Mater.* **2011**, *23*, 4679.
[30] S. J. Park, H. Zhao, G. Ai, C. Wang, X. Song, N. Yuca, V. S. Battaglia, W. Yang, G. Liu, *J. Am. Chem. Soc.* **2015**, *137*, 2565.
[31] H. Zhao, Z. Wang, P. Lu, M. Jiang, F. Shi, X. Song, Z. Zheng, X. Zhou, Y. Fu, G. Abdelbast, X. Xiao, Z. Liu, V. S. Battaglia, K. Zaghib, G. Liu, *Nano Lett.* **2014**, *14*, 6704.
[32] M. Wu, X. Song, X. Liu, V. Battaglia, W. Yang, G. Liu, *J. Mater. Chem. A* **2015**, *3*, 3651.
[33] A. Magasinski, B. Zdyrko, I. Kovalenko, B. Hertzberg, R. Burtovyy, C. F. Huebner, T. F. Fuller, I. Luzinov, G. Yushin, *ACS Appl. Mater. Interfaces* **2010**, *2*, 3004.
[34] J. S. Bridel, T. Azais, M. Morcrette, J. M. Tarascon, D. Larcher, *Chem. Mater.* **2010**, *22*, 1229.
[35] I. Kovalenko, B. Zdyrko, A. Magasinski, B. Hertzberg, Z. Milicev, R. Burtovyy, I. Luzinov, G. Yushin, *Science* **2011**, *334*, 75.
[36] F. Bonino, S. Brutti, P. Reale, B. Scrosati, L. Gherghel, J. Wu, K. Müllen, *Adv. Mater.* **2005**, *17*, 743.
[37] A. Caballero, L. Hernan, J. Morales, *ChemSusChem* **2011**, *4*, 658.
[38] I. R. M. Kottegoda, Y. Kadoma, H. Ikuta, Y. Uchimoto, M. Wakihara, *J. Electrochem. Soc.* **2005**, *152*, A1595.
[39] Ó. Vargas, Á. Caballero, J. Morales, *Electrochim. Acta* **2015**, *165*, 365.
[40] C. Chae, H. Park, D. Kim, J. Kim, E.-S. Oh, J. K. Lee, *J. Power Sources* **2013**, *244*, 214.
[41] J. Hassoun, F. Croce, I. Hong, B. Scrosati, *Electrochem. Commun.* **2011**, *13*, 228.
[42] R. Kataoka, T. Mukai, A. Yoshizawa, T. Sakai, *J. Electrochem. Soc.* **2013**, *160*, A1684.
[43] K.-L. Lee, J.-Y. Jung, S.-W. Lee, H.-S. Moon, J.-W. Park, *J. Power Sources* **2004**, *130*, 241.
[44] R. Verrelli, J. Hassoun, A. Farkas, T. Jacob, B. Scrosati, *J. Mater. Chem. A* **2013**, *1*, 15329.
[45] Y. Wang, Y. Wang, D. Jia, Z. Peng, Y. Xia, G. Zheng, *Nano Lett.* **2014**, *14*, 1080.
[46] M. Shimizu, H. Usui, T. Suzumura, H. Sakaguchi, *J. Phys. Chem. C* **2015**, *119*, 2975.
[47] J. Nanda, M. K. Datta, J. T. Remillard, A. O'Neill, P. N. Kumta, *Electrochem. Commun.* **2009**, *11*, 235.
[48] R. C. Teixeira, I. Doi, M. B. P. Zakia, J. A. Diniz, J. W. Swart, *Mater. Sci. Eng. B* **2004**, *112*, 160.
[49] D. M. Piper, J. J. Travis, M. Young, S. B. Son, S. C. Kim, K. H. Oh, S. M. George, C. Ban, S. H. Lee, *Adv. Mater.* **2014**, *26*, 1596.
[50] V. Aravindan, J. Sundaramurthy, P. S. Kumar, N. Shubha, W. C. Ling, S. Ramakrishna, S. Madhavi, *Nanoscale* **2013**, *5*, 10636.
[51] S. Jayaraman, V. Aravindan, P. Suresh Kumar, W. Chui Ling, S. Ramakrishna, S. Madhavi, *ACS Appl. Mater. Interfaces* **2014**, *6*, 8660.

[52] M. Wu, X. Xiao, N. Vukmirovic, S. Xun, P. K. Das, X. Song, P. Olalde-Velasco, D. Wang, A. Z. Weber, L. W. Wang, V. S. Battaglia, W. Yang, G. Liu, *J. Am. Chem. Soc.* **2013**, *135*, 12048.

CHAPTER VII

SUMMARY

1. Particle/polymer electrospinning was used to prepare fiber mat Li-ion battery (LIB) electrodes containing active material nanoparticles and electronically conductive carbon powder distributed throughout a polymer binder. The preservation of the polymer binder in the final electrode structure distinguishes this work from previous studies where electrospun electrodes were prepared by pyrolyzing fiber mats containing a polymer precursor. In this dissertation, ink composition and electrospinning conditions were identified to produce particle/polymer fiber mats with uniform particle distributions and average fiber diameters on the order of 1 μm for the following electrode systems:
    a. Titania-based anodes containing 40 wt % TiO_2 nanoparticles, 25 wt % carbon black, and 35 wt % poly(acrylic acid) (TiO_2/C/PAA)
    b. Carbon-based anodes containing 65 wt % carbon nanoparticles and 35 wt % poly(vinylidene fluoride) (C/PVDF)
    c. $LiCoO_2$-based cathodes containing 70 wt % $LiCoO_2$ nanoparticles, 10 wt % carbon black, and 20 wt % poly(vinylidene fluoride) ($LiCoO_2$/C/PVDF)
    d. Si-based anodes containing Si nanoparticles, carbon black, and poly(acrylic acid) where the Si/C/PAA weight ratio was either 40/25/35 or 15/50/35 (Si/C/PAA)

e. Si-based anodes prepared with electronically conductive polymer binders where the Si content ranged from 35 – 50 wt % (e.g., Si/PFM/PEO)

2. $LiCoO_2$ nanoparticles were synthesized from a commercially available Co_3O_4 nanoparticle precursor. Appropriate solution and processing conditions were identified to produce $LiCoO_2$ nanoparticles with diameters ranging from 270 – 980 nm. X-ray powder diffraction (XRD) and Raman spectroscopy confirmed the $LiCoO_2$ had the desired $R\bar{3}m$ crystal structure, and Rietveld analysis of the XRD pattern indicated that the unit cell parameters of the synthesized $LiCoO_2$ agreed well with values reported in the literature. The $LiCoO_2$ nanoparticles were electrospun with carbon powder and PVDF binder to produce fiber mat cathodes for LIBs.

3. The active material in electrospun fiber mat electrodes containing carbon powder (i.e., TiO_2/C/PAA, C/PVDF, Si/C/PAA, and $LiCoO_2$/C/PVDF) was fully utilized at a 0.1 C charge/discharge rate. Cyclic voltammograms and charge/discharge curves for particle/polymer fiber mats indicated that the electrospinning process did not adversely affect fundamental lithiation/delithiation properties of the active material.

4. Electrospun TiO_2/C/PAA anodes, C/PVDF anodes, and $LiCoO_2$/C/PVDF cathodes exhibited higher capacities at fast charge/discharge rates (e.g., 2 C) compared to conventional slurry cast electrodes of the same composition. The excellent performance of the electrospun electrodes is attributed to: (i) complete electrolyte infiltration throughout the mat's intra and interfiber void space, (ii) a large

electrode/electrolyte interfacial area, and (iii) short Li^+ transport pathways between the electrolyte and active material nanoparticles in the radial fiber direction. These results show that the performance of LIB electrodes at high C-rates is limited by Li^+ transport rates.

5. Electrospun TiO_2/C/PAA, C/PVDF, Si/C/PAA, and $LiCoO_2$/C/PVDF fiber mat electrodes exhibited outstanding electrochemical and physical stability in an operating battery. The electrodes had minimal capacity fade during cycling (e.g., 91.7 % capacity retention after 510 cycles at 0.1 C for a C/PVDF nanofiber anode). Post-mortem analysis of the electrospun electrodes showed that the interfiber void space and fiber structure were well-maintained during cycling. For anodes with operating potentials < ~ 0.5 V vs. Li/Li^+ (i.e., Si/C/PAA and C/PVDF), preservation of the fiber mat structure demonstrated that the solid-electrolyte interphase (SEI) layer formed during cycling did not disrupt the overall pore structure of the electrospun fiber mats.

6. Whereas anodes and cathodes produced using many nanofabrication techniques (e.g., nanowires, carbon nanofibers, etc.) are restricted to low areal and/or volumetric capacities, electrospun particle/polymer fiber mat electrodes were made thick (up to 1.4 mm) with a high fiber volume fraction (up to 0.85) to achieve high areal and volumetric capacities. For example, compacted Si/C/PAA fiber mat anodes had high reversible capacities of 4.5 $mAh\,cm^{-2}$ and 750 $mAh\,cm^{-3}$ at 0.1 C.

7. The areal capacity at 0.1 C for electrospun C/PVDF fiber mats with a fiber volume fraction ~ 0.60 scaled linearly with electrode thickness where mats with thicknesses of 40 – 510 μm had areal capacities ranging from 0.32 – 3.94 mAh cm^{-2} at 0.1 C. Similarly, volumetric capacity at 0.1 C was directly proportional to the mat's fiber volume fraction. C/PVDF mats with fiber volume fractions of 0.25 – 0.79 had volumetric capacities of 36 – 102 mAh cm^{-3} at 0.1 C.

8. The areal capacity up to 2 C for thick C/PVDF anodes was improved by increasing the mat's interfiber void volume. C/PVDF mats with mass loadings ~ 24 mg cm^{-2}, fiber volume fractions of 0.42 and 0.63 (and thicknesses of 820 and 510 μm, respectively) exhibited similar areal capacities ~ 4 mAh cm^{-2} at 0.1 C, but the anode with a lower fiber volume fraction had a 4-fold higher capacity at 2 C (0.70 vs. 0.17 mAh cm^{-2}).

9. The capacity and cycling stability of electrospun Si/C/PAA anodes was significantly improved by compacting the mats to a high fiber volume fraction (~ 0.85) followed by welding the interfiber contacts via exposure to methanol vapor. A compacted/welded Si/C/PAA nanofiber mat had an initial capacity of 1,484 mAh g^{-1} which was 28 % higher than that of an as-spun mat (1,064 mAh g^{-1}). After 50 cycles at 0.1 C, the compacted/welded mat retained 73 % of its initial capacity compared to only 20 % capacity retention for the as-spun mat. Mats which were either only compacted or only welded had intermediate performance with initial capacities of

1,444 and 1,148 mAh g^{-1}, respectively, and 56 % capacity retention for each electrode after 50 cycles at 0.1 C.

10. Compacted/welded Si/C/PAA fiber mat anodes prepared with 15 wt % Si exhibited a lower capacity but better cycling stability compared to anodes containing 40 wt % Si. Fiber mats with 15 and 40 wt % Si had initial capacities of 582 and 1,484 mAh g^{-1} at 0.1 C, respectively, and capacity retentions of 90 % and 73 %, respectively, after 50 cycles at 0.1 C. The superior cycling stability of the anode with the lower Si content is attributed to its smaller volumetric changes during battery charging and discharging.

11. Full cells containing either an electrospun C/PVDF or Si/C/PAA anode and an electrospun $LiCoO_2$/C/PVDF cathode were prepared and characterized. The reversible capacity and specific energy density of the C/$LiCoO_2$ full cells were 49 mAh g^{-1} and 144 Wh kg^{-1} at 0.1 C. The electrospun C/$LiCoO_2$ full cell exhibited a high areal capacity of 0.64 mAh cm^{-2} at 2 C compared to only 0.34 mAh cm^{-2} for a cell containing slurry cast electrodes of the same composition. The Si/$LiCoO_2$ cells had a reversible capacity of 75 mAh g^{-1} and an energy density of 270 Wh kg^{-1} which are the highest values reported in the literature for an electrospun full cell. The electrospun Si/$LiCoO_2$ cell exhibited moderate cycling stability with 70 % capacity retention after 10 cycles at 0.1 C.

12. Fiber mats containing an electronically conductive polymer [PFM, which was synthesized by Gao Liu and coworkers at Lawrence Berkeley National Laboratory (LBNL)] were produced using electrospinning. Neat PFM fibers had an undesired bead-on-fiber morphology, but adding 1 wt % poly(ethylene oxide) (PEO) as a carrier polymer allowed for the production of uniform PFM/PEO fibers. Si/PFM/PEO fibers were also electrospun with up to 50 wt % Si nanoparticles. Fiber diameters of these materials ranged from 1.5 – 9 μm depending on the Si loading and electrospinning conditions. Relative humidity (rh) during electrospinning had a significant impact on the fiber structure; fibers spun at 15 % rh had a dense surface whereas spinning at 75 % rh produced fibers with surface pores ~ 100 nm in diameter.

13. Electrospun and slurry cast Si/PFM/PEO anodes containing 50 wt % Si exhibited very low reversible capacities (< 15 mAh g^{-1}) when cycled at 0.1 C. Similar results were obtained for a Si/PFM slurry cast anode (containing no PEO polymer), indicating that PEO is not the cause of the electrodes' low capacity. The PFM binder in these anodes likely formed a thick, ionically insulating layer on the Si nanoparticles which inhibited Li^+ transport to the active material during cycling. Experiments on slurry cast Si/PFM anodes showed that the PFM content should be ≤ 33 wt % to prevent electrochemical isolation of the Si nanoparticles. Similar experiments on slurry cast anodes containing another electronically conductive polymer binder (PEFM, which was synthesized by Gao Liu and coworkers at LBNL) showed that anodes prepared with 45 wt % PEFM exhibited high capacities and good cycling stability. The presence of the PEO side groups in PEFM likely increased the

binder's electrolyte uptake which allowed Si/PEFM slurry cast anodes to maintain good electrochemical performance at higher binder contents.

CHAPTER VIII

CONCLUSIONS

1. Particle/polymer electrospinning is a robust platform which can be used to prepare a wide range of fiber mat Li-ion battery (LIB) electrodes with high capacities at fast charge/discharge rates. The rate capabilities of electrospun particle/polymer fiber mats are insensitive of the electrode's active material and polymer binder. As shown in Appendix B, electrospun TiO_2/C/PAA anodes, C/PVDF anodes, and $LiCoO_2$/C/PVDF cathodes all retained ~ 67 % of their 0.1 C capacity at a 2 C charge/discharge rate.

2. The cycling stability of particle/polymer fiber mat electrodes containing active materials which undergo large volumetric changes during lithiation/delithiation (e.g., Si) can be significantly improved by welding interfiber contacts throughout the mat. The improved interfiber connectivity of welded fiber mats stabilizes the electrode structure during battery operation. In comparison, fiber mats containing active materials which experience small volumetric changes (e.g., TiO_2, C, and $LiCoO_2$) do not require welded interfiber contacts to achieve good cycling stability.

3. The thickness and fiber volume fraction of electrospun particle/polymer fiber mats must be optimized to meet the energy and power density requirements of a given application. For fiber mats of a specific fiber volume fraction, the areal capacity at

slow charge/discharge rates (e.g., 0.1 C) can increased by utilizing thicker electrodes, but very thick mats (e.g., > 500 μm) exhibit worse rate capabilities due to increased Li^+ transport distances throughout the electrode. To improve the rate capabilities of these thick electrodes, the mat's fiber volume fraction should be decreased. However, reducing the fiber volume fraction results in lower volumetric capacity. Thus in general, mat thickness and fiber volume fraction must both be optimized for a given application.

4. The meso- and macrostructure of LIB electrodes must be optimized to achieve high capacities at fast charge/discharge rates. Whereas conventional electrode fabrication techniques (e.g., slurry casting) provide little to no control over the pore structure throughout the electrode, electrospun particle/polymer fiber mats contain intra- and interfiber porosity where pore sizes range from a few nm to several μm. The hierarchical design allows rapid Li^+ transport throughout the electrode during battery operation and thus superior performance at high C-rates compared to conventional slurry cast electrodes.

CHAPTER IX

SUGGESTIONS FOR FUTURE WORK

1. The electrospun Si/C/PAA fiber mat anodes discussed in Chapter VI were prepared with Si/C/PAA weight ratios of 40/25/35 and 15/50/35. Electrodes with different amounts of Si, C, and PAA should be prepared and tested in coin cells to better understand how electrode composition affects the electrochemical performance of these materials.

2. Si/C/PAA fiber mat anodes should be prepared with a fiber volume fraction ~ 0.80 and thicknesses of at least 200 μm to achieve an areal capacity ~ 14 mAh cm^{-2}. The cycling performance of these electrodes should be evaluated over at 500 cycles at charge/discharge rates ranging from 0.1 – 5 C.

3. To prevent the electrochemical isolation of Si nanoparticles in electrospun anodes prepared with electronically conductive polymer binders (e.g., PFM and PEFM), ink compositions and electrospinning conditions to form Si/PFM and Si/PEFM fiber mats containing at least 67 wt % Si and 55 wt % Si, respectively, should be identified. The electrochemical performance of these electrospun electrodes should be compared to that of slurry cast anodes of the same compositions. In these studies, various carrier polymers should also be investigated including, poly(ethylene oxide) (PEO) and poly(vinylpyrrolidone) (PVP).

4. Electrospun mats containing etched Si nanowires (where the SiO_x passive layer is either partially or fully removed) should be prepared and characterized. The effect of the SiO_x layer on reversible capacity and cycling stability of these electrodes should be determined, and the performance of electrospun Si/C/PAA fiber mats containing either Si nanoparticles or Si nanowires with comparable SiO_x layer thicknesses should be compared.

5. Chapter IV describes the fabrication and characterization of electrospun fiber mat C/PVDF anodes prepared with Vulcan XC-72R carbon powder. The charge/discharge curves collected for these anodes had sloping profiles over 0.015 – 1.5 V vs. Li/Li^+ due to the non-graphitic nature of the carbon particles. In comparison, typical graphite anodes have a flat potential profile which is desired for some applications where battery voltage should remain relatively constant during discharging. Thus, particle/polymer electrospinning should be used to prepare graphitic carbon nanofiber mat anodes, and these materials should be characterized in half cells and full cells.

6. In Chapters III – VI, the capacities of electrospun particle/polymer fiber mat electrodes were normalized with respect to the total electrode mass and volume. For commercial battery applications, the mass and volume of other cell components (e.g., current collectors, separators, electrolyte, and cell packaging) must also be considered. Future studies should account for these inactive components to evaluate the cell-level energy density of batteries containing electrospun anodes and cathodes.

7. The performance of electrospun particle/polymer fiber mat electrodes should be evaluated in coin cells containing different electrolyte formulations (e.g., glymes and ionic liquids) which have wider electrochemical stability windows compared to conventional electrolytes containing liquid organic carbonates. These studies should focus on reducing or eliminating irreversible Li consumption due to formation of a solid-electrolyte interphase (SEI) layer.

8. This dissertation explored electrospun Li-ion battery (LIB) anodes and cathodes where the average fiber diameter in the mats was on the order of 1 μm. Ink composition and electrospinning conditions should be adjusted to change the average fiber diameter of the electrodes, and the effect of fiber diameter on LIB performance in half cells and full cells should be evaluated.

9. Particle/polymer nanofiber mat anodes and cathodes with different porosities, thicknesses, and active material loadings should be prepared and evaluated. Such experiments should be used to optimize anode and cathode designs for use at 0.1 – 5 C.

10. Sulfur-based fiber mat cathodes should be prepared by: (i) electrospinning sulfur-infiltrated carbon particles with a polymer binder and/or (ii) infiltrating sulfur into an electrospun carbon/polymer fiber mat. The effects of different carbon particles and polymer binders on the reversible capacity, polysulfide dissolution, and cycling stability of these sulfur cathodes in half cells and full cells should be evaluated.

11. Mn-based spinel cathodes with high operating potentials (e.g., 4.7 V vs. Li/Li^+) have been developed to increase the energy density of full cells as described in Chapter II. Electrospun fiber mat cathodes containing these high voltage active materials (in the form of nanoparticles) with carbon powder and polymer binder (e.g., PVDF) should be prepared and characterized.

12. Electrospinning should be used to prepare LIB separators and membranes. Electrospun PVDF nanofiber mats can be used directly as the separator in cells containing a liquid electrolyte. The effects of separator thickness, average pore size, and pore size distribution on LIB performance should be evaluated. Electrospun solid-state Li^+ conducting membranes containing ceramic nanoparticles (e.g., lithium lanthanum titanate, LLTO) should also be developed and assessed. The performance of these electrospun separators and membranes should be compared to that of commercial polyolefin separators.

13. An all-electrospun battery containing fiber mats as the anode, separator/membrane, and cathode layers should be fabricated. This fully integrated nanofiber system can, in principle, be prepared using a roll-to-roll process where each layer is electrospun sequentially or by electrospinning the electrodes on either side of a pre-fabricated membrane/separator.

14. A dual fiber electrospinning approach should be investigated to prepare nanofiber mats containing two different electrospun fibers. Electrospun anodes containing

separate Si/PAA fibers for high lithium capacity and C/PAA fibers for high electronic conductivity should be prepared where the weight ratio of the two fiber types is systematically changed. The performance of the dual fiber electrodes should be compared to that of single fiber mats of the same composition (i.e., mats containing Si, C, and PAA in the same fiber) to determine how the location of carbon powder affects cycling stability. Dual fiber mats with varying amounts of electronically conductive fibers should be prepared to determine the percolation threshold to achieve complete active material utilization of the Si/PAA fibers. Dual fiber mats should be prepared with different electrode thicknesses in the range of 50 – 200 μm and evaluated in half cells and full cells.

15. Core-shell electrospinning should be used to prepare fibers with concentric layers of anode, separator, and cathode materials. For example, a fiber would contain an anode core and cathode shell which are separated by a thin, ionically conductive membrane layer. At one end of the fiber, the anode should be exposed by etching away the cathode shell and membrane layer such that opposite ends of the fiber represent the battery's positive and negative terminals. Multiple fibers should be electronically wired together to increase the amount of energy that can be stored in the battery. This envisioned battery architecture has a very high material packing efficiency and would thus have a high systems-level energy density.

16. Electrospun particle/polymer nanofiber mats should be used to optimize the electrode/electrolyte interface for energy storage and conversion devices beyond

LIBs. Fiber mat electrodes for next-generation battery systems (e.g., Na-ion, Mg-ion, and Li-air) and supercapacitors should be developed. The effects of mat thickness and pore structure on the performance of these devices should be studied.

APPENDIX A

SYNTHESIS OF $LICOO_2$ NANOPARTICLES

A.1 Experimental Methods and Results

In addition to the sonochemical synthesis method described in Chapter V, $LiCoO_2$ nanoparticles were prepared using a sol-gel reaction as described in the literature.[1-3] For the sol-gel method, an aqueous solution containing a 1/1/2 molar ratio of $LiNO_3/CoN_2O_4 \cdot 6\ H_2O$/poly(acrylic acid) ($M_w$ = 1,800 Da) was magnetically stirred and evaporated at 80 °C overnight until a thick, pink gel was obtained. The resulting gel was then heated in air for 1 h at 300 °C followed by 1 h at 750 °C. Figures A.1a and A.1b show scanning electron microscopy (SEM) images of the resulting $LiCoO_2$ powder which contained primary particles (~ 200 – 500 nm in size) that were fused together. This sintered structure is undesired for electrospinning since individual particles need to be dispersed within the fibers. Therefore, $LiCoO_2$ nanoparticles prepared via a sol-gel method were not further investigated in the present study. In comparison, $LiCoO_2$ nanoparticles prepared using the synthesis method described in Chapter V were well-separated with diameters ranging from ~ 300 – 1,000 nm as shown in Figures A.1c and A.1d.

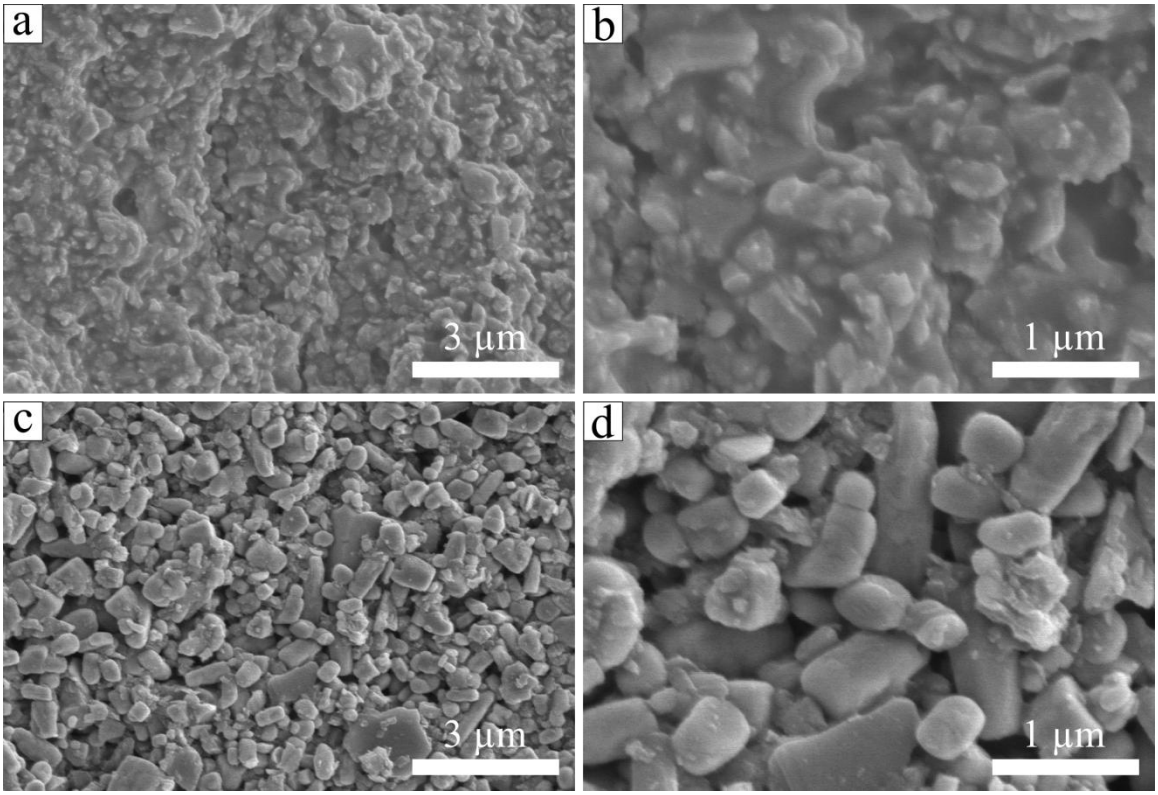

Figure A.1. SEM images of $LiCoO_2$ nanoparticles synthesized using a (a,b) sol-gel method and (c,d) the sonochemical method described in Chapter V.

A.2 References

[1] Y.-K. Sun, I.-H. Oh, S.-A. Hong, *J. Mater. Sci.* **1996**, *31*, 3617.
[2] I.-H. Oh, S.-A. Hong, Y.-K. Sun, *J. Mater. Sci.* **1997**, *32*, 3177.
[3] Z. S. Peng, C. R. Wan, C. Y. Jiang, *J. Power Sources* **1998**, *72*, 215.

APPENDIX B

RATE CAPABILITIES OF TIO_2/C/PAA, C/PVDF, and $LICOO_2$/C/PVDF FIBER MAT ELECTRODES

The performance of electrospun TiO_2/C/PAA anodes, C/PVDF anodes, and $LiCoO_2$/C/PVDF cathodes were compared in half cells at 0.1 – 2 C. As shown in Figure B.1, each electrode was prepared with an areal capacity ~ 0.1 mAh cm^{-2} at 0.1 C, and the electrospun anodes and cathodes exhibited similar performance at higher C-rates with capacity retentions of 67 ± 4 % at 2 C. These results demonstrate that particle/polymer electrospinning can be used to prepare a wide range of electrodes with good performance up to 2 C where the rate capabilities are insensitive to the active material and polymer binder used.

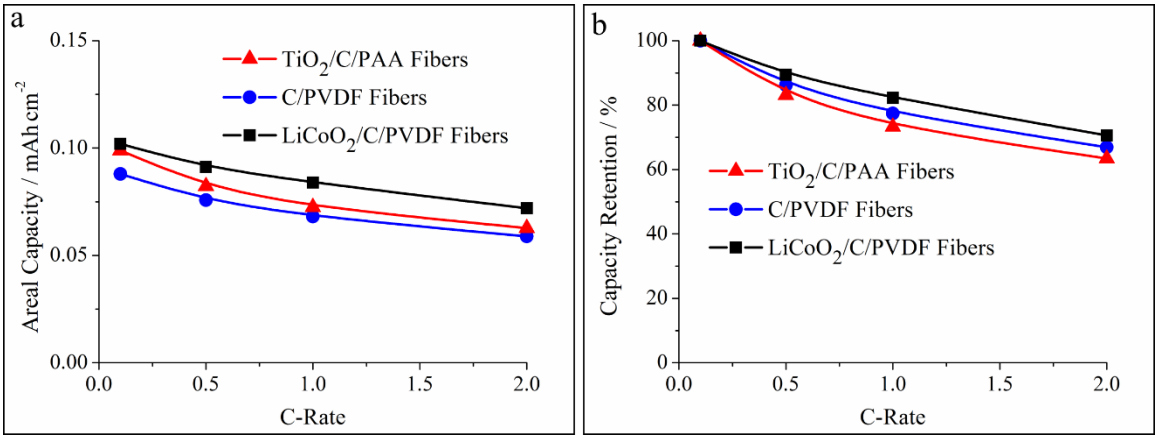

Figure B.1. (a) Areal capacity and (b) capacity retention of electrospun fiber mat TiO_2/C/PAA, C/PVDF, and $LiCoO_2$/C/PVDF electrodes at 0.1 – 2 C in half cells. Capacity retention in (b) is calculated by normalizing the capacity with respect to the capacity measured at 0.1 C for each electrode. The electrodes contained TiO_2/C/PAA, C/PVDF, and $LiCoO_2$/C/PVDF in a 40/25/35, 65/35, and 70/10/20 weight ratio, respectively.

APPENDIX C

ELECTROSPUN FIBER MAT ANODES PREPARED WITH SI NANOWIRES

As an alternative to Si nanoparticle-based fiber mat anodes, electrospun anodes containing Si nanowires (shown in Figures C.1a and C.1b) were prepared and characterized. The Si nanowires (provided by Professor Sreeram Vaddiraju and coworkers at Texas A&M University) were ~ 50 nm in diameter and ~ 5 μm in length. Electrospun fiber mats containing Si nanowires, carbon powder, and poly(acrylic acid) (PAA) in a 40/25/35 weight ratio were ~ 1 μm in diameter, and the nanowires were nicely aligned along the fiber axis as shown in Figures C.1c and C.1d. The performance of Si/C/PAA anodes containing either Si nanoparticles or Si nanowires was compared in half cells. The electrolyte in these cells contained 1.0 M $LiPF_6$ in a mixture of ethylene carbonate, dimethyl carbonate, and diethyl carbonate (1:1:1 by volume), and 10 wt % fluoroethylene carbonate was added to the electrolyte to ensure stable solid electrolyte interphase (SEI) layer formation. These experiments were conducted with as-spun mats only; neither mat compaction nor welding steps were performed prior to electrochemical characterization.

As shown in Figure C.2, the gravimetric capacity at 0.1 C of the electrospun mat containing Si nanowires was significantly lower than that of the Si nanoparticle anode (432 vs. 1,001 mAh g^{-1}). The lower capacity of the Si nanowires may be due to the presence of a thick (~ 10 nm) SiO_x passive layer on the nanowire surface, as determined by x-ray photoelectron spectroscopy conducted by Jagjit Nanda and coworkers at Oak

Ridge National Laboratory (results not shown). Despite its lower capacity, the Si nanowire anode exhibited superior cycling stability, retaining 68 % of its initial capacity after 50 cycles, as compared to only 21 % capacity retention for the nanofiber anode containing Si nanoparticles. The superior cycling stability of the anode containing Si nanowires could be attributed to one or more of the following: (i) improved fiber strength due to the presence of aligned Si nanowires along the fiber axis, (ii) anisotropic volumetric changes during lithiation/delithiation due to the unique nanowire aspect ratio, and/or (iii) the lower capacity and thus less severe volumetric changes during cycling of the Si nanowires.

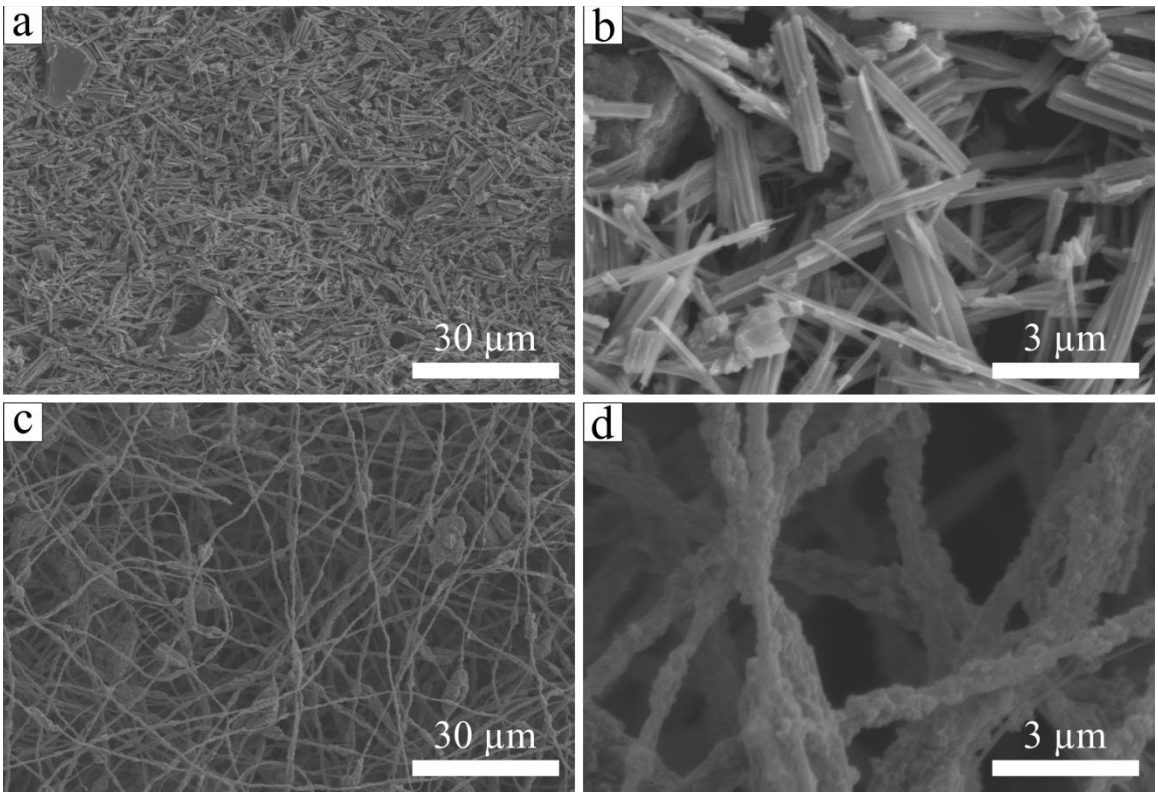

Figure C.1. SEM images of (a,b) Si nanowires and (c,d) electrospun nanofibers containing Si nanowires, carbon black, and PAA in a 40/25/35 weight ratio.

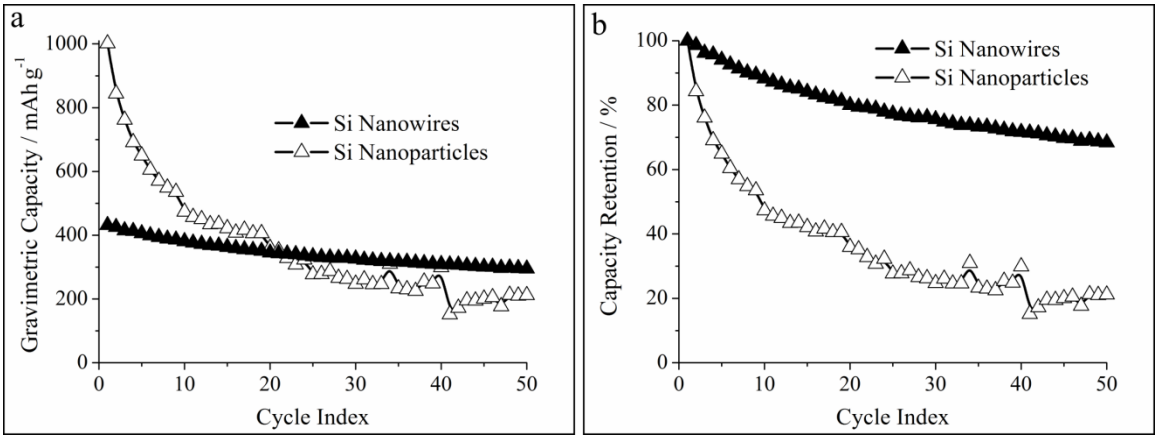

Figure C.2. Electrochemical performance of as-spun Si/C/PAA nanofiber mats where the Si active material is either in the form of nanowires or nanoparticles. (a) Gravimetric capacity and (b) capacity retention over 50 cycles at 0.1 C.